**Title**
Overcoming the limitations of silver nanowire electrodes for light emitting applications



**Author**
Chen, Dustin Yuan

**Publication Date**
2017

Peer reviewed|Thesis/dissertation

UNIVERSITY OF CALIFORNIA

Los Angeles

# Overcoming the limitations of silver nanowire electrodes for light emitting applications

A dissertation submitted in partial satisfaction of the

requirements for the degree of

Doctor of Philosophy in Materials Science and Engineering

by

Dustin Yuan Chen

2017

ABSTRACT OF THE DISSERTATION

Overcoming the limitations of silver nanowire electrodes for light emitting applications

by

Dustin Yuan Chen

Doctor of Philosophy in Materials Science and Engineering

University of California, Los Angeles, 2017

Professor Qibing Pei, Chair

The global lighting market is projected to exceed 100 billion dollars by 2020, undergoing rapid transitions driven by technological advancements. In conjunction with increased demand for new technology, global regulations have become increasingly stringent, mandating the development and implementation of more fuel-efficient light sources. As prior generations of lighting technology such as incandescent bulbs and florescent lighting progressively become phased out, newer technologies such as light emitting diodes (LEDs) and organic light emitting diodes (OLEDs) have become progressively popular and commonplace. Though they still lag behind LEDs in terms of market penetration, OLEDs have garnered increasing amounts of attention in recent years due to unique attributes such as their exotic and large scale form factors, mechanical flexibility, and potential for high volume, low-cost manufacturing. Unfortunately, the costs for OLED manufacturing are currently still prohibitively high for several applications, with the anode and substrate representing 20-25 percent of this total cost. Significant technical and

processing improvements for OLED substrates are of utmost necessity for fiscal cost reduction and commercialization of OLED technology.

Silver nanowires have gained traction as a potential replacement for the current status quo, indium tin oxide (ITO) due to attributes such as flexibility, low cost processing, and high optoelectronic properties. However, due to nanoscale size effects, the integration of silver nanowires in both process flows and operational use has proven to be problematic. This work makes several key contributions towards enabling the use of silver nanowires for practical and commercial applications within the lighting industry. First, a novel method for the fabrication of a high temperature-stable, flexible substrate with surface roughness ($R_a$) < 2 nm is presented, based on atomic layer deposition of a conformal metal oxide film on silver nanowires. This development of a thermally stable AgNW based substrate is critical for the future of flexible OLEDs, as both polymers and AgNWs are unstable at elevated temperatures required for certain OLED processing. However, at the time publication, no solutions existed for flexible OLED substrates simultaneously having thermal stability in excess of 230 °C for more than a few minutes while maintaining a smooth surface for subsequent device fabrication. The thermally stable silver nanowires developed in this work are able to withstand temperatures of 500 °C in ramping tests, and when integrated with a thermally stable polymer matrix, withstand temperatures of 300 °C for at least 6 hours, representing an increase in allowable processing temperatures of 70 °C for several hours longer. Resulting polymer light emitting devices (PLEDs) requiring high temperature processing fabricated on this thermally stable exhibit comparable performance to the same devices fabricated on ITO, validating its compatibility for integration in traditional process flows, and validity for use in extreme processing conditions.

Secondly, the aforementioned method is applied to understanding the electrical stability of silver nanowires. At the time of publication, previous works on the electrical failure of silver nanowires centered on the observation of failure under current flow, without a solution offered for how to mitigate the phenomenon. However, because the underlying purpose of these electrodes is to transport current, providing a solution for the failure flow is paramount to the success of AgNWs in future commercial applications. The importance of the development of this solution cannot be understated, especially in light of the fact that silver nanowires have been shown to fail under electrical stresses below typical operating conditions of various optoelectronic devices. The same technique mentioned previously can be leveraged for electrically stable silver nanowire networks, which show significant morphological stability over pristine silver nanowires when electrically stressed at normal operating conditions for OLEDs. These electrically stable substrates were able to produce high performance OLEDs with lifetimes 140% longer than the same devices fabricated on ITO, and 20% higher than non-electrically stable AgNW-based substrates.

Thirdly, the thermally and electrically stable substrate was used to fabricate a high performing perovskite quantum dot light-emitting device exhibiting high flexibility. The use of quantum dots instead of perovskite precursors and post treatment to convert the precursors to perovskite allowed for several new innovations. Due to the elimination of highly polar solvents typically required with perovskite precursors, a broadened range of architectures can be achieved. Furthermore, due to the small dimensions of the quantum dots in contrast to thick films of perovskite formed from precursors, the active layer can extremely thin, allowing for high

mechanical flexibility. The performance metrics achieved of 10.4 cd/A, 8.1 lm/W, and 2.6% EQE at a brightness of 1000 cd/$m^2$ were enabled in part by the substrate, which further allowed for the high mechanical performance. The electroluminescence performance of the perovskite quantum dot LEDs was found to be virtually fully recoverable after being subjected to a bending radius of 2.5 mm, or repeated cycles of bending and unbending to a 4 mm radius, representing the first report of a highly flexible and mechanically perovskite quantum dot light emitting device with high electroluminescence performance.

The improved stability of AgNWs with regards to both manufacturing and operational use, in addition to proof of concept in various light emitting devices demonstrates the potential of this technology for large-scale, commercial lighting applications.

The dissertation of Dustin Yuan Chen is approved.

Jaime Marian

Yunfeng Lu

Ioanna Kakoulli

Qibing Pei, Committee Chair

University of California, Los Angeles

2017

Dedicated to my parents
for their unwavering love and support

# Contents

# List of Figures

# List of Tables

# Acknowledgments

First and foremost I would like to thank my advisor, Professor Qibing Pei, for his guidance, mentorship, and help over the past few years. The work presented in this dissertation would not be possible without his continuous support.

Furthermore, I'd like to express my gratitude to Professors Jaime Marian, Yunfeng Lu, Ioanna Kakoulli, and Yu Huang for serving as my committee members for my qualifying exam and dissertation defense. Their guidance and suggestions have been invaluable for the completion of this dissertation.

Other current and past members of the Pei research group have also played an instrumental role in my research. I would like to specifically thank Kwing Tong, Chao Liu, Gillian Saldanha, Dr. Fangchao Zhao, Dr. Xiaofeng Liu, and Dr. Jiang Liu, and Dr. Jiajie Liang for valuable discussion and collaboration these past years, especially for their work on contributing to the thoughts and ideas presented in Chapters 2-4.

From other research facilities, I would like to thank Dr. Wilson Lin of the UCLA Nanolab, Dr. Ignacio Martini from UCLA Molecular Instrumentation Center, Dr. Sergey Prikhodko from the

Materials Science department, and Dr. Adam Steig from CNSI for help and training on various machines used through the course of my research.

To other friends at UCLA - H.C.; M. H.; J. G.; B. K. – thank you – you guys helped make long days on campus pass by much more quickly.

M. L.; E. B.; C. C.; R. N.; S. R.; - I've known all of you forever – thank you for your encouragement and friendship not only during my time at UCLA, but over the last decade or more.

Z. D.; and H. C. – thank you for your patience and support. We truly make a great team.

And finally to my family – my parents F. C.; and Y. C.; and my sister C. C.; - thank you for your unconditional and selfless love.

# Vita

2008 B.S., Materials Science and Engineering, University of California, Berkeley, Berkeley, CA

2014 M.S., Materials Science and Engineering, University of California, Los Angeles, Los Angeles, CA

2016 Intern, Advanced Display Manufacturing, Apple Inc., Cupertino, CA

# Publications

## First author / co-first author

[1] **D. Chen** *et al*., *Thermally Stable Silver Nanowire-Polyimide Transparent Electrode Based on Atomic Layer Deposition of Zinc Oxide on Silver Nanowires*, Advanced Functional Materials, Vol. 25, Issue 48, 7512-7520 (2015)

[2] **D. Chen** *et al*., *Flexible and stretchable electrodes for next generation polymer electronics: a review*, Science China Chemistry, doi:10.1007/s11426-015-5520-9 (2016)

[3] Q. Pei, **D. Chen**, J. Liang, *Thermally Stable Silver Nanowire Transparent Electrode,* Docket 30435.295-US-P1, *patent pending*

[4] **D. Chen** *et al., Mitigation of Electrical Failure of Silver Nanowires under Current Flow and the Application for Long Lifetime Organic Light-Emitting Diodes*, Advanced Electronic Materials, doi:10.1002/aelm.201600167 (2016)

[5] F. Zhao, **D. Chen** *et al., Highly flexible organometal halide perovskite quantum dot based light-emitting diodes on a silver nanowire-polymer composite electrode*, Journal of Materials Chemistry C, doi:10.1039/C6TC04934F (2016)

[6] J. Liu, X. Luan, **D. Chen** *et al., Vertical electrolyte-gated phosphorescent light-emitting transistors*, submitted for publication (2016)

[7] **D. Chen**, Q. Pei, *Electronic muscles and skins: a review of soft sensors and actuators*, Chemical Reviews, submitted for publication (2017)

## Other publications

[8] C. Liu, T. Hajagos, **D. Chen**, Y. Chen, D. Kishpaugh, Q. Pei, *Efficient One-Pot Synthesis of Colloidal Zirconium Oxide Nanoparticles for High-Refractive Index Nanocomposites*, ACS Applied Materials & Interfaces, Vol. 8, Issue 7, 4795-4802 (2016)

[9] J. Liang, L. Li, **D. Chen**, J. Hajagos, Z. Ren, S. Chou, W. Hu, Q. Pei, *Intrinsically stretchable and transparent thin-film transistors based on printable silver nanowires, carbon nanotubes, and an elastomeric dielectric*, Nature Communications, Vol. 6, 7647 (2015)

[10] Z. Ren, X. Niu, **D. Chen**, Q. Pei, *A new bistable electroactive polymer for prolonged cycle lifetime of refreshable Braille displays*, SPIE 9056, Electroactive Polymer Actuators and Devices (2014)

[11] X. Niu, R. Leo, **D. Chen**, W. Hua, Q. Pei, *Multilayer stack actuator made from new prestrain-free dielectric elastomers*. Proceedings of SPIE, Volume 8687 (2013)

# Chapter 1

# Introduction

In recent years, wearable electronics have transformed from a concept once posited by writers of science fiction to a functional reality permeating the everyday lives of everyday people. With the rapid development of these next generation electronics, the search for high performing flexible or stretchable transparent conductive electrodes (TCEs) has been highlighted as a critical barrier to surmount before the realization of high efficiency, high performance optoelectronic devices. In the selection of TCEs, the two parameters most commonly discussed are high conductivity and transparency,[1] with these parameters being compared to the standard, indium tin oxide (ITO). Adding to these two parameters, next generation TCEs must also exhibit mechanical compliancy, retaining their properties under various applied loadings and strains.

Networks of metallic nanowires have been shown to exhibit high transparency, conductivity, mechanical compliancy, and can be solution processed. In particular, silver nanowires (AgNW) have garnered significant attention, being used for applications ranging from organic light emitting diodes (OLEDs),[2–4] solar cells,[3,5,6] transparent heaters,[7] thin film transistors,[8,9] to electronic circuits.[10] These AgNW based devices have exhibited comparable performance, or in

some cases, exceeded the performance of devices fabricated using traditional electrode technology.

Though we focus primarily on the use of AgNW electrodes, several other materials are being explored for potential applications as well. Carbon nanotubes have been research extensively due to excellent mechanical behavior as well, but often times the higher sheet resistance prohibit use in high performing devices. Graphene has similarly garnered significant interest in electrode technology. Due to its high Fermi-velocity and the ability to be doped, graphene films exhibit extremely high in-plane conductivities.[1] Wu *et al.* demonstrated OLEDs on graphene substrates approaching the performance of ITO based devices.[11] Furthermore, due to the mechanical properties of this carbon based material, graphene based electrodes can be fabricated to be flexible or stretchable,[12] and can similarly be roll-to-roll processed.[13] However, though pristine graphene is an excellent candidate for a TCE, the difficulties in fabricating high quality films render the material cumbersome to use. Due to their combination of optoelectronic and mechanical performance, and their time and fiscal efficient fabrication, silver nanowires are currently at the forefront to replace ITO in next generation optoelectronics. This chapter first highlights the fabrication, development, and advancements we have made in recent years in the field of AgNW based electrodes. Second, the application of these electrodes for the fabrication of discrete devices and integrated systems is elucidated upon. Finally, this chapter concludes with a motivation for the work presented in subsequent chapters.

# 1.1. Fabrication, development, and advancement of AgNW based electrodes

## 1.1.1. Flexible AgNW electrodes

In a typical fabrication, AgNW flexible electrodes are fabricated by first coating a layer of AgNW from a dispersion of isopropyl alcohol (IPA) and methanol through wet deposition techniques such as drop casting, Meyer rod coating, dip coating, or spin coating onto a smooth release substrate. A bifunctional monomer with photoinitiator is overcoated on top of the AgNW coating, infiltrating the pores between the nanowires, and contacting the underlying release substrate.[14–16] After UV irradiation to crosslink the monomer, the flexible freestanding film is peeled off, resulting in an embedded AgNW network inlaid within a polymer matrix that can undergo bending at a 5 mm radius for 1000 cycles without deterioration of electrical properties.[17]

The AgNW films can be tailored to the desired transparency and conductivity by controlling the amount of solid nanowires deposited on the release surface, as shown in **Figure 1.1a**.[16] At transparency of 82%, freestanding films have a sheet resistance of approximately 10 ohm/□, comparable to commercially available ITO on PET substrates, and significantly higher than the typical 200 ohm/□ value observed for flexible CNT electrodes.[16]

In addition, embedding the AgNW within a polymer matrix drastically decreases the surface roughness, making devices such as OLEDs or solar cells built on top of the electrode significantly more efficient in contrast to rough electrodes with the same sheet resistance. **Figure 1.1b** illustrates the AFM topographical image of an embedded AgNW electrode at a sheet resistance of 10 ohm/□.[14] The average surface roughness for these embedded electrodes can be

up to one order of magnitude lower than those described in the previous section detailing CNT electrodes. The use of AgNWs instead of CNTs also lowers the barrier for charge injection into conjugated polymers, further increasing efficiency for optoelectronic devices built on top.

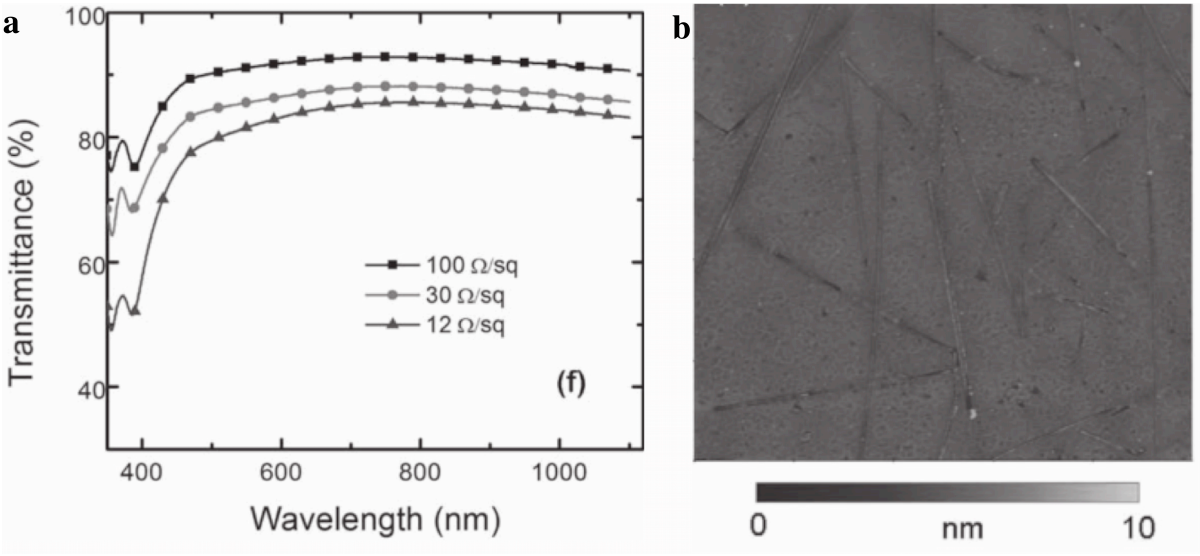


**Figure 1.1.** a) Transmittance as a function of wavelength for AgNW-acrylate freestanding electrodes at different sheet resistances. b) AFM topographical image of a freestanding AgNW-acrylate embedded electrode with a sheet resistance of 10 ohm/sq. [14,16]

Additional degrees of variability can be introduced into the electrode by selection of the polymer matrix. Li *et al.* embedded the AgNW percolation network within a heat resistant acrylate material to allow for subsequent device fabrication requiring temperatures up to 200 °C.[17] Yu *et al.* used a shape memory acrylate to reform and refreeze the electrode into new shapes when heated and cooled above the glass transition temperature ($T_g$) of the polymer.[16] The electrodes can further be made stretchable with the introduction of stretchable polymer matrices.

## 1.1.2. Stretchable AgNW electrodes

As a significant amount of optoelectronic applications requiring high conductivity and

transparency similarly require low surface roughness ($R_a$ < 2 nm), all silver nanowire based stretchable electrodes were fabricated by embedding the nanowires within a polymer matrix.[18–22] In the fabrication of stretchable electrodes, the selection of the polymer matrix is paramount to the performance, with selection criteria involving parameters including the bonding between nanowires and polymer, glass transition temperature, modulus, and transparency.

Yun *et al.* embedded the AgNWs in a copolymer of tert-butly acrylate (TBA) and acrylic acid (AA) to form a stretchable electrode with shape memory properties.[19] Though TBA by itself exhibits good elasticity and shape memory performance, the hydrophobicity of the homopolymer results in poor bonding with the nanowires. The addition of AA allows increased bonding between the copolymer and AgNWS via the carboxylic acid group, preventing sliding between the nanowires and polymer during repeated stretching cycles, and thus, minimizing the rate of increase of resistance when stretched. However, excessive concentrations of AA raises the $T_g$ value of the copolymer, leading to prohibitively high power consumptions for the electrode if used for shape memory applications. **Figure 1.2** illustrates the evolution of the nanowire electrodes with increasing strain (**Figure 1.2a**), and cyclical testing (**Figure 1.2b**), with various weight percentages of AA added.[19] A weight percentage of 5% AA was seen to improve the overall stretchability of the electrode both in uniaxial stretching and in cyclical testing. These electrodes were found to recover 98% of the resistance change after relaxing the electrode following stretching at 30% strain, 95% at 70% strain, and 90% at 90% strain, verifying the efficacy of the TCE as a stretchable electrode.[19] Lower recovery at higher strains were correlated with the viscoelasticity of the polymer matrix, exhibiting irreversable damage at high strains.

For stretchable electrodes not requiring shape memory properties, Hu *et al.* embedded the AgNW within an elastomeric polyurethane (PU) matrix.[20] The freestanding electrodes exhibited

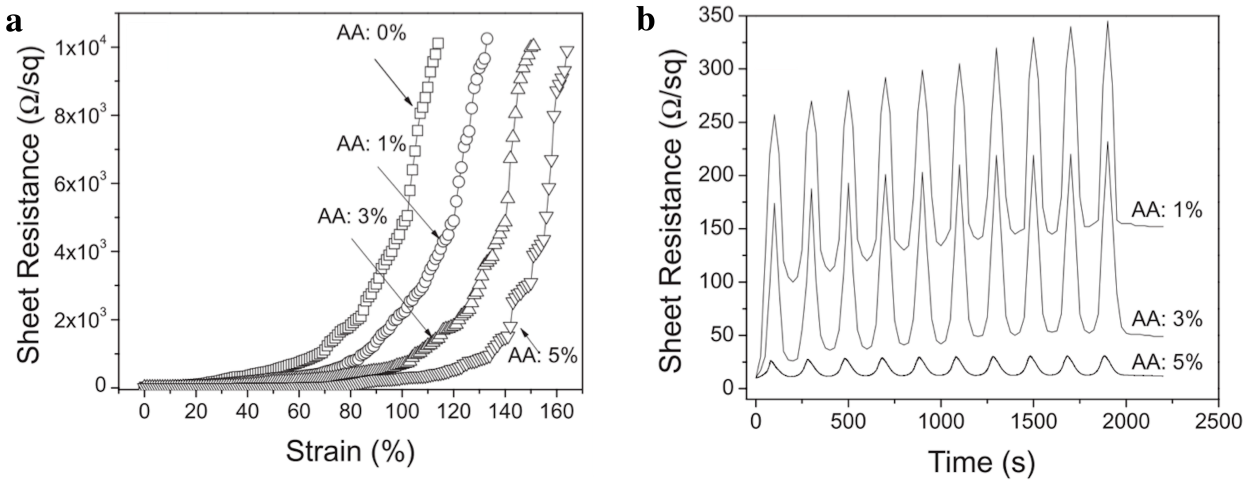


**Figure 1.2. | Electro-mechanical performance of stretchable AgNW-TBA/AA composite electrode.** a) Change in sheet resistance of stretchable AgNW-TBA/AA composite electrode with increasing strain. b) Change in sheet resistance of stretchable AgNW composite during 10 cyclic loadings of strain between 0 and 50% strain at a constant strain rate of 0.005 /s. [19]

a sheet resistance of 8 ohm/□ at a transparency of 75%, similar to the transparency value observed on the release glass substrate.[20] Using the rubbery PU matrix, the stretchable electrode was able to be reversibly stretched up to 170% strain, with the strained electrodes rapidly relaxing back to its original shape upon removal of the external load.

The AgNWs themselves can be manipulated as well to obtain enhanced performance. Liang *et al.* soldered the nanowires with a thin layer of graphene oxide (GO) before embedding the nanowires within the polymer matrix.[22] Fabrication of the GO-soldered AgNW remained largely the same as the general process of stretchable AgNW electrode fabrication, with the introduction of a soaking step in a 1 mg/mL GO Dispersion in distilled water and IPA following AgNW coating on a release substrate. The SEM image in **Figure 1.3a** shows that the percolation network remains intact, through a GO layer is evident at the nanowire junctions. This fusing at the nanowire junction is able to prevent inter-nanowire sliding at the junctions when the

composite electrode is stretched. **Figure 1.3b** shows the stretching performance of the composite electrode after the GO-soldered AgNWs are embedded within a polyurethane matrix, with a non-GO soldered AgNW stretchable electrode for comparison. The GO-soldered AgNWs were seen to have smaller resistance increase with strain in contrast to the control device, increasing in resistance by 2.3, 5.3, and 10.6-fold at strains of 40, 60, and 80%, respectively. In contrast, the control electrode increased 5.4, 9.8, and 17.2 fold.

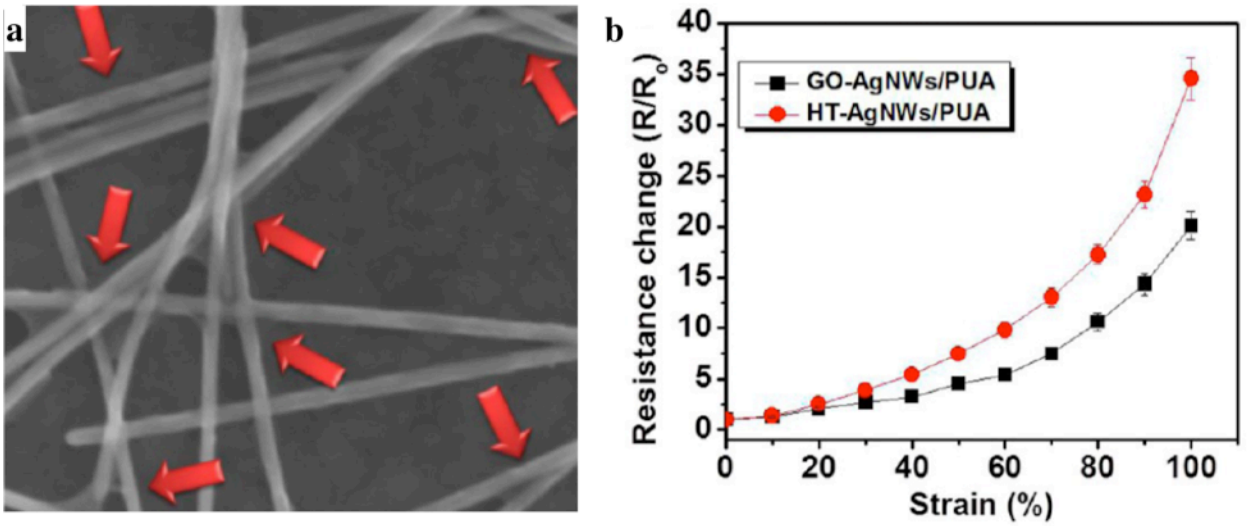


**Figure 1.3. | GO-soldered AgNW networks** a) SEM image of GO-soldered AgNW networks, with fused junctions indiciated by red arrows. b) Normalized resistance of GO-AgNW-PU and AgNW-PU electrodes stretched at 1 mm/s (20%/s). [22]

These electrodes described above are the basis of several optoelectronic devices. Detailed description of these devices will be elucidated upon in further sections.

## 1.2. Lighting applications: discrete devices and integrated systems

### 1.2.1. Flexible light emitting electrochemical cell

In previous works, rigid light emitting electrochemical cells have been fabricated on ITO.[23,24] Briefly, the polymer LEC consists of a single active layer comprising a light emitting polymer (LEP), an electrolyte to supply dopants, and an ionic conductor, sandwiched between two electrodes. The LEC exhibits light emitting properties due to the formation of a dynamic p-i-n junction in the polymer layer upon application of a bias, which effectively removes the charge injection barrier at the polymer-electrode interfaces.[24] The formation of excitons from the recombination of electrons and holes near this junction is the mechanism of light formation for these devices. Though the performance of polymer LECs (PLECs) lag behind polymer LEDs, the use of a single polymer layer that can be wet processed is highly appealing, resulting in thorough investigation through the years in increasing the stability, luminance, and efficiency of these devices.

However, the use of ITO as the anode still requires one component manufactured through expensive batch based vacuum processing, in addition to rendering the LEC rigid, as the electrode material is known to be brittle even under low loadings. Yu *et al.* fabricated a PLEC using spray coated SWCNT on PET as both the anode and cathode.[25] Though conventional light emitting devices require high smoothness for optimal performance, the high thicknesses of the emissive layer that can be utilized within PLECs without sacrificing performance renders this method of electrode fabrication sufficient. PF-B, a blue emissive luminescent polymer, an

ethoxylated trimethylopropane triacrylate (ETT-15) as the ionic conductor, and lithium trifluoromethane sulfonate (LiTf) as the salt were used as the polymer layer in a weight ratio of 20:10:1, respectively.[25] The polymer was spin-coated onto the SWCNT/PET anode, with the resulting stack subsequently laminated underneath another SWCNT/PET cathode using a roll lamination machine at 120 °C.[25] For flat devices, the PLEC had a turn-on voltage of 3.8 V, a maximum intensity of 1400 cd/m$^2$ at 10 V, and a maximum efficiency of 2.2 cd/A at 480 cd/m$^2$.[25] The device performance (J-V and luminance-voltage, and efficiency-luminance) is shown below in **Figure 1.4**. No change in light emission intensity and uniformity was observed after being bent to a 2.5 mm radius. Furthermore, as seen in **Figure 1.4a**, the electrical characteristics of the blue-emission devices remained virtually identical after being bent to a 2.5 mm radius, highlighting the efficacy of the two SWCNT based flexible electrodes. A slight decrease in efficiency was observed in the bent device, as seen in **Figure 1.4b.**

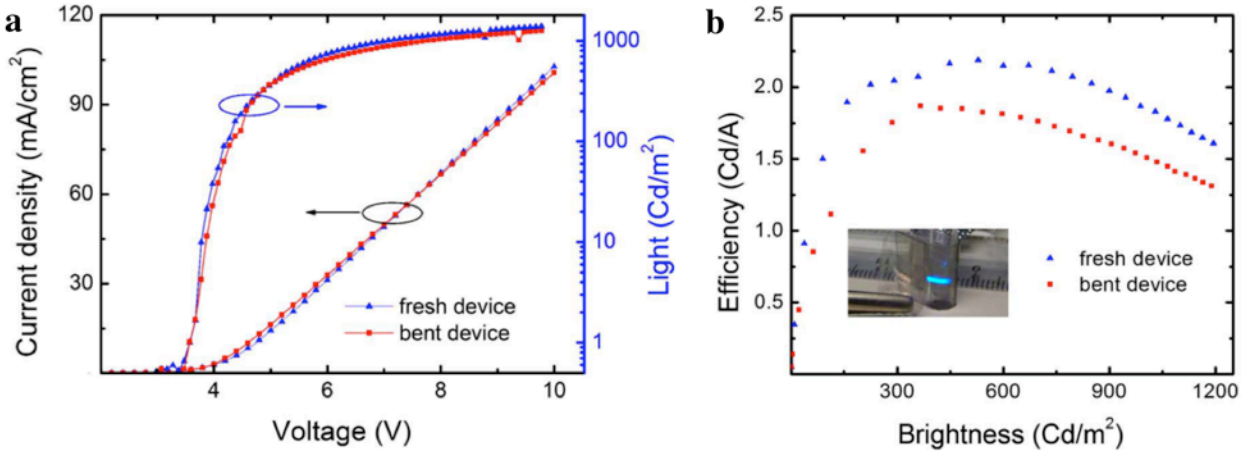


**Figure 1.4. | Performance of the bendable blue polymer light emitting device.** a) Current and light emission as a function of voltage for a bent and flat blue-emission device. b) Efficiency as a function of brightness of a bent and flat blue-emission device, with bent device shown in inset. [25]

Liang *et al.* demonstrated a PLEC using a bilayer SWCNT/AgNW anode fabricated by sequentially Meyer rod coating layers of SWCNTs and AgNWs before embedding the hybrid

conductive percolation layer in a urethane acrylate, difunctional methacrylate monomer, and tert-butyl acrylate monomer mixture.[26] The use of the bilayer anode is to improve the area coverage of conductive material; AgNWs by themselves yield relatively low surface coverage, resulting in non-uniform charge injection, and non-active regions of emission. Yellow PLECs were fabricated with the bilayer electrode as anode, an active layer comprising SuperYellow as the emissive material, a cross-linked trimethylolpropanetriacrylate (ETPTA) as an ionic conductor, and LiTf as the salt, and an evaporated aluminum (Al) layer as cathode.[26] To evaluate the performance of the bilayer anode, the same devices were also fabricated on control anode of ITO/glass and a single AgNW layer composite electrode.

The performance of the yellow PLECs on the three anodes described above are shown in **Figure 1.5**. **Figure 1.5a** illustrates the J-V curve of the devices. The bilayer composite electrode has higher current density than both devices on ITO/glass and the AgNW composite electrode. The high current density is a result of the low resistivity of the highly conductive AgNW network, in conjunction with the uniform surface coverage due to the small dimensions of the SWCNT network. The high current density leads to high charge injection, and thus, high emission intensity. Because the area coverage of the bilayer electrode is higher than that of the AgNW electrode, there is more charge distribution into the emissive layer, leading to a larger lighted area. Thus, the emission characteristics of the bilayer anode device are higher than that of the AgNW electrode, and resemble those devices built on ITO/glass, as seen in **Figure 1.5b**. Furthermore, the efficiency of the PLEC on the composite electrode exceeds that on ITO/glass **(Figure 1.5c**). This can be attributed in part by the surface plasmon scattering of emitted light by the nanowires, increasing the out-coupling efficiency.[26]

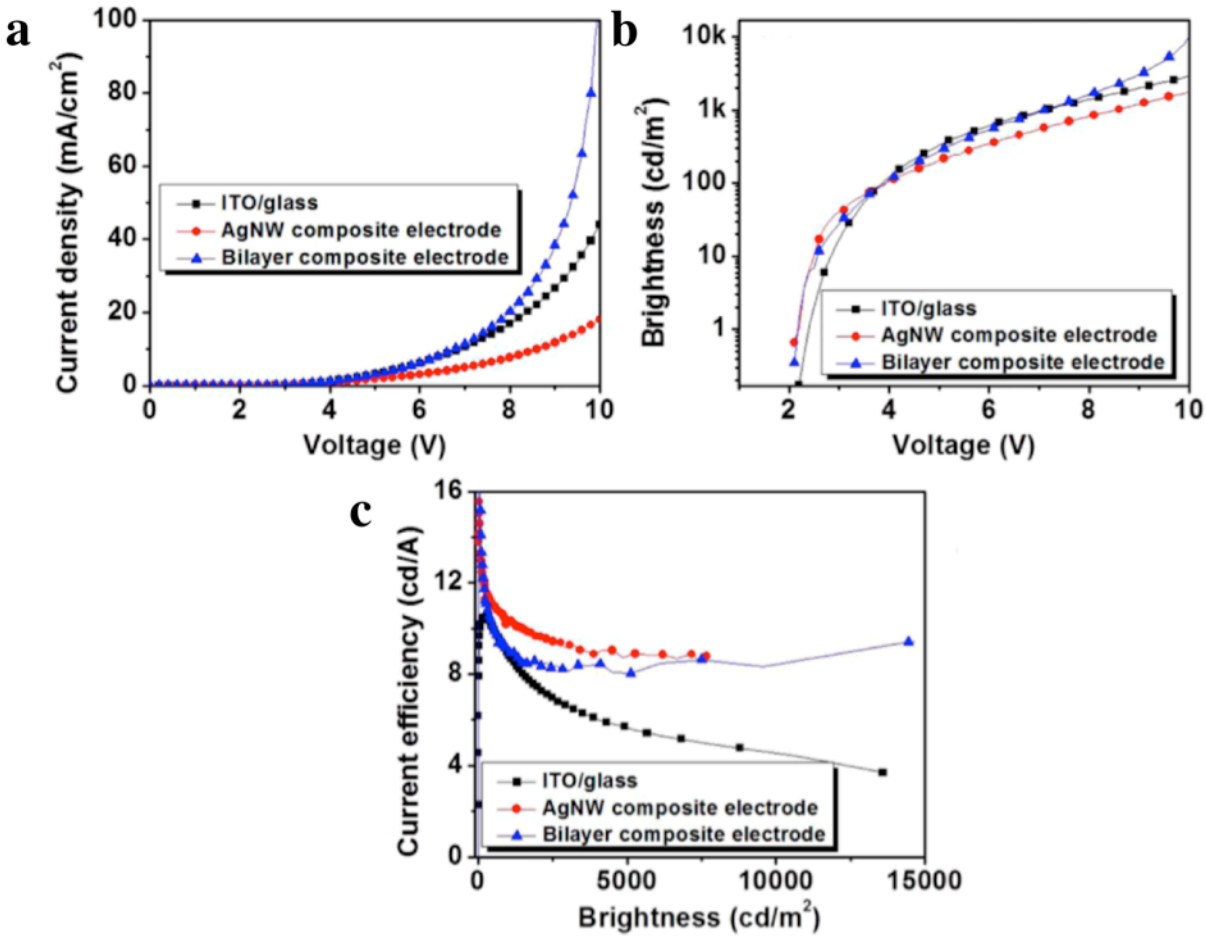


**Figure 1.5 | Performance of yellow PLEC.** a) J-V characteristics of yellow PLEC fabricated on a bilayer anode, a mono-layer AgNW anode, and ITO/glass. b) Luminance-voltage characteristics of a yellow PLEC fabricated on the three different anodes. c) Current efficiency as a function of brightness for yellow PLECs fabricated on the three different anodes. [26]

## 1.2.2. Flexible organic light emitting diodes

Though OLEDs or PLEDs require additional processing in contrast with PLECs, the enhancement in performance, stability, and efficiency largely outweigh the additional time and fiscal costs brought about by the more complex fabrication. Like the aforementioned PLECs, AgNW or hybrid AgNW/SWCNT substrates provide a cost and performance efficient platform to build OLEDs or PLEDs on top of. Several devices for a variety of different applications have

been reported using these composite electrodes as the basis.[15,16,27,28] Yu *et al*. fabricated shape-memory PLEDs using a bifunctional acrylate polymer as the matrix supporting the AgNWs for the anode, followed by subsequent layers of poly (3,4-ethylenedioxythiophene) polystyrene sulfonate (PEDOT:PSS) as a hole injection layer (HIL), an alkoxyphenyl substituted yellow emissive poly(1,4-phenylene vinylene) (SY-PPV), cesium fluoride (CsF) as the electron injection layer (EIL), and Al as the cathode.[16] To evaluate the shape change properties and performance of the PLED, the device was heated above the $T_g$ of the polymer substrate, bent to a 2.5 mm radius, and relaxed back to the flat shape. The devices were able to operate at a high brightness during the shape change process occurring at 120 °C, as seen in **Figure 1.6a**.[16] Furthermore, the current efficiency of the device remains unchanged at approximately 14 cd/A after several cycles of bending and recovery, as seen in **Figure 1.6b**.[16] The operational lifetime of the PLED was also similar to control devices fabricated on ITO, with the emission intensity reducing to 80% of its maximum value after 24 hours of continuous operation, in contrast to the 88% observed with ITO as the anode. This difference in lifetime may be due to a higher operating voltage needed to drive the AgNW based devices.

For higher efficiency lighting, Li *et al.* fabricated white polymer phosphorescent LEDs (WPLED) using the AgNW composite substrates. Like the previously discussed PLED, the WPLED fabricated was fully solution processed for low fabrication cost, using PEDOT:PSS as the HIL and CsF and Al as the EIL and cathode, respectively. The emissive layer comprised a mixture of host material poly(vinylcarbazole) (PVK) and electron transporting (ET) material 1,3-bis[4-*tert*-butylphenyl)-1,3,4-oxidiazolyl]phenylene (OXD-7), doped with blue phosphorescent dopant bis[4,6-difulorophenyl)-pyridinato-N,$C^2$] (picolinato)Ir(III) (FIrpic), green phosphorescent dopant tris(2-(4-toyl) pyridinato-N,$C^2$) (Ir((mppy)$_3$), and red phosphorescent

dopant bis(1-phenylisoquinoline) (acetylacetonate) (IR(piq)).[27] PVK was selected as the host due to its high triplet energy level, good surface topography, thermal stability, and its ability to conduct holes.

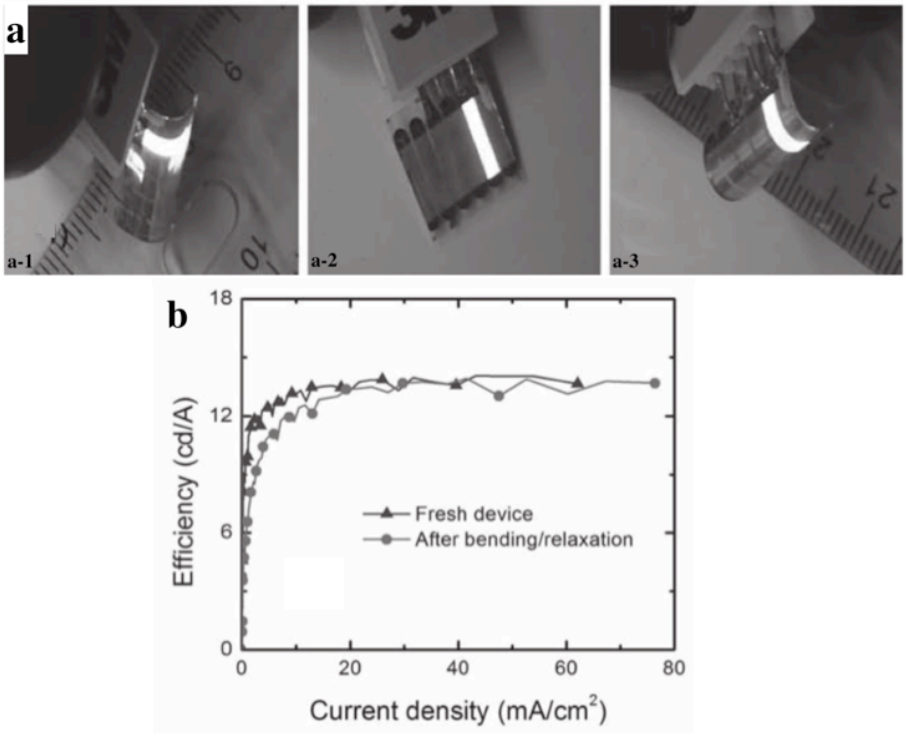


**Figure 1.6.** a) Shape memory PLEDs bent and frozen to a 2.5 mm radius, recovered to flat position, and bent and frozen to the opposite direction. b) Current efficiency as a function of current density for fresh PLEDs, and PLEDs subjected to 10 cycles of bending and recovery. [16]

It was reported that the use of the AgNW polymer substrate had the additional benefit of extracting more light emitted from the emissive layer in comparison to devices built on ITO/glass. **Figure 1.7** illustrates the architecture of the WPLEDs on both ITO/glass and AgNW/polymer. Due to total internal reflection, light beams emitted at small angles (L1 and L2) from the WPLED on ITO/glass are trapped. However, the composite substrate has a twofold

benefit. First, the AgNWs serve to scatter light, allowing smaller angle rays (R1) to change course, and be extracted from the opposite side of the substrate. Second, the index mismatch between emissive layer and polymer substrate is smaller than that between emissive layer and ITO, allowing wider angles to be extracted from the WPLED.

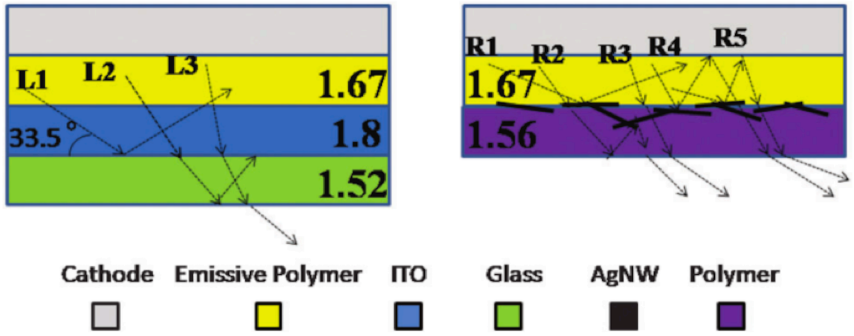


**Figure 1.7.** Schematic cross sectional views of WPLEDs on ITO/glass (left), and AgNW/polymer (right). The refractive of the layers are shown in the schematic, in addition to the modes of light extraction in the devices. [27]

As a result of the enhanced light extraction of WPLEDs built on AgNW/polymer, the current efficiency measured exceeded that of control devices fabricated on ITO/glass by 41%.[27] Current density as a function of luminance and power density as a function of current density are shown in **Figure 1.8a**. A maximum current efficient of 42.3 cd/A for the three primary color device, with the current density remaining in a narrow range around 40 cd/A up to a luminance of 10,000 cd/m$^2$ was obtained. The enhanced light extraction is further evident in **Figure 1.8b**, where the edge emission of the WPLED built on AgNW/polymer is significantly weaker due to a majority of the light being extracted from the substrate. Also apparent in **Figure 1.8b** is the wide viewing angle, which is quantified in **Figure 1.8c** with WPLEDs on AgNW/polymer having a higher luminance than those on ITO/glass at all angles except extremely low angles.

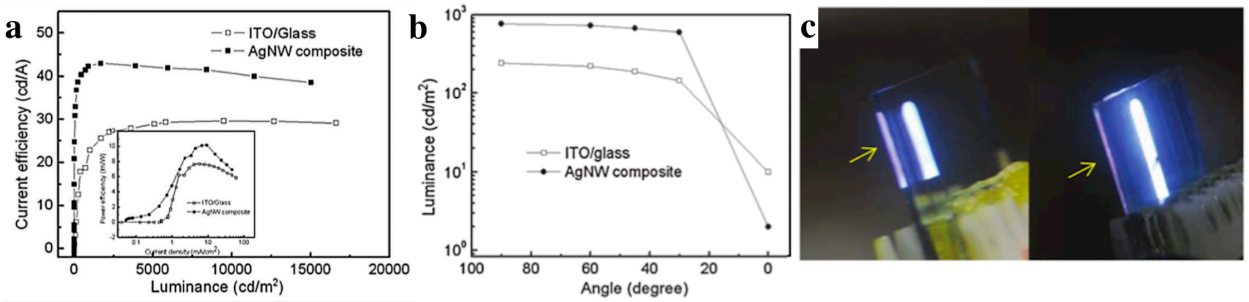


**Figure 1.8. | Light emission for WPLEDs** a) Current density as a function of luminance for WPLEDs fabricated on ITO/glass and AgNW/polymer. Power efficiency as a function of current density is shown in the inset. b) Luminance as a function of angle. c) Electroluminance photograph of WPLEDs on ITO/glass (left) and AgNW/polymer (right) during operation, with arrows pointing to the location of edge emission. [27]

To further increase the efficiency of WPLEDs, Li *et al.* dispersed nanoparticles of barium strontium titante (BST) in a AgNW/SWCNT/polymer matrix.[28] Using finite-difference time-domain (FDTD) analysis, the light extraction enhancement as a function of diameter and refractive index of the nanoparticle (**Figure 1.9a**) was determined. A maximum enhancement of 3.61 was obtainable for nanoparticle diameters of 500 nm and a refractive of 2.6, when the doping concentration was 1 wt%.[28] The peak enhancement factor as a function of wt.% was also simulated (**Figure 1.9b**), with 1 wt.% being the optimal concentration for 500 nm BST nanoparticles, and 2 wt.% being optimal for 200 nm nanoparticles.[28] **Figure 1.9c** illustrates the benefit of using BST dispersed within the polymer matrix. With the nanocomposite polymer matrix, two major trapping modes in PLEDs fabricated on ITO/glass are eliminated or suppressed: (1) the waveguide mode in ITO is eliminated; and (2) the glass mode is suppressed as light propagation can be altered by the nanoparticles and nanowires.

Following simulation results, SWCNT/AgNW/polymer electrodes were fabricated with 2 wt.% of 200 nm BST nanoparticles dispersed within.[28] The 200 nm nanoparticles were selected instead of larger dimension nanoparticles due to the ease of dispersion of smaller nanoparticles within

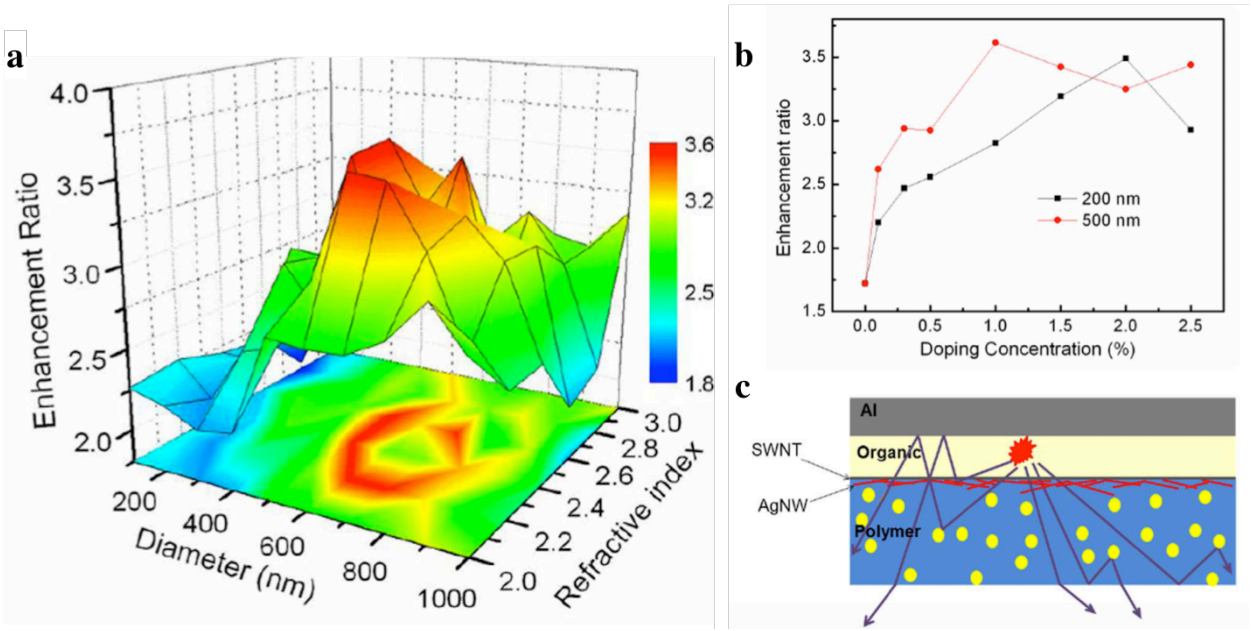


**Figure 1.9 | Light enhancement using BST nanoparticles.** a) Simulated enhancement in WPLEDs as a function of diameter and refractive index of nanoparticles dispersed within the substrate. b) Simulated enhancement factors as a function of doping concentrations with the refractive index fixed at 2.6. c) Schematic cross section of the AgNW/polymer substrate with nanoparticles dispersed illustrating the light scattering by the nanoparticles. [28]

the acrylate monomer. WPLEDs were fabricated with a sandwich structure of Al / CsF / emissive layer / PEDOT:PSS / anode, with the emissive layer being a blend of a white polymer (WP) and OXD-7 in a 100:40 wt. ratio. As control devices, WPLEDs were fabricated on an additional four substrates: ITO/glass; AgNW/polymer; SWCNT/AgNW /polymer; and AgNW/BST/polymer. **Figure 1.10** shows the current (**Figure 1.10a**) and power efficiency (**Figure 1.10b**) of the AgNW/SWCNT/BST/ polymer, compared to the four reference devices. The values of current, power, and external quantum efficiency of the AgNW/SWCNT/BST/polymer based device was 44.7, 44.0, and 28.8, respectively, representing an enhancement of 119%, 140%, and 120% compared to respective values obtained from devices built on ITO/glass. The efficacy of the BST nanoparticles in enhancing the efficiency was seen in the enhancement of current, power and

external quantum efficiencies of 55%, 48%, and 82% compared to SWCNT/AgNW/polymer based devices.

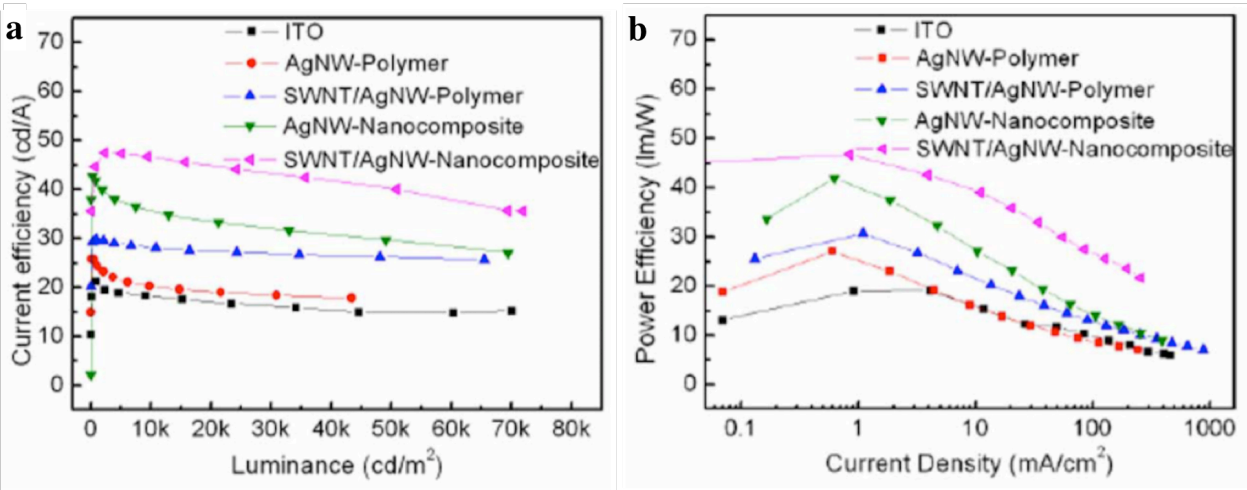


**Figure 1.10 | Device performance for WPLED on various substrates.** a) Current efficiency as a function of luminance for WPLEDs fabricated on five different substrates. b) Power efficiency as a function of current density for WPLEDs fabricated on five different substrates. [28]

The OLEDs described in this section verify the efficacy of AgNW or AgNW/SWCNT based electrodes for different applications. Careful selection and engineering of the polymer matrix can be used to tailor the properties desired for specific W/PLEDs. The same type of engineering can be applied to various stretchable electronics.

## 1.2.3. Stretchable lighting

Yu *et al.* first fabricated stretchable PLECs on SWCNTs embedded in a shape memory PtBA matrix.[29] The PLECs consisted of the stretchable SWCNT electrodes sandwiching an emissive layer comprising a blue emissive polyfluorene copolymer (Pf-B); poly(ethylene oxide) dimethacrylate ether (PEO-DMA), an ionic conductor, and LiTf as the salt.[29] To analyze the compliance of the PLECs, the devices were heated above the $T_g$ of the shape memory polymer,

anchored on two edges of a homemade stretching apparatus, and prestrained by 10% to flatten the device. The PLECs were subsequently stretched an additional 20% and 45%, and cooled to room temperature to freeze the deformed shape.

Emission from the stretched devices was observed to be uniform throughout the active layer. Though the current density and luminance decrease with increasing strain, the efficiency exhibits slight enhancement at larger strains, as seen in **Table 1.1**.

**Table 1.1.** Electroluminescence characteristics of the stretchable PLEC driven at 8V at different strains. [29]

| Property | Longitudinal strain: 0% | 20% | 45% |
|---|---|---|---|
| Luminance [cd $m^{-2}$] | 45 | 30 | 18 |
| Current density [A $m^{-2}$] | 59.4 | 35.7 | 20.8 |
| Efficiency [cd $A^{-1}$] | 0.76 | 0.84 | 0.87 |

For improved PLEC performance, Liang *et al*. used embedded AgNWs in a rubbery poly(urethane acrylate) (PUA) matrix.[21] The PLEC was fully solution processed with an emissive layer comprising SuperYellow as a yellow light emitting polymer, ETPTA as the ionic conductor, PEO as a second ionic conductor to enhance the stretchability of the ETPTA network, and LiTf as the salt, sandwiched between two AgNW-PUA electrodes.[21] To avoid damage to the electrode from solvent attack, a thin layer of PEDOT:PSS was spun on the anode side prior to the deposition of the emissive layer.

The PLEC turned on at 6.8 V, and reached a peak brightness of 2200 cd/$m^2$.[21] Unstretched, an EQE of 4.0% was obtained, comparable to state of the art PLECs based on SuperYellow on ITO at the time. When stretched, these devices increased in brightness up to 20% strain, then decreased at higher strains up to 120%, after which light emission was no longer observed. As the opposite trend was observed in current density, the current efficiency initially increases up to

80% strain, before leveling off and decreasing gradually until 120% strain. The current density exhibited this opposite trend due to an increase in sheet resistance of the composite electrode.

Due to the mechanical robustness of the device, the PLEC can be stretched, bent, or collapsed, promising easily deployable lighting that can conformally attach on non-uniform surfaces. **Figure 1.11** illustrates the capability of the PLEC to withstand mechanical deformation, with the device stretched to various strains illustrated in **Figure 1.11a**, and wrapped around the edge of a 400 micron thick piece of cardboard (**Figure 1.11b**). The high flexibility and stretchability of the composite electrode allows the device to operate under these extreme conditions while maintaining uniform emission as evidenced by the absence of dark areas, and emission ~30% of the original luminance.

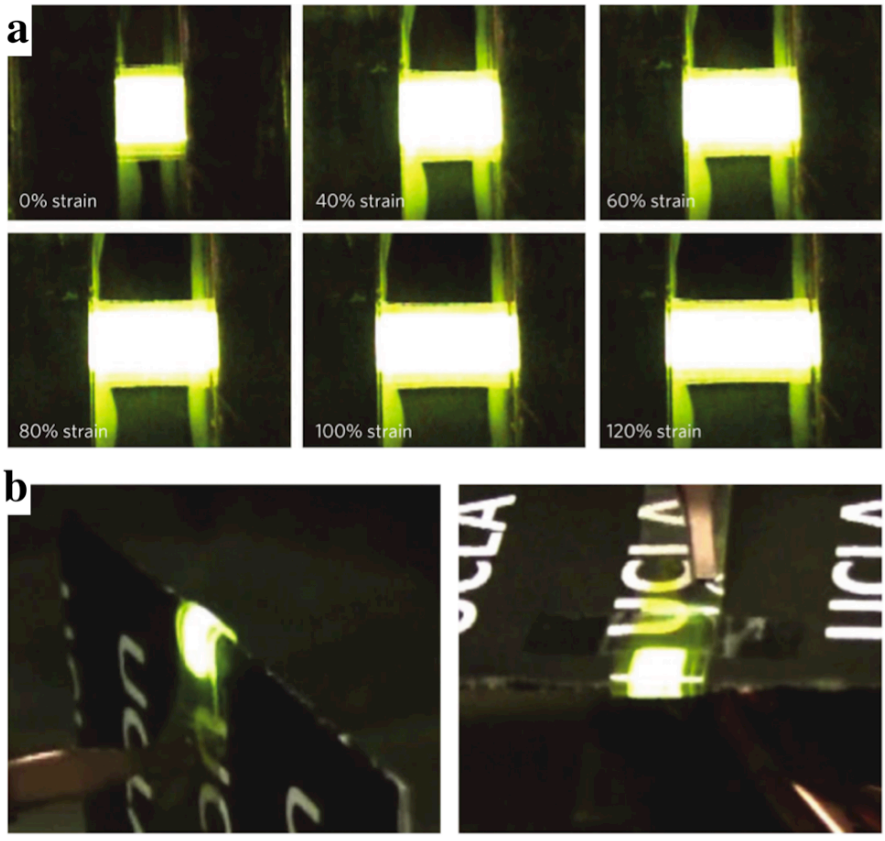


**Figure 1.11 | Mechanical deformation of an elastomeric PLEC.** a) PLECs stretched from 0 – 120% strain. b) PLECs bent around a 400 micron thick piece of cardboard. [21]

Liang *et al*. also fabricated stretchable white PLEDs using a graphene oxide soldered AgNW electrode embedded in a PUA matrix.[22] The devices were fabricated with the architecture: GO-AgNW/PUA anode; PEDOT:PSS as the hole transport layer (HTL); an emissive layer comprising a white light emitting polymer and OXD-7; and a second GO-AgNW/PUA electrode coated with polyethylenimine (PEI) acting as a electron transport layer (ETL). The performance of these devices were comparable to that observed with the stretchable PLEC. These stretchable lighting devices pave the foundation for rollable displays and other consumer tunable electronics of the future.

### 1.2.4. Integrated system: Stretchable transistor and display

For display technology, thin film transistor (TFT) arrays are required to control the pixels. In the case of stretchable lighting, a stretchable TFT array is a critical component in the development of a fully functioning stretchable display. Liang *et al.* demonstrated an intrinsically stretchable, fully solution processed TFT using an AgNW/PUA electrode as the source and drain, SWCNT as the network channel, and polyacrylate-*co*-polyethylene glycol (PA-*co*-PEG) as an elastomeric dielectric.[30]

Transfer characteristics (**Figure 1.12a**) and device performance (**Figure 1.12b**) under applied strain are shown in **Figure 1.12**. A mobility of 30 $cm^2/V$ s was obtained, with an on off ratio of $10^3 – 10^4$, switching current > 100 μA, and transconductance > 50 μS.[30] At a strain of 50%, the mobility decreased to 16.2, due to the decrease in capacitance from the dielectric layer, while the on-off ratio remains relatively constant from strains ranging from 0 – 50%. In addition, the TFT was able to undergo repeated stretching of 20% strain over hundreds of cycles without significant loss in electrical property.

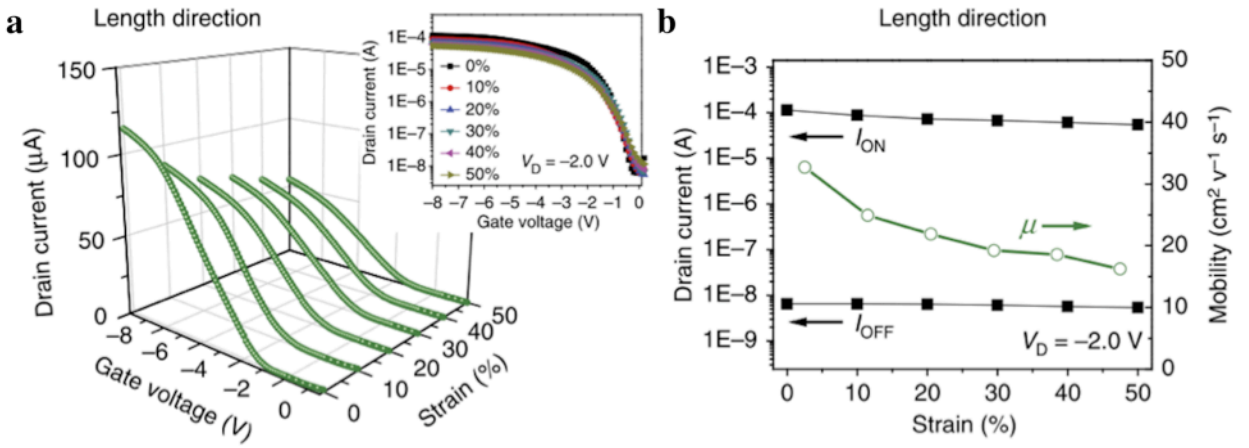


**Figure 1.12 | Device performance of the stretchable, transparent TFT under strain.** a) Transfer characteristics (VD =- 2.0 V) of the stretchable TFT under strain. b) ION, IOFF, and mobility as a function of applied strain along the channel length direction. [30]

As a proof of concept of the efficacy of the stretchable TFT, the device was connected to a white-light OLED with the structure architecture glass/ITO/PEDOT:PSS/white emissive polymer layer/CsF/Al.[30] The I-V characteristics of the OLED connected circuit is shown in **Figure 1.13a**, showing the device lighting up slowly as the voltage is increased. Good diode behavior with clear cutoff and triode region is observed in **Figure 13b**, indicating the ability of the TFT to control the OLED.

The OLED test circuit was further characterized when the TFT was stretched under 0 (**Figure 1.14a**), 20 (**Figure 1.14b**), and 30% strain (**Figure 1.14c**). At higher strains, the field-effect behavior characteristic of TFTs is still observed verifying the efficacy of the TFT to operate under strains to drive lighting devices. Though $I_{ON}$ decreases slightly with elevated strains, the current is still high enough to drive the lighting device. This decrease in current is at higher strains is manifested in a decrease in brightness (68% decrease when stretched up to 30%) However, this even with reduced luminance, the brightness is still sufficient for display applications. The luminance of the OLED under different inputs is shown in **Figure 1.14d**.

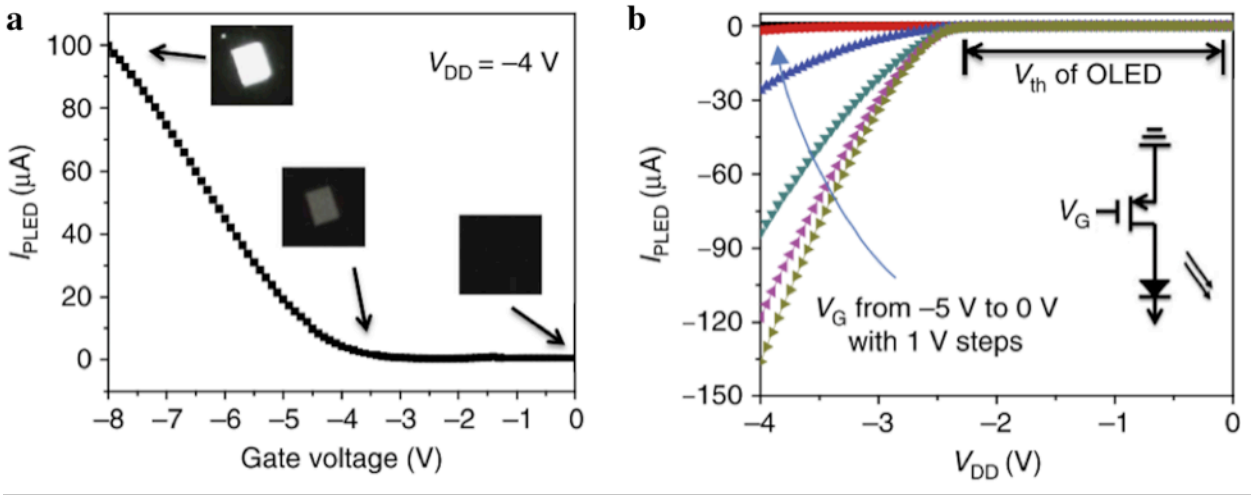


**Figure 1.13 | TFT used to drive a white OLED (unstretched).** a) $I_{OLED}$ as a function of $V_G$ with $V_{DD}$ = -4.0 V. The OLED at different brightnessnes are shown in the insets correlated to specific $V_G$ values. b) Output characterisitcs of the OLED control circuit as a function of gate voltage, with a schematic diagram of the OLED control circuit in the inset. [30]

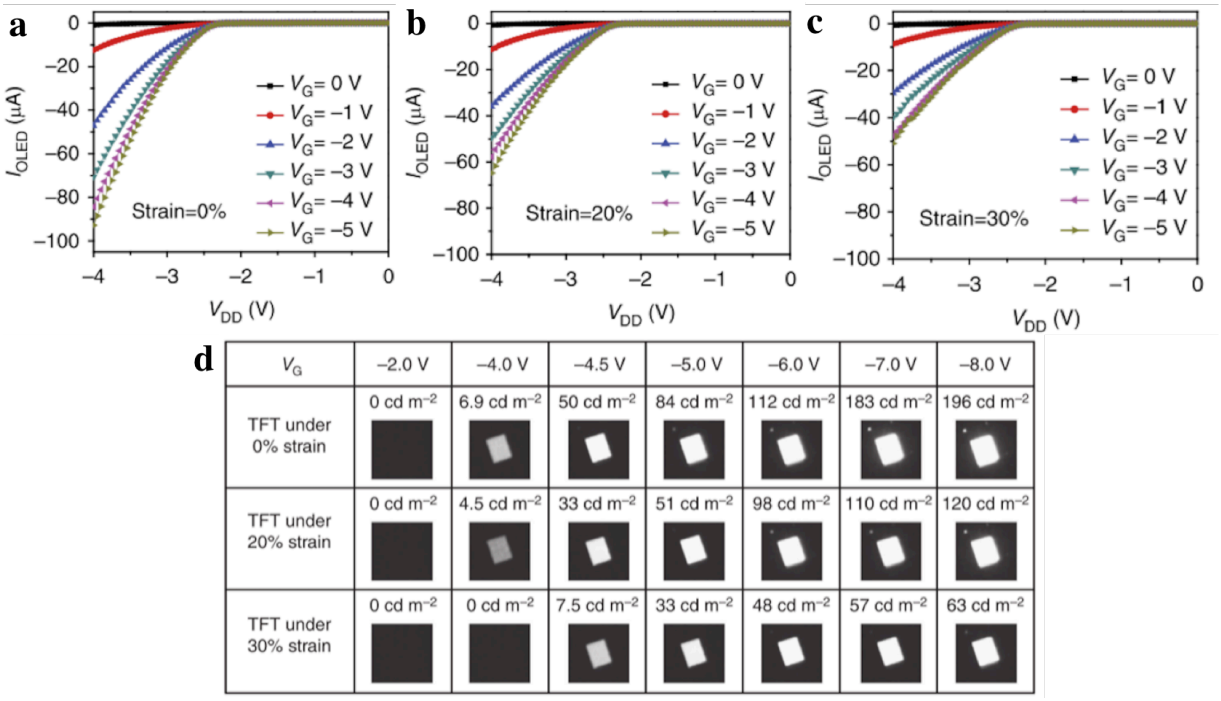


**Figure 1.14 | TFT used to drive a white OLED under different srains.** a) $I_{OLED}$ as a function of $V_G$ with $V_{DD}$ = -4.0 V. The OLED at different brightnessnes are shown in the insets correlated to specific $V_G$ values. b) Output characteristics of the OLED control circuit as a function of gate voltage, with a schematic diagram of the OLED control circuit in the inset. [30]

Although the TFT was not used to drive a stretchable PLED, the demonstrated proof of concept highlights the potential efficacy of this technology in stretchable display technology with the further improvement of materials, fabrication procedure, and processing. These integrated systems give hope to the future of widely available, efficient stretchable devices for a vast array of applications.

## 1.3. Motivation for this work

Silver nanowires have been shown to display outstanding properties such as high transparency, conductivity, and mechanical compliance. Due to their ability to form a percolation network, these conductive materials can be embedded within a polymer matrix to form conductive electrodes with low roughnesses ($R_a$ < 2 nm) for optoelectronic applications. The versatility of these electrodes allows for a wide range of devices to be fabricated on top, ranging from various lighting devices, TFT arrays, and capacitive sensors. Furthermore, the properties of the electrodes can be tailored individually for the application at hand.

Polymer light emitting electrochemical cells, polymer light emitting diodes, and transistors have been discussed at length in this chapter. Additional applications that have been demonstrated on the basis of the technology discussed include solar cells, touch sensors, and actuators. Further improvements on applications based on these alternative TCEs continue, rapidly driving demand for next generation devices. As for the basis of the TCE technology itself, the fabrication and processing of the electrodes in and of itself has reached a relatively mature stage. However, new process developments to further reduce financial consideration of this developing technology are still critical. These alternative TCEs already promise cheaper devices than respective devices built on traditional ITO technology. An analysis conducted by Emmott *et al*. found that AgNW electrodes have the potential to reduce device cost per Watt by 17%.[31] A rough estimation by this group found that for OLED substrates, AgNW substrate cost per meter are slightly lower to that of ITO, though the AgNW substrate based substrate is able to more than double the efficiency of the lighting device compared to ITO. However, these estimations do not take into account the potential for degradation and shorter lifetimes of devices built on these substrates.

Thus, the most critical TCE improvement involves improving the stability of AgNW electrodes. These factors such as lifetime stability, thermal stability, and processing stability in extreme manufacturing and usage conditions will serve to greatly expedite the future of wearable electronics. Continual improvements and development promise a myriad of stretchable and wearable electronics, bringing us one step closer to the futuristic vision of electronics envisioned for so many years. This following chapters detail some the work done in improving the thermal and electrical stability of AgNWs.

In addition to the stability of AgNWs, the scope of this dissertation also includes the incorporation of these AgNWs towards various lighting applications, a market which represents a 43 billion dollar global industry. As the necessity to curtail energy usage becomes increasingly evident, the development of environmentally friendly lighting sources has become a topic of significant research interest in recent years. In the quest for greener lighting, traditional technology such as fluorescence tube lighting and incandescent bulb lighting are continuously being phased out in favor of solid-state lighting. Currently, inorganic light emitting diodes (LEDs) take up the bulk of the replacement lighting market due to higher performance and stability, and cheaper costs. However, organic light emitting diodes (OLED) have garnered progressively higher levels of attention due to their aesthetics, energy efficiency, flexibility, and ability to be fabricated in large area panel displays without experiencing a significant drop in efficiency, unlike their inorganic counterparts.[32–36] Due to these advantages, niche industries such as hospitality and the architectural market have begun adopting this technology in recent years. As costs continue to be driven down, more industries have opened up, such as the landscape architecture, automotive applications, and commercial and industrial offices. However, for mass production, significant improvements still need to be made. In particular, OLEDs lag

behind LEDs in several key aspects. As the scope for this dissertation centers around the use of AgNW technology, an increasingly commonly used anode for OLED technology, key issues directly related to OLED substrates required to drive OLED commercialization are the cost barrier, efficiency, and lifetime. The following few chapters further expound on the stability of the AgNWs for lighting applications in a quest for a brighter, greener future.

# Chapter 2

# Thermally stable silver nanowire - polyimide transparent electrode based on atomic layer deposition of zinc oxide on silver nanowires

## 2.1. Introduction

Transparent conductive electrodes (TCEs) are critical components in optoelectronic devices, and can be found in devices ranging from touch sensors, display technology, to organic light emitting diodes (OLEDs).[37] The current industry standard for TCEs is indium tin oxide (ITO), which has been ubiquitous for most practical thin-film transparent electrode applications over the course of the past several decades.[1] However, ITO is expensive due to the scarcity of indium, there are potential health issues due to the exposure of indium based powders,[38] and ITO films are brittle and the underlying glass substrate thick, restricting their use for flexible optoelectronic devices.[39] These inherent drawbacks of ITO necessitate the development of alternative TCEs for next generation optoelectronic devices. In the selection for TCEs, the two critical requirements

most commonly discussed are high conductivity and transparency, seemingly contradictory as these two parameters vary inversely with film thickness.[40]

Leading candidates for TCEs that satisfy these requirements include carbon based materials such as carbon nanotube (CNT)[41,42] and graphene,[12,13] metal grids,[37,43] and networks of metallic nanowires.[5,21] Though promising candidates, carbon nanostructured based materials do not have the combined transparency and conductivity requirement necessitated for optoelectronic applications such as solar cells and OLEDs, and metal nanogrids require expensive batch based processing, making them impractical for large scale applications.[37] In comparison, metal-based nanowires such as silver nanowires (AgNW) networks have desirable electrical, mechanical, and optical properties, in addition to being solution processed, allowing for high speed, low cost, roll-to-roll processing.

Despite significant advantages over leading competitors, AgNW films still suffer from inherent drawbacks, most notably the rough surface topology and poor thermal stability of the AgNW composite electrode.[44] Several attempts at ameliorating these issues have been reported, though a solution simultaneously resolving both the aforementioned problems has not yet surfaced. Embedding the AgNW layer within the polymer has been shown to drastically reduce the surface roughness,[2,14,17,28,44,45] which can prevent short circuits that can lead to device failure. With this technique, a glass substrate is typically used to provide a smooth release for the AgNW infused with polymer, yielding surface roughnesses below 2 nm.[28] To improve thermal stability, polymers with a higher glass transition temperature ($\mathbf{T_g}$) such as polyimide, or reinforced hybrid polymers have been used.[2,17,44–46] As an example, one of our previous works used AgNWs inlaid

in the surface of a heat-resistant acrylate matrix to be used as a thin film heater, though the device was only tested at a maximum temperature of 230 °C for time scales under 5 minutes.[17] However, TCEs with thermally stable polymer matrices do not account for the thermal stability of the AgNW themselves, which exhibit an increase in sheet resistance at 180 °C when the nanowires are freestanding, and often at even lower temperatures when embedded in a polymer matrix.[47] This increase of resistivity is due to nanoscale size effects, causing NWs to melt at a significantly lower temperature than the melting temperature of bulk silver.[48] A sandwich layer of zinc oxide (ZnO) / AgNW / ZnO has been shown to increase the thermal stability of the silver nanowires,[46,49,50] but the continuous layer of ZnO over the AgNW film prohibit the infiltration of a polymer precursor to form a percolation network, leading to a high surface roughness which cause shorts and device failure. Chen et al. used stamp-transferred graphene on AgNW to allow graphene to dissipate heat in order to protect the AgNWs, but were only able to main stability at 200 °C for three hours, in addition to not fabricating freestanding films.[48] The use of neutral-pH poly(3,4-ethylenedioxythiophene): poly(styrenesulfonate) (PEDOT:PSS) was reported to improve thermal stability of the AgNW electrode, but could only withstand 20 minutes annealing at 210 °C due to the degradation of PEDOT:PSS at high temperatures.[51]

In this chapter, the use of a low temperature atomic layer deposition (ALD) process to coat a conformal, thin layer of ZnO around individual nanowires to enhance the thermal stability of AgNWs while maintaining a porous structure is reported. ALD on AgNW has been shown to improve the stability of AgNW,[52,53] albeit no reports on the long term thermal stability have been conducted, and freestanding films have not been fabricated. Thermally stable and colorless polyimide (PI) was chosen as the polymer matrix to embed the coated AgNWs. The resulting

composite electrode successfully resolves the issue of thermal stability for both the AgNWs and polymer matrix, while still embedding the AgNW within the polymer matrix for low surface roughness. The composite sheets show high long-term thermal stability up to 300 °C, mechanical flexibility, resistance to atmospheric corrosion, and outperform ITO/ polyethylene terephthalate (PET), a common transparent flexible electrode, in visual transparency, surface conductivity, and surface smoothness. The efficacy of the new ZnO-AgNW-PI TCE was demonstrated by solution-processing polymer LEDs (PLEDs), with the ZnO-AgNW-PI TCE having performance comparable to ITO, and vastly outperforming control non-coated AgNW based TCEs.

## 2.2. Experimental Section

### 2.2.1. Materials

Graphene oxide (GO) was prepared from graphite by the modified Hummers method.[54]AgNWs were purchased from Zhejiang Kechuang Advanced Materials Co., LTD. PI was obtained from Nexolve Materials. 2,2-Dimethoxy-2phenylacetophenone (photoinitator), anhydrous chlorobenzene, chlorobenzene, and bis(acetylacetonato) dioxomolybdenum(VI) were obtained from Sigma-Aldrich. PEDOT:PSS (Clevios VP AL4083) was purchased from H.C. Starck Inc. Zonyl FS-300 fluorosurfactant was purchased from Fluka Analytical. A white-light-emitting polymer (WP) was provided by Cambridge Display Technology, and 1,3-bis[(4-tert-butylphenyl)-1,3,4-oxidiazolyl)phenylene (OXD-7) was obtained from Lumtech.

### 2.2.2. Preparation of ZnO-AgNW networks and freestanding ZnO-AgNW-PI composite electrodes:

GO powder was dispersed in deionized (DI) water at a concentration of 2 mg/mL in an ultrasonic bath for 15 minutes. The resulting solution was further diluted with isopropyl alcohol (IPA) to 0.2 mg/5mL, and sonicated for 15 minutes before use. A glass slide was placed flat, and the solution of GO drop-casted into a thin line at the top of glass and drawn down with a Meyer rod. The resulting films were annealed on a hot plate at 150 °C for 30 minutes. Subsequently, AgNW solution was drawn down on the GO covered glass slide prior to annealing at 150 °C for 3 minutes, soaking in DI water for 10 minutes, and a second annealing at 165 °C for 8 minutes. GO-AgNW slides were introduced into a Fiji ALD chamber from Cambridge NanoTech. $Al_2O_3$ was deposited at 100 °C from TMA and $H_2O$ precursors, with pulse and purge times for the two

precursors both being 0.06 and 30 s. ZnO was deposited at 100 °C following $Al_2O_3$ deposition from $(C_2H_5)_2Zn$, diethyl zinc (DEZ) and $H_2O$, with pulse times for the two precursors being 0.06 / 45 seconds, and 0.06 / 60 s, respectively.

PI solution was made by dissolving 20% PI in chlorobenzene. The soluble PI was spun onto the ZnO-AgNW or bare AgNW coated glass before peeling off.

### 2.2.3. Fabrication of white PLED

In a typical procedure for ZnO-AgNW-PI electrode based devices described, freestanding electrodes were cleaned in an ultrasonic bath with detergent and DI water for 30 minutes, before being soaking and rinsing with ethanol. A solution of 0.3 wt.% $MoO_2(acac)_2$ in IPA was spin-coated on the substrate at 2000 rpm for 60 s, and then annealed at 250 °C or 300 °C for 1 hr. The films were next spun with a solution of 2000:1 vol.% (PEDOT:PSS):(Zonyl FS-300) at 1100 rpm for 30 seconds, followed by annealing at 130 °C for 30 min to dry off any residual solvent. The white polymer emissive layer was spun from a solution of 100:10 wt.% WP:OXD-7 in chlorobenzene. A 1 nm layer of cesium fluoride (CsF) and 100 nm of aluminum (Al) were evaporated onto the substrate through a shadow mask at $10^{-6}$ Torr.

### 2.2.4. Characterization methods

Scanning electron microscopy (SEM) was performed on a JOEL JSM-6701F scanning electron microscope. Transmittance spectra were obtained with a Shimadzu UV-1700 spectrophotometer. Surface topography was carried out on a Dimension Icon Scanning Probe Microscope (SPM) from Bruker. Electrical measurements for the white PLED were carried out in a nitrogen

atmosphere glovebox, with the current and light voltage curves being measured with a Keithley 2400 source meter and calibrated silicon photodetector by sweeping the applied voltage from 0 to 6 V at 500 mV increments per step. All characterization tests were carried out at room temperature.

## 2.3. Results and Discussion

### 2.3.1. Morphological characterization of pristine and ZnO-coated AgNWs on glass at elevated temperatures

Fabrication of the porous electrode network was achieved by drawing down liquid solution with a Mayer rod onto a release glass substrate. First, a solution of graphene oxide (GO) was drawn down to act as a sacrificial layer when transferring the AgNW to PI matrix. **Figure 2.1a** illustrates the Raman spectra before and after the transfer process to confirm the presence of GO with the same Raman intensity. The characteristic D and G bands of graphene oxide[55] are present before and after transferring both pristine AgNW and ZnO-AgNW, confirming its use as a sacrificial layer. Following GO coating, a AgNW network was coated to a sheet resistance ($R_{sh}$) of 10 ohm $sq^{-1}$ and 91% transparency. The solution-processed electrode on glass was subsequently brought into an ALD chamber for low temperature thermal deposition. Because ALD deposition relies exclusively on surface reactions, with hydroxylated surfaces typically being the most reactive with ALD precursors, a thin layer of aluminum oxide ($Al_2O_3$) was deposited as an adhesive layer prior to ZnO deposition. $Al_2O_3$ was selected as the adhesive layer as its precursor, trimethyl aluminum (TMA), has been shown to react well with Ag and provides a hydroxylated surface for subsequent deposition processes.[53,56] ZnO was deposited immediately following $Al_2O_3$. Both materials were deposited using a low temperature thermal deposition process to prevent oxidation and melting of the AgNWs.

ZnO coated and pristine AgNW electrodes were heated at 150, 200, and 250 °C for 30 minutes to verify the stability of the electrodes at high temperatures. It has been reported that at

temperatures above 180 °C, a sharp increase in $R_{sh}$ is observed due to the coalescence of the nanowires into discrete particles and the formation of a thin oxide layer that decrease electrical performance.[44,47] While both pristine (**Figure 2.1b**) and ZnO coated AgNWs were found to remain intact in a percolating network at 150 °C, the beginning of coalescence into isolated particles was observed at 200 °C (**Figure 2.1c**), and complete conversion of nanowires into discrete Ag nanoparticles at 250 °C for pristine AgNWs, as seen in **Figure 2.1d**.

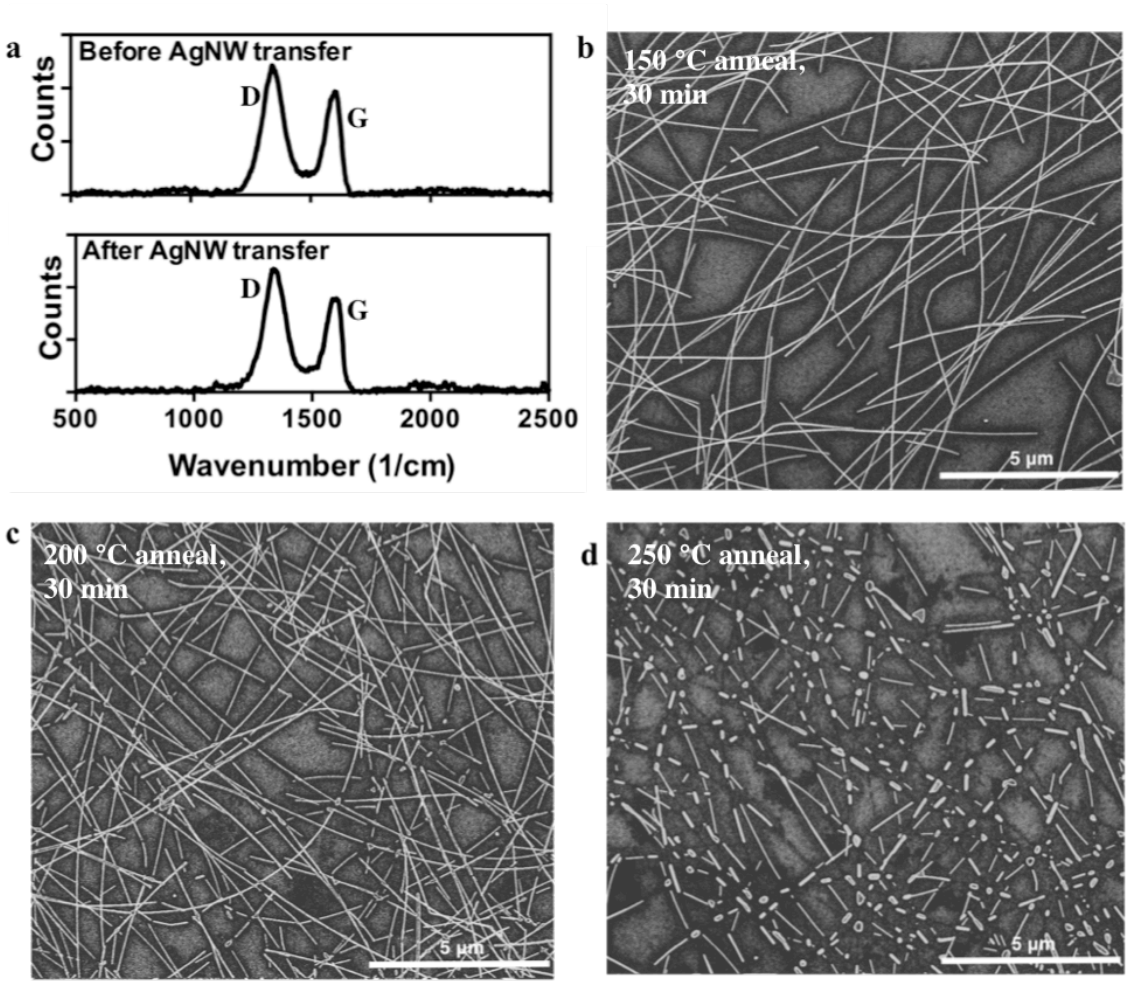


**Figure 2.1.** a) Raman spectra of the GO-coated glass release substrate before (top) and after (bottom) PI transfer of ZnO-AgNW film. b) AgNW bar coated on a glass slide after a 150 °C anneal for 30 min. c) AgNW coated on a glass substrate after a 200 °C anneal for 30 min. d) AgNW coated on a glass substrate after a 250 °C anneal for 30 min.

The coating of AgNW with ZnO was expected to greatly enhance the thermal stability of the electrodes. The melting temperature of bulk ZnO greatly exceeds that of silver, with the $T_m$ for the metal oxide approaching 2000 °C.[57] When accounting for melting point depression brought about by the size effects, the melting point of ZnO nanostructures with radii under 10 nm still exceed 1000 °C,[57] well over the processing temperatures required for OLED processing. Furthermore, to hinder the fragmentation of the nanowires from surface diffusion, the conformal metal oxide coating serves to limit the source of vacancies to allow for substitutional diffusion, in addition to having strong ionic bonds, which require a higher energy to overcome to break the bonds. To verify the enhanced thermal stability of the electrodes endowed by the ZnO coating, AgNW samples were coated with 1.0, 1.5, 3, 4.5, 6, and 7.5 nm of ZnO, and subsequently annealed at temperatures between 200 and 300 °C. The resulting electrodes were analyzed with SEM imaging to determine the minimum thickness of ZnO at which the additional thermal stability afforded to the AgNW remained intact. Silver was sputtered onto glass slides to be used as a reference before being brought into the ALD chamber to concurrently deposit ZnO on the reference and AgNW films, and the thicknesses of the ZnO layers were subsequently measured using a FilmTek 2000 ellipsometer. Transmission electron microscopy (TEM) images of AgNWs with and without ZnO are shown in **Figure 2.2a** to illustrate the ZnO wrapping completely around the AgNW. A sample with 7.5 nm ZnO thickness measured with ellipsometry was imaged, matching well with the 7.8 nm measured from TEM. Though the bare AgNW shown is thicker than the ZnO coated AgNW, with different thicknesses of nanowires evident in SEM imaging as well (**Figure 2.2b**), the ability to coat the desired ALD thickness on different dimension nanowires highlights the efficacy of this approach.

Standridge *et al.* conducted a study of ALD deposited $TiO_2$ on AgNW and found that below a certain thickness threshold, the resulting incomplete coverage of $TiO_2$ lead to significantly enhanced etching rates when placed in corrosive $I^-/I_3^-$ solutions.[53] Similarly, it is hypothesized that below a certain thickness threshold for ZnO, incomplete coverage would enable the underlying Ag to fragment into discrete Ag droplets. While no samples showed adverse effects of annealing at 200 °C, the beginning of junction deterioration was observed for samples with a ZnO thickness below 3 nm when annealed at 250 °C. The fragmentation at the junction is believed to be caused in part by incomplete coverage of the protective ZnO coating at very low thicknesses. Because the AgNW film is comprised of layers of AgNWs stacked on top of each other, the bottom layers may not be exposed to precursor flow for long enough periods to render complete coverage, similar to high aspect nanostructures experiencing thinning regions in deeper portion of the nanostructure.[58,59] According to the Gibbs-Thomson theory, $\Delta G = \gamma \Omega r^{-1}$, where $\Delta G$ is the change in Gibbs Thomson potential, $\gamma$ is the surface energy, Ω is the volume per atom, and r is the radius, the Gibbs-Thomson potential is inversely related to the radius of the nanowire. At the junction between nanowires, a negative curvature is present, leading to a negative value of the Gibbs-Thomson potential, as illustrated in **Figure 2.2c**. However, the radius of individual nanowires is positive, leading to a positive Gibbs-Thomson potential, and thus, a large potential difference between the junction and regions immediately adjacent to the junction. This large potential gradient is a driving force for diffusion, causing the migration of atoms into the junction, which, over time, leads to the fragmentation of nanowires close to the junction. This phenomenon is clearly observed through the enlarged area around certain junctions, in addition to the discontinuity of select nanowires immediately adjacent to junctions as shown **in Figure 2.2d**.

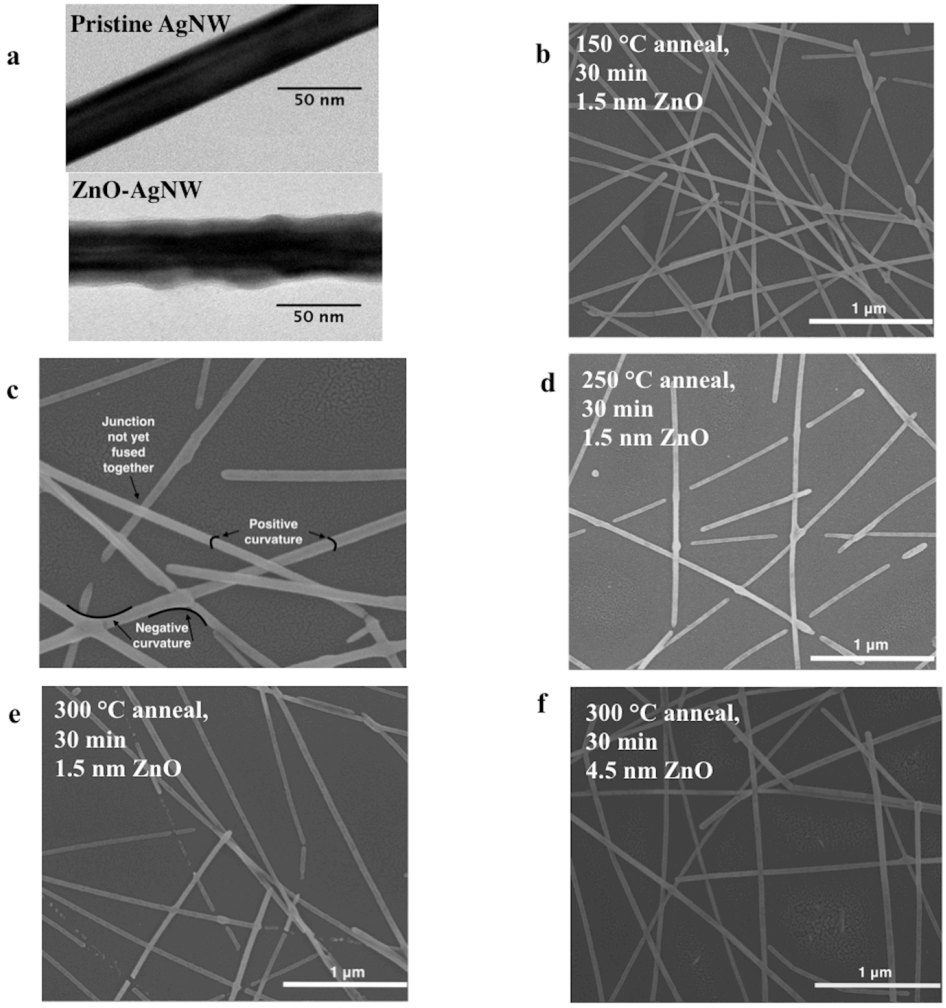


**Figure 2.2.** a) TEM image of pristine (top), and ZnO coated AgNW (bottom). b) SEM image of ZnO-coated AgNW on glass substrate without annealing. c) SEM image illustrating positive and negative curvatures. d) SEM image of 1.5 nm of ZnO-AgNW after a 250 °C anneal for 30 min. e) SEM image of 1.5 nm ZnO-AgNW after a 300 °C anneal for 30 min. f) SEM image of 4.5 nm ZnO-AgNW after a 300 °C anneal for 30 min.

At samples heated to 300 °C, partial coalescence of nanowires into droplets for samples with a ZnO thickness below 1.5 nm is observed. This phenomenon is attributed again to surface diffusion as evidenced by the conservation of volume. At even higher temperatures, the nanowires could experience melting, which would be evidenced by the formation of spherical nanoparticles with specific spacing between the nanodrops as the melted metal cools in a way to

minimize the total surface energy. In **Figure 2.2e**, the formation of Ag nanoparticles is evident in nanowires with shorter radii, as the diffusion of atoms is proportional to the gradient of the curvature of the wire surface as highlighted by the definition of Gibbs-Thomson potential. In comparison, **Figure 2.2f** shows a 4.5 nm ZnO coated AgNW film annealed at 300 °C for 30 minutes with no significant fragmentation or coalescence of the nanowires.

### 2.3.2. Optical and electrical characterization of pristine and ZnO-coated AgNW on glass at elevated temperatures

In the selection of the optimal thickness of ZnO, the effect of the ZnO thicknesses on transparency and conductivity of the AgNW based electrode was analyzed. **Figure 2.3** illustrates the transparency of AgNW electrodes before and after deposition of 1.5 (**Figure 2.3a**), 3.0 (**Figure 2.3b**), 4.5 ((**Figure 2.3c**), and 7.5 nm ZnO (**Figure 2.3d**). The transparency before and after ZnO deposition was virtually unchanged for all four samples with different thicknesses of ZnO. In addition, the sheet resistance of all samples remained essentially unchanged, with only variations below 1% observed when measuring sheet resistance before and after ZnO deposition. Thus, the selection of ZnO thickness was relegated to the lowest thickness of ZnO in which highly effective thermal protection was still present, as the minimization of the process times requiring high vacuum application is desirable. It is important to note that even though the bulk of the nanowire networks remained intact after high temperature annealing even with low thicknesses of ZnO, remaining experiments were conducted using AgNW electrodes coated with 4.5 nm of ZnO to ensure optimal performance.

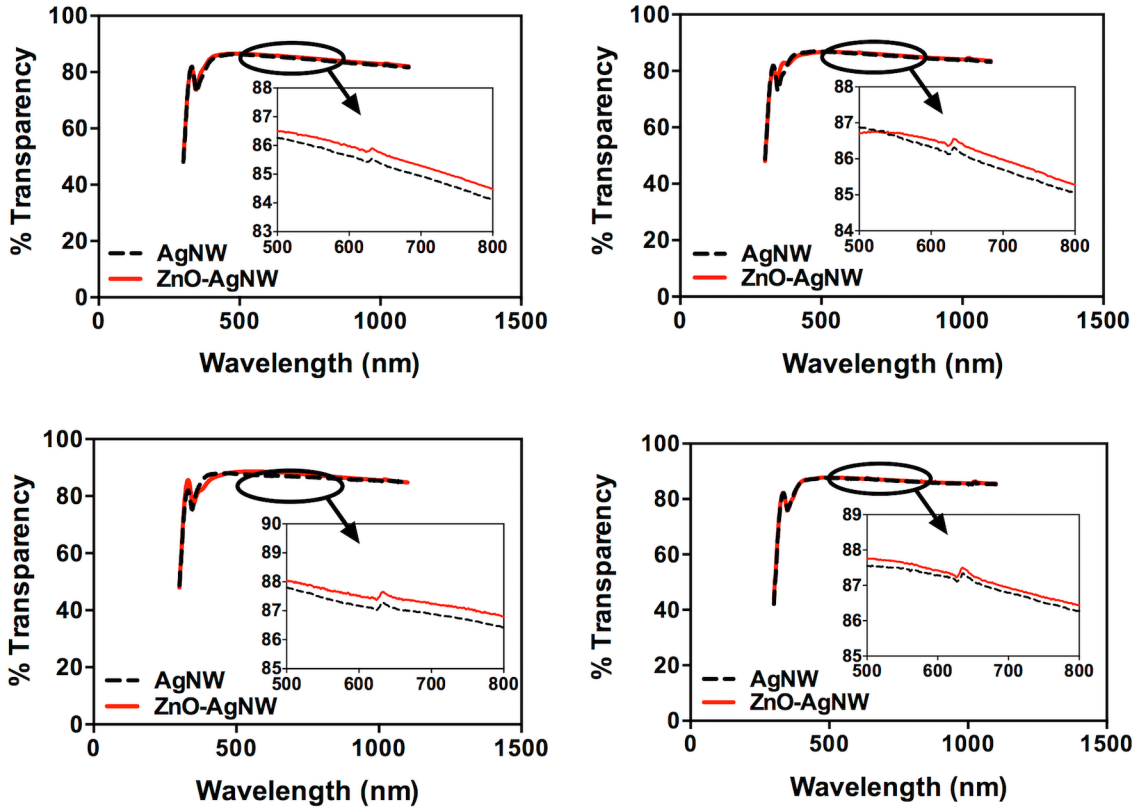


**Figure 2.3.** a) Transparency of the same AgNW electrode on glass before and after 1.5 nm ZnO coating. b) Transparency of the same AgNW electrode on glass before and after 3.0 nm ZnO coating. c) Transparency of the same AgNW electrode on glass before and after 4.5 nm ZnO coating. d) Transparency of the same AgNW electrode on glass before and after 7.5 nm ZnO coating.

To quantitatively analyze the efficacy of the ALD coated AgNW film for high temperature processing, the sheet resistance and transmittance were evaluated and compared with pristine AgNWs before and after annealing. An electrical thermal stability test was performed by measuring the sheet resistance as a function of the annealing temperature to highlight the superior electrical performance of the ZnO-AgNW electrode. A ZnO-AgNW film coated on glass was annealed on an Instec mK1000 high precision temperature controller with a ramp rate of 5 °C $min^{-1}$. The hot stage was sealed with a cover on top under ambient conditions to prevent

heat loss from the surface sample due to convection. Two electrical leads were formed on the samples with silver paste, with connections leading outside of the testing stage to measure the sheet resistance *in situ* every twelve seconds. In the case of the pure AgNW film, an increase in sheet resistance deviating from the slight increase of resistance associated with increasing temperature in metals was observed, with a dramatic increase in $R_{sh}$ beginning at 250 °C (**Figure 2.4a**). At temperatures above 300 °C, the sheet resistance exceeded the maximum measuring limit of the voltmeter. The ZnO enhanced electrode showed only the expected slight continuous increase in resistance as a function of temperature, with no rapid increase in resistance up to 500 °C, at which the test was stopped due to the limitations of the instrument.

Though the poor electrical performance after high temperature annealing is largely attributed to the fragmentation of nanowires due to the high driving force for atomic diffusion into the junctions, atmospheric corrosion, primarily sulfidation and oxidation, which can occur at low temperatures, with increasingly deleterious effects with higher anneal temperatures, can also have detrimental effects for optoelectronic devices requiring high temperature processing.[62] The corroded AgNW films, in addition to increasing in sheet resistance, show significant transparency loss when compared to unannealed samples. In contrast, the ZnO-AgNW film exhibited excellent optical performance in the visible spectrum after annealing at 300 °C for 30 minutes, as seen in the inset of Figure 2.4b. Whereas the black background is clearly visible in the transparent ZnO coated electrode, the pristine AgNW sample subjected to the same annealing conditions is virtually fully opaque due to the atmospheric corrosion of silver by sulifdation and oxidation. Numerically, a 15 percent loss in transparency at 550 nm due to oxidation is observed in the non-coated AgNW when compared to non-coated, unannealed samples, as shown in

Figure 3b. However, the ZnO coated nanowire showed no decrease in transparency after annealing in contrast to pristine, unannealed AgNWs, showing its efficacy in protecting the underlying AgNWs not only from melting, but oxidation as well. The optoelectronic performance can be compared between the AgNW and control sample through comparison of the percolative figure of merit and percolation exponent, two parameters often used in describing optoelectronic performance of metals nanowires.[63] These two parameters can be solved with the following equation:[45,63]

$$T = \left[1 + \frac{1}{\Pi}\left(\frac{Z_0}{R_{sh}}\right)^{1/n+1}\right]^{-2} \quad \text{(Eq. 2.1)}$$

where Π and n are the percolative figure of merit (PFOM) and percolation exponent (PE), respectively, T is the optical transmittance, and $Z_0$ is the impedance of free space (377 Ω). This equation comes about by combining the Beer-Lambert law of transparency in conjunction with the definition of sheet resistance to obtain a relationship linking conductivity and transparency. Upon solution of the equation, it is found that high values of Π and low values of n are conducive to higher performing optoelectronic performance for metal nanowire based TCEs. Six pairs of $R_{sh}$ and T at each annealing temperature were used, and curve fitted to obtain the respective PFOM and PE. As can be seen in **Figure 2.4c**, the desirable trends for these two parameters, a high value of Π and a low value of n, are observed for ZnO-coated AgNW electrodes for different annealing temperatures, whereas a deterioration of the parameters is observed with higher annealing temperatures in the case of the pristine AgNWs. This optoelectronic performance signifies that pristine AgNW electrodes are not suitable for applications requiring processing temperatures in excess of 200 °C.

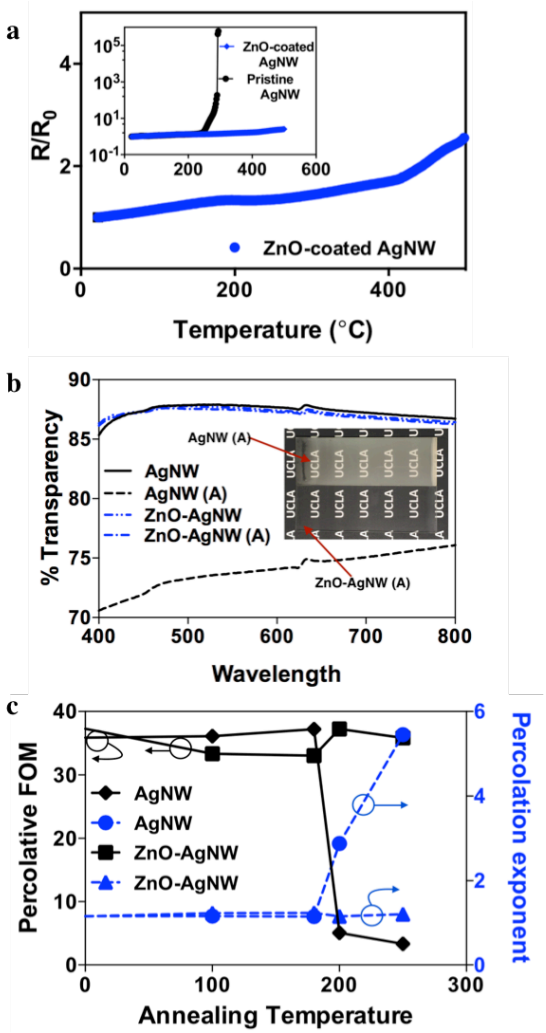


**Figure 2.4.** a) Normalized sheet resistance of ZnO-coated AgNW, with the normalized sheet resistance for ZnO-AgNW and pristine AgNW plotted on a logarithmic scale in the inset. b) UV-vis spectrum of annealed and non-annealed ZnO-coated AgNW films and pristine AgNW films (A) denotes annealed samples. c) Percolative figure of merit and percolation exponent as a function of annealing temperature for both ZnO-coated AgNW films and pristine AgNW films.

## 2.3.3. Fabrication, and optical and electrical characterization of freestanding thermally stable electrodes

To create freestanding electrodes for optoelectronic devices, the coated nanowire network were embedded and transferred from the glass substrate with a similar method reported in one of our previous publications, shown in **Figure 2.5a**.[28] Briefly, a PI solution was spun onto the ZnO-AgNW electrode, and then heated at 130 °C in a vacuum oven to remove excess solvent. A freestanding ZnO-AgNW-PI film of approximately 50 μm thickness was separated from the glass after solvent removal (**Figure 2.5b)**. The embedding of the ZnO coated AgNW into the surface of the PI allows for a sub-2 nm $R_a$ topography, as shown in **Figure 2.5c**, critical for the performance of certain optoelectronic devices such as OLEDs. Additional SEM images depicting the embedding of the AgNW within the polymer matrix are shown in **Figure 2.6**. Following separation of the ZnO-AgNW-PI electrode from glass, a bending test was conducted, flexing the electrode repeatedly to a 3.0 mm radius, as seen in **Figure 2.7.** During 5,000 cycles of bending and unbending the resistance of the ZnO-AgNW-PI electrode remained stable, increasing in sheet resistance by less than 2%.

It is important to note that the very top of the freestanding electrode consist of a portion of AgNWs not coated with ZnO. This region of AgNWs is the portion of nanowires intimately in contact with the release glass substrate, preventing the infiltration of ALD precursors to coat the protective ZnO coating. However, this uncoated region comprises merely a small area of the AgNW surface. **Figure 2.8** illustrates a SEM image of coated AgNWs on glass, highlighting the individual nanowires on the very bottom of the percolation network in contact with the glass.

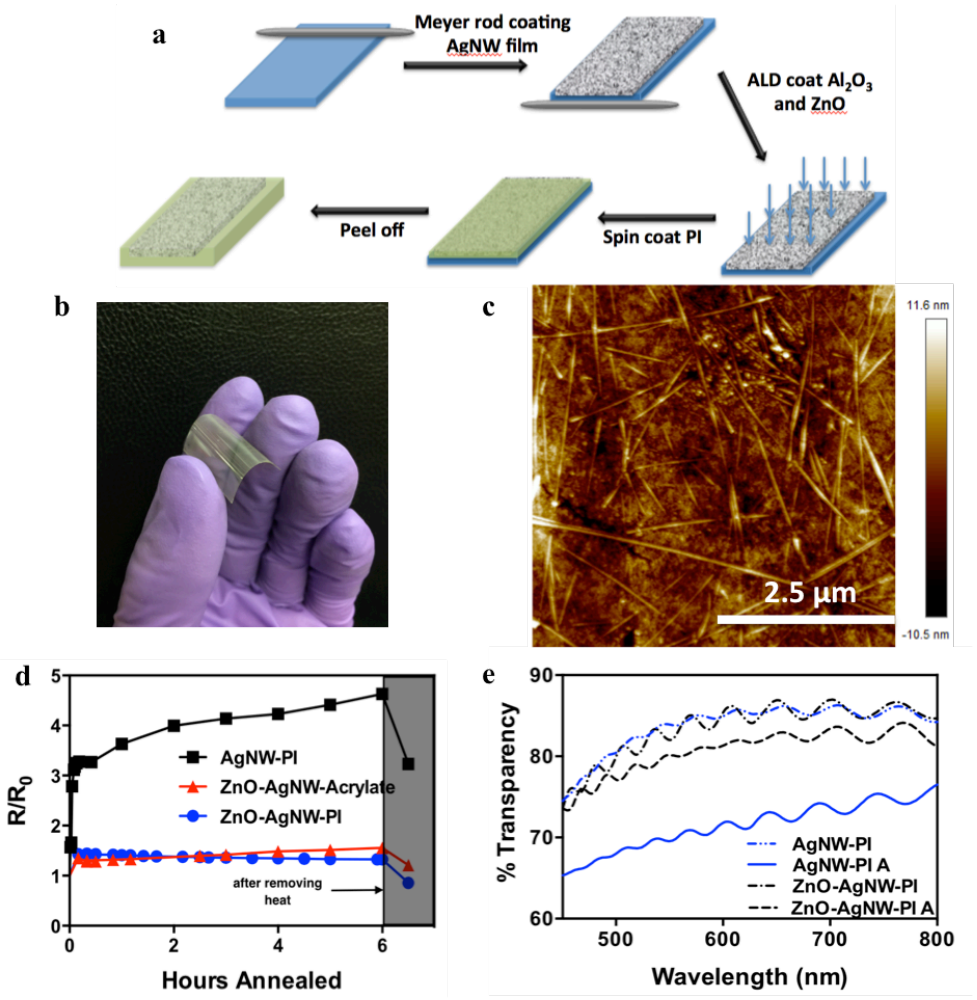


**Figure 2.5.** a) Fabrication process for a freestanding ZnO-AgNW-PI film. b) Optical image of a ZnO-AgNW-PI composite electrode. c) AFM image of embedded ZnO-AgNW-PI substrate. d) Normalized sheet resistance of the ZnO-AgNW-PI heated at 300 °C, and two reference electrodes annealed at 250 °C as a function of hours annealed. e) UV-vis spectra of ZnO-AgNW-PI film annealed at 300 °C for 1 hour and AgNW-PI film at 250 °C for one hour.

Because the percolation network consists of layers of AgNWs deposited on top of each other, only this very bottom layer consists of full nanowires intimately in contact with the glass, a fraction of the total nanowire network. Furthermore, of these bottom layer nanowires, less than fifty percent of the surface area actually will contact the release glass surface. Tilted SEM imaging of AgNWs show a relatively small area of nanowires actually pressed against the

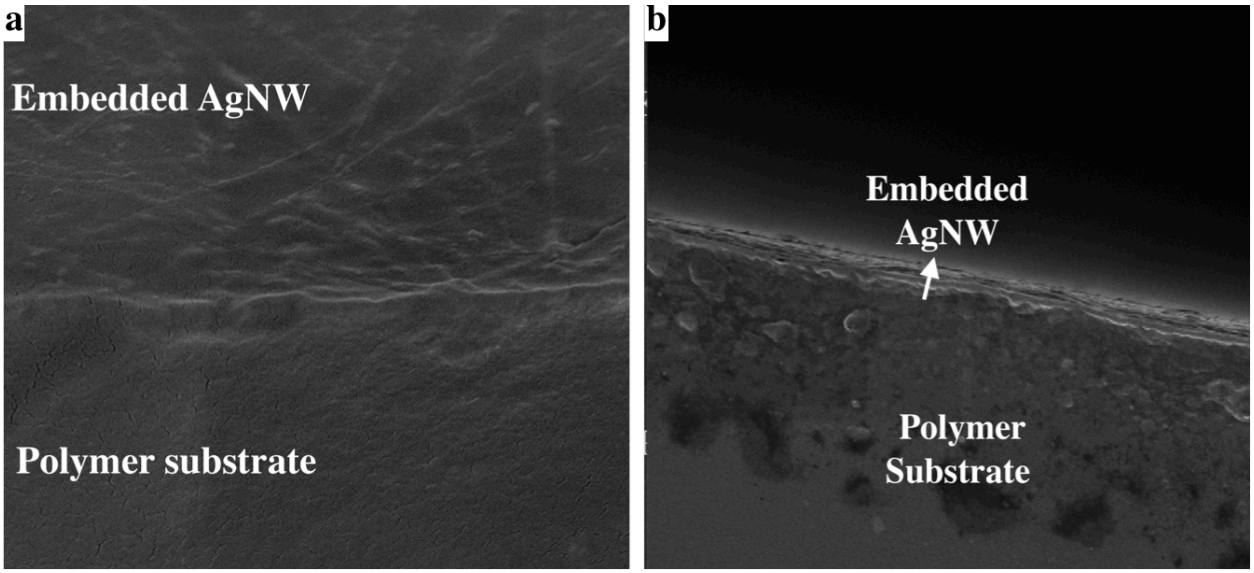


**Figure 2.6.** a) Tilted SEM image of embedded ZnO-AgNW within a polymer matrix (500 nm scale). b) Cross-sectional SEM image of freestanding ZnO-AgNW-PI film, with the ZnO coated AgNW seen embedded in the top layer of the polymer (2 μm scale).

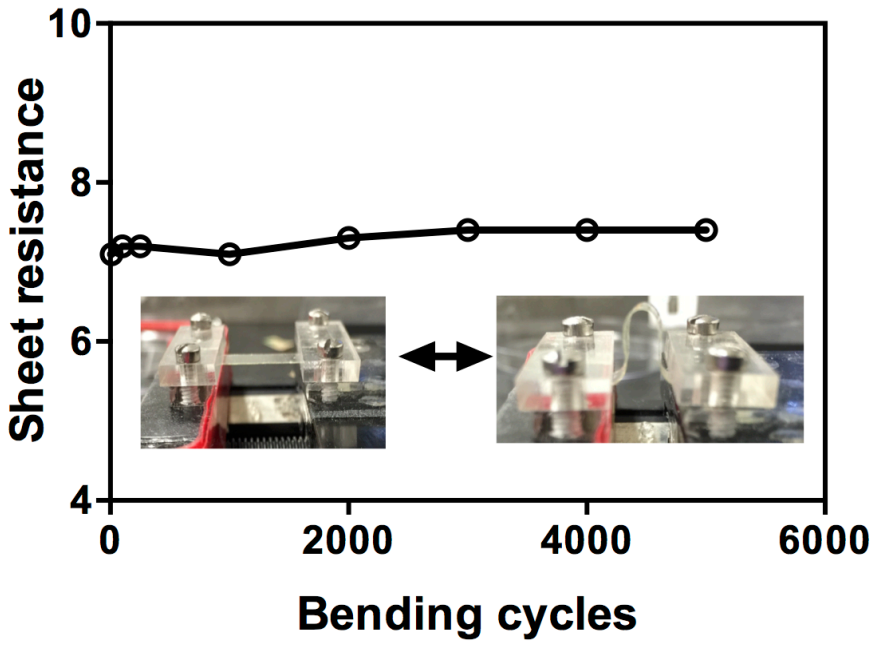


**Figure 2.7.** Sheet resistance as a function of bending cycles of the ZnO-AgNW-PI freestanding electrode. Home-made testing setup for bending the electrode to a 3.0 mm radius is shown in the inset.

glass.[60] Because the mechanism of electrical decay with thermal annealing primarily consists of the fragmentation of the AgNWs into discrete nanoparticles, the partial, but majority coating of the bottom layer of nanowires is still sufficient to protect these nanowires. As the majority of the nanowires are fully coated, and the few that are not have coatings exceeding half of the surface area, the transferred AgNW network still exhibit high thermal stability.

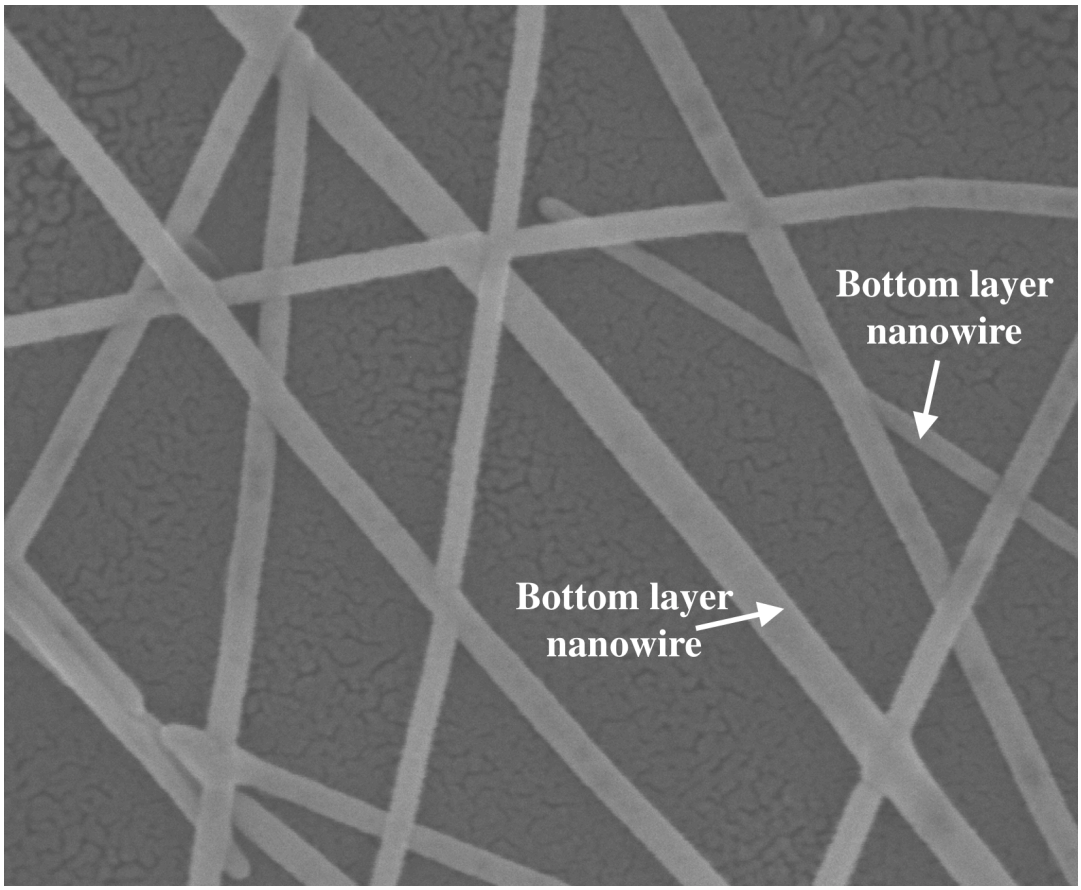


**Figure 2.8.** AgNW network on glass depicting individual nanowires on the very bottom of the percolation network.

To evaluate this thermal stability with regards to electrical and optical performance of the freestanding composite hybrid electrode, the sheet resistance of the as-prepared films was analyzed *in situ* with the mK 1000 high precision temperature controller, and UV-vis spectra were obtained before and after annealing. The efficacy of both thermally stable components, PI

and ZnO, were evaluated by comparing the ZnO-AgNW-PI films with three control electrodes: a pristine AgNW-PI film, a ZnO-AgNW-acrylate film, and a AgNW-acrylate film. The acrylate utilized in the reference electrode was previously used for flexible PLED devices with enhanced light extraction in our previous publication.[28] ZnO-coated AgNW films were heated at 300 °C, for 6 hours, while the reference films with pristine AgNW were heated to 250 °C also for 6 hours, due to the inability of bare AgNWs to withstand higher temperatures. Regarding electrical stability, the AgNW-acrylate films failed in the first few minutes, with the resistance increasing over 10 MΩ, the limit of the voltmeter used to measure the resistance. **Figure 2.5d** shows the change in sheet resistance as a function of time for the two other reference electrodes, and the ZnO-AgNW-PI electrode. The AgNW-PI showed a linear increase in sheet resistance, with the final resistance after cooling back down to room temperature more than three times the original sheet resistance. The AgNW-PI electrode was also tested at 300 °C, where similar to the AgNW-acrylate films, the electrode failed to register a resistance within a few minutes. In contrast, the ZnO coated films showed significantly better electrical performance, with the ZnO-acrylate electrode increasing in sheet resistance by only 21%, and the ZnO-AgNW-PI decreasing in sheet resistance by 15%. This decrease in sheet resistance is attributed to the fusing of nanowires at the junction, as the high annealing temperature allows the non-coated regions at the point of intersection of the nanowires to melt and fuse together, while the outer ZnO shell prevents the complete melting of the nanowires. The fusing of nanowires at the junction lowers the junction resistance of the nanowires, which in turn, lowers the overall sheet resistance of the electrode.

In addition to the electrical stability, the ZnO-AgNW-PI electrode was also able to withstand the 6 hour anneal at 300 °C without significant optical deterioration of the films, as seen in the UV- vis spectra in **Figure 2.5e**. Figure 4e illustrates a control AgNW-PI electrode before and after heating at 250 °C, along with the ZnO-AgNW-PI electrode before and after heating at 300 °C to demonstrate the efficacy of ZnO in preventing oxidation of the nanowires within the PI polymer matrix. The wave-like characteristics of the spectrum are characteristic of the PI polymer.[64] For the pristine AgNW embedded within the PI matrix, a 14.4% decrease in transparency is observed before and after heating at 250 °C, in contrast to a 1.9% loss in transparency in the ZnO-AgNW-PI freestanding electrode after heating at 300 °C. An AgNW-acrylate, and ZnO-AgNW-acrylate electrode were also analyzed before and after heating at 250 °C to highlight the thermal resistance of the PI substrate. The acrylate substrate exhibited significant yellowing of the film, quantified by a 31% transparency loss for the ZnO-AgNW-acrylate electrode, and a 43% loss for the pristine AgNW-acrylate electrode. This yellowing in the acrylate is a deterioration often observed in plastic films due to radical-activated oxidative degeneration of the hydrocarbon backbone in the polymer material.[65]

### 2.3.4. Proof of concept of efficacy of the thermally stable substrate in fabrication of PLEDs required high temperature processing

To demonstrate the viability of the ZnO-AgNW-PI film as a flexible TCE, solution-processed white PLEDs were fabricated in a typical bottom-emissive structure. Solution processed bis(acetylacetonato) dioxomolybdenum(VI) [$MoO_2(acac)_2$] was used as the precursor for the hole injection layer, and was seen empirically from thermogravimetric analysis (TGA) and x-ray photoelectron spectroscopy (XPS) to require a minimum temperatures of 250 °C to begin the

conversion to $MoO_x$. This solution processed $MoO_x$ (s-$MoO_x$) has been reported as an effective hole-injection material to enhance hole injection in OLEDs and hole collection in organic photovoltaic cells.[66,67] A White Polymer (WP) from Cambridge Display Technology blended with 1,3-bis[(4-*tert*-butylphenyl)-1,3,4-oxidiazolyl)phenylene (OXD-7) was used for the emissive layer, with cesium fluoride and aluminum evaporated for the electron injection layer and cathode, respectively. Further detailed procedures of materials for the s-$MoO_x$ and the PLED fabrication processes are described in the Method section. The white PLEDs were fabricated on five different substrates: a ZnO-AgNW-PI hybrid electrode; a ZnO-AgNW-acrylate electrode, a pristine AgNW-PI electrode, the pristine AgNW-acrylate electrode used in our previous paper;[28] and sputtered ITO on a glass substrate. All polymer based electrodes were analyzed after heating the $MoO_2(acac)_2$ precursor both at 250 and 300 °C. Characteristic current density (J-V) and luminance-voltage curves are shown in **Figure 2.9a** and **Figure 2.9b**, respectively. Data for PLEDs based on the pristine AgNW-acrylate electrode at both temperatures, in addition to the pristine AgNW-PI electrode at 300 °C are not shown as no light could be observed from these devices due to the immeasurably high resistance of the electrodes as discussed above. For the ZnO-AgNW-PI electrode, enhanced luminance at the higher annealing temperature was observed due to the formation of $Mo^{4+}$ and $Mo^{5+}$ species at higher temperatures. These reduced species lead to the formation of gap states in $MoO_x$, lowering the potential barrier height in contrast to what is expected from the phenomenological model, and in turn, enhancing PLED performance at devices annealed at higher temperatures and longer annealing times. The PLED based on the AgNW-PI electrode annealed at 250 °C was capable of light emission, though an increased resistance and decreased transparency resulted in a 63.7% lower luminance at 6 V as compared to the ZnO-AgNW-PI annealed at 300 °C. ZnO-AgNW-acrylate based diodes were capable of

light emission at both annealing temperatures, though significant transparency loss for both samples annealed at 250 and 300 °C resulted in a 64.0% and 87.0% luminance loss at 6 V, respectively in contrast with the ZnO-AgNW-PI based diode. Furthermore, with higher annealing temperatures, the presence of localized shorts in the devices was observed, as seen in the inset of Figure 5a. These shorts in the device may also contribute to the lower luminance, as illustrated in Figure 5b. The ZnO-AgNW-PI electrode annealed at 300 °C exhibited similar luminance to ITO using the same device structure and processing conditions. The maximum external quantum efficiency (EQE) and current efficiency (CE) for ITO based devices was 7.7% and 14.7 cd/A, while corresponding efficiencies for the ZnO-AgNW-PI PLED was 6.9% and 13.2 cd/A. All other EQEs and CEs for PLEDs based on reference electrodes were under 5% and 10 cd/A, respectively. The comparable performance of the ZnO-AgNW-PI PLED and ITO/glass PLED with the same processing condition verifies the new composite substrate's efficacy for use in optoelectronic devices requiring high processing temperatures. It is expected that significantly improved performance can further be obtained with the dispersion of nanoparticles within the polymer matrix to enhance light extraction.[28] We anticipate that the ZnO-AgNW-PI composite electrode can be used for emerging flexible optoelectronic devices requiring high temperature fabrication processing in a transition away from conventional TCE materials.

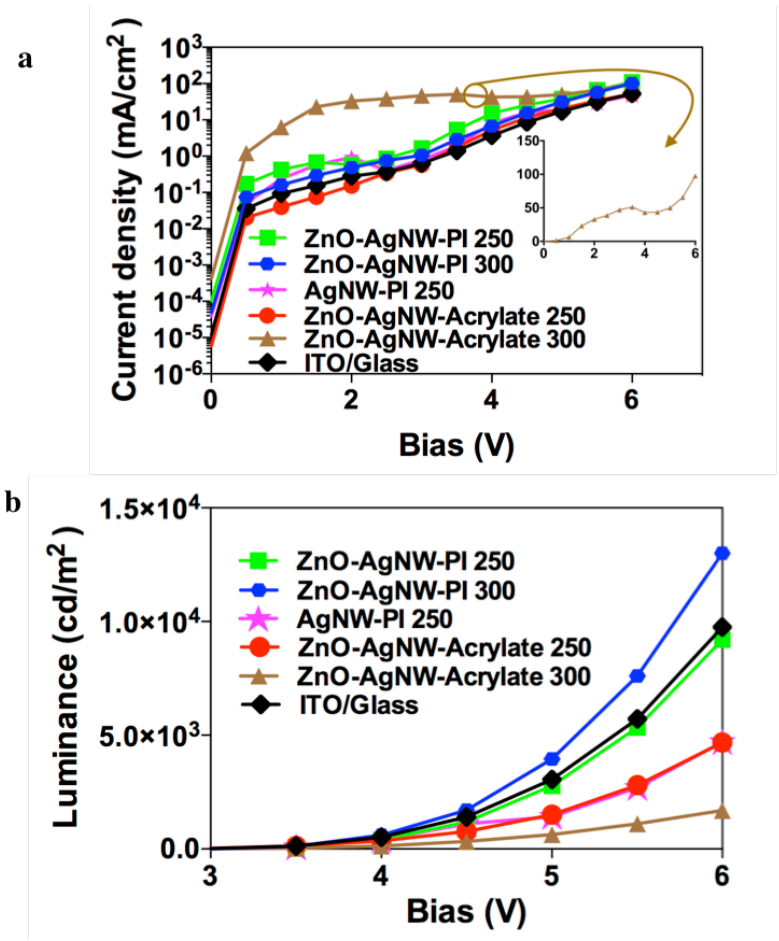


**Figure 2.9.** a) Current density as a function of voltage for various substrates annealed at 250 and 300 °C. ITO is annealed at 300 °C. PLED based on ZnO-AgNW-Acrylate heated at 300 °C is shown in the inset on a linear scale. b) Luminance as a function of voltage for the PLED devices with various substrates annealed at 250 and 300 °C. ITO is annealed at 300 °C.

## 2.4. Conclusion

A TCE has been fabricated for high performance optoelectronic devices requiring high processing temperatures. The TCE is comprised of AgNW coated with a thin, conformal layer of ZnO deposited with ALD, embedded within a PI matrix. Enhanced thermal stability based on electrical and optical performance of the ZnO coated AgNW film was observed. The freestanding ZnO-AgNW-PI film also showed excellent thermal stability in regards to both electrical and optical performance. Because the high temperature stable AgNWs are embedded within the PI, the resulting TCE has a smooth surface topography, allowing its use for optoelectronic devices requiring smooth interfaces. As proof of viability, a white PLED was fabricated on the ZnO-AgNW-PI film comprising a layer of $MoO_x$ processed from solution followed by annealing at 250 or 300 °C. The PLED exhibited comparable performance to controls on ITO/glass, and vastly outperforming control devices with one or no thermally stable component (ZnO and PI). The ZnO-AgNW-PI electrode shows great promise for replacing ITO as it ameliorates two significant limitation of flexible, plastic TCEs hindering their widespread adoption – low thermal stability and high surface roughness.

# Chapter 3

# Mitigation of electrical failure of silver nanowires under current flow and the application for long lifetime organic light emitting diodes

## 3.1. Introduction

As the necessity to curtail energy usage becomes increasingly evident, the development of environmentally friendly lighting sources has become a topic of intense research interest. In the quest for greener lighting, traditional technology such as fluorescence tube lighting and incandescent bulb lighting are continuously being phased out in favor of solid-state lighting. In recent years, organic light emitting diodes (OLED) have garnered progressively higher levels of attention due to their aesthetics, energy efficiency, flexibility, and ability to be fabricated in large area panel displays without experiencing a significant drop in efficiency, unlike their inorganic counterparts.[32–36] Though niche industries such as hospitality and architectural adopted OLED technology in early years due in part to the aforementioned attributes and exotic form factors,

widespread adoption of OLEDs still remains contingent upon continued improvements to meet the market drivers required for commercial viability.[68] To address these market drivers, our group has previously demonstrated solution-processed plastic substrates to replace the standard indium tin oxide (ITO)/substrate and light extraction structures for OLED fabrication in an effort to drive down cost and enhance efficiency.[15,27,28] Furthermore, several other groups have demonstrated ITO-free substrates with scaled up processing such as roll-to-roll, demonstrating the potential application for low cost, high volume manufacturing.[13,69–75] However, the lifetime of OLEDs remains a critical barrier to surmount before this new lighting technology can establish itself as a competitor to inorganic LEDs.[68]

The rate of degradation in OLEDs is a function of current density and total charge passed through the device.[76] As such, the use of OLED substrates built on a silver nanowire (AgNW) platform should improve the lifetime of OLEDs due to the potential for more efficient devices. With the presence of the AgNW / polymer boundary at the interface between substrate and emissive layer, the waveguide mode can be significantly reduced by the scattering and altering of light rays from the emissive layer, preventing total internal reflection as in the case of ITO substrates.[27,77,78] Furthermore, low-cost, internal light extraction mechanisms such as light scattering nanoparticles can further reduce out-coupling losses due to the substrate mode.[28,79–81] The resulting performance has been shown to greatly enhance the efficiency of organic and polymer light emitting diodes, with efficiency enhancement reaching over 100%,[27,28] manifested empirically by the lower driving current required to reach the same luminance as devices fabricated on ITO. This reduction in current density is anticipated to extend the lifetime of OLEDs by reducing the excited states generated by recombining charges.[76] Specifically, the

lifetime is expected to scale approximately as $1/J^2$, with J the current density passing through the device.[82,83]

However, in contrast with the bulk ITO standard for industry production of OLEDs, the nanostructured AgNWs may experience instability during processing or operational use due to size effects, leading to shorter than expected lifetimes. Curiously, though AgNW networks are designed and utilized for conducting electricity, there are very few reported works on the electrical stability of AgNW based conductors, and to the authors' knowledge, none on the lifetime of OLEDs built on AgNW substrates. Regarding the electrical stability of the substrates themselves, a study by Zhao *et al.* found that the electrical breakdown of a single AgNW was due to stresses induced by electromigration.[84] However the findings do not expand further to failure mechanisms of AgNW networks, where high junction resistances between nanowires should be expected to have a profound effect on electrically induced failure due to enhanced Joule heating at the junctions. Khaligh *et al.* and Mayousse *et al.* reported that under normal current densities, AgNW networks could fail within two days due to Joule heating causing the nanowires to create electrical discontinuities in the networks,[85,86] but the scope of their studies were limited solely to observation of the failure. Other attempted approaches to improve the stability of AgNW electrodes include post treatment processes to weld the nanowire junction through laser sintering,[87] chemical processes,[88] electrical welding,[4,60] or heat treatment,[17,28] or the use of overcoats such as neutral poly(3,4-ethylenedioxythiophene): poly(styrenesulfonate) (PEDOT:PSS) to reduce acidic corrosion during operational use.[51] However, AgNW networks subjected to post treatment processes have already been shown to fail under typical operational currents of solar cells,[85] and the use the neutral PEDOT:PSS[51] merely mitigated harsh

environmental conditions typically observed with traditionally acidic PEDOT:PSS without addressing the underlying issue of electrical instability of AgNW networks.

In this chapter, several issues regarding the electrical stability of AgNW networks, and the application of these networks towards electrodes for improving the lifetime of OLEDs are reported. First, a thorough analysis on the failure mechanism of AgNW networks under current flow is presented. Second, we report on the use of a low temperature atomic layer deposition process to coat a thin, conformal layer of zinc oxide (ZnO) around individual nanowires to enhance the current stability of AgNWs while maintaining a porous nanowire network. Third, the efficacy of the electrically stable ZnO-AgNW based electrode in enhancing OLED lifetime is demonstrated by fabricating OLEDs and comparing resulting performance to ITO and pristine AgNW electrodes. It is noted that the use of ZnO in conjunction with AgNWs have been previously reported.[5,49,89] Kim *et al*. sandwiched a layer of AgNWs between two sputtered layers of aluminum doped zinc oxide (AZO) for enhanced thermal for use in thin film solar cells.[49] Chalh *et al*. spun solution processed ZnO nanoparticles both before and after solution processing AgNWs to form a tri-layer electrode for use as organic solar cell electrodes.[89] However, the use of these continuous layers of ZnO, while suitable for some applications, may lead to potential downfalls such as increased absorbance, decreased flexibility, and higher surface roughness, due to the prohibition of a polymer precursor to form a percolation network. In contrast, the use of an ALD coated ZnO layer retains the benefits of the utilization of ZnO while mitigating these issues, as the conformal coating allows the network to maintain or increase the mechanical properties of the network, retains the high open area for high transparency, and can be infiltrated by polymer precursors for low surface roughness. The potential for these electrically robust

AgNW electrodes extends past applications solely in the lighting industry. With continual research and improvement in the stability of silver nanowire electrodes, the field of wearable, stretchable, and optoelectronics can be advanced, benefiting applications such as driving circuitry,[30,90–92] solar cells,[14,93] and conformal sensors.[20,94–97]

## 3.2. Experimental Section

### 3.2.1. Materials

AgNWs were purchased from Zhejiang Kechuang Advanced Materials Co. GO was synthesized from graphite according to the modified Hummers method.[54] BST nanoparticles were obtained from NanOxide, and were admixed in a liquid monomer solution comprising ethoxylated bisphenol A dimethacrylate and siliconized urethane acrylate oligomer supplied by Sartomer, and 2,2-dimethoxy-2phenylacetophenone purchased from Sigma-Aldrich (photoinitator) at 3 wt.%. Willow® glass was supplied by Corning®. 3-(Trichlorosilyl)propyl methacrylate was purchased from Gelest, Inc. PEDOT:PSS (Clevios VP AL4083) was obtained from H.C. Starck. All organic materials for OLED fabrication were purchased from Lumtech. CsF and Al were purchased from Sigma-Aldrich.

### 3.2.2. Preparation of ZnO-AgNW networks and freestanding ZnO-AgNW/Willow® glass substrates

Willow® glass was treated in a solution of 3% 3-(Trichlorosilyl)propyl methacrylate in toluene. The treated glass was washed with acetone and dried before use. GO was dispersed in deionized water and isopropyl alcohol (IPA) at a concentration of 0.2 mg/5mL, and sonicated for 15 minutes before use. The GO solution was drop cast on top of a release glass substrate and drawn down with a Meyer rod. Resulting GO coated films were annealed for 30 minutes at 150 °C. A AgNW in IPA solution was subsequently drawn down on top of the GO, followed by post-treatment processing comprising annealing at 150 °C for 3 minutes, soaking in DI water for 10 minutes, and further annealing at 165 °C for 8 minutes. Following wet processing of the

nanowires and GO, the conductive glass slides were introduced into a Fiji ALD system from Cambridge NanoTech, where $Al_2O_3$ and ZnO were deposited from precursors of TMA and $H_2O$, and diethyl zinc (DEZ) and $H_2O$, respectively at 100 °C. The pulse and purge times for the precursors of $Al_2O_3$ were 0.06 / 30 seconds, while the times for the ZnO precursors were 0.06 / 45 and 0.06 / 60 for DEZ and $H_2O$, respectively.

After removal from the ALD chamber, the pre-treated Willow® glass was placed over the ZnO-AgNW coated release glass substrate with a 40 micron thick spacer in between the two glass slides. A mixture of 3 wt.% BST in the monomer solution was flowed between the glass slides before exposure to 365 nm ultraviolet radiation. The ZnO-AgNW/Willow® glass substrate was peeled off and rinsed with soap and water before soaking in acetone and IPA.

### 3.2.3. Fabrication of white OLED

In a typical procedure, ITO/glass, AgNW/Willow® glass, and ZnO-AgNW/Willow® glass were spun with a solution of PEDOT:PSS at 5000 RPM for 1 minute, followed by annealing at 130 °C for 30 minutes to dry off any residual solvent. The PEDOT:PSS coated substrates were brought into an evaporation chamber inside a glovebox for OLED fabrication. The sandwich stack of TAPC / NPB:PO-01 / $Bepp_2$ / CsF / Al were deposited with thicknesses of 60 nm, 10 nm, 35 nm, 1 nm, and 80 nm.

### 3.2.4. Characterization methods

SEM-EDX was conducted on a JOEL JSM-6701 scanning electron microscope. Electrical stressing was performed using a Keithley 2400 source meter. Sheet resistance measurements

were obtained by forming electrical leads on the nanowires to define a unit square, with the leads connected to the Keithley 2400 source meter measuring the sheet resistance every second. Transmittance spectra were obtained with a Shimadzu UV-1700 spectrophotometer. OLED analysis was conducted in a nitrogen atmosphere glovebox using a Keithley 2400 source meter and calibrated silicon photodetector by passing a constant current between anode and cathode. The surface morphology of the substrates was analyzed with a Dimension Icon Scanning Probe Microscope from Bruker. All characterization was conducted at room temperature.

## 3.3. Results and Discussion

### 3.3.1. Current flow through AgNWs

Current flow through silver nanowire electrodes differs from that in ITO, as electronic transport can only occur through the individual nanowires. Due to the small dimensions of the nanowire (on average 30 nm in diameter and 30 μm length), the corresponding current density may be several orders of magnitude higher than that in ITO. To obtain reasonable estimates of the current flow under normal operating conditions, the upper bound of biasing during operational testing of our OLEDs (0-6 V) was selected, corresponding to a current density through the OLED of 150 mA/cm$^2$. With this device current density, the approximate current density in individual nanowires was estimated to be $\sim 5.0 \times 10^6$ A/cm$^2$, in line with values reported by other groups.[60] Using this current density, the finite-element method was used to model an isolated two-nanowire system to understand nanowire behavior under current flow, with the longitudinal cross-section down the middle of the two nanowires shown to better observe current distribution through the system. For simulation parameters, the average dimensions of the nanowires (30 nm in diameter and 30 μm length) was used, along with a conductivity of $1 * 10^7$ S/m.[98,99] **Figure 3.1** shows the current flow through the reacted contact morphology nanowire system with a high current concentrating at the junction due to the increased resistance between individual nanowires at the said junction. This reacted contact is an intermediate state between a point contact and a fully ripened junction. With a point contact, the current density at the junction can be several orders of magnitude higher, while current crowding will be less pronounced in ripened junctions. However, because of differences in contact morphologies at junctions due to different thicknesses and junction resistances, all three morphologies are present

in nanowire networks, with the reacted contact being selected as an illustration of phenomenon occurring in the network under current stressing.

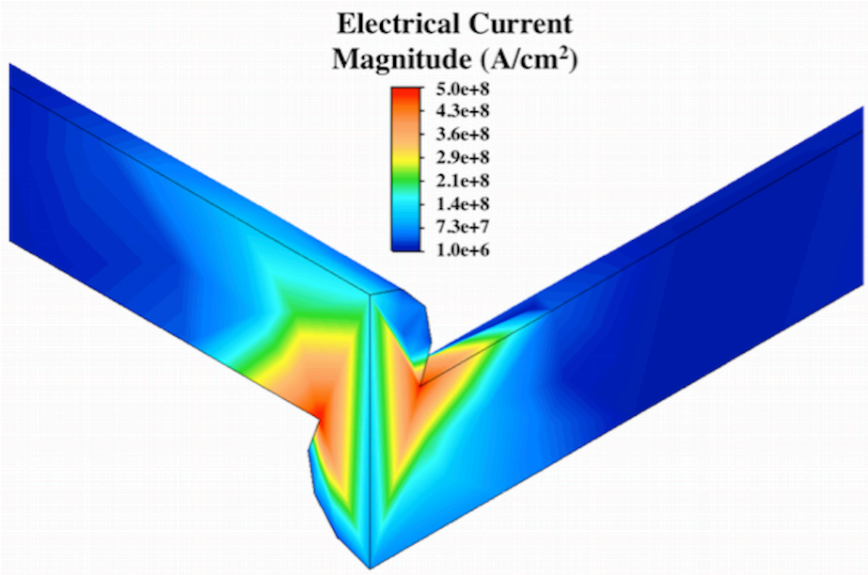


**Figure 3.1.** Finite element simulation of the current flow through a two-nanowire network.

As a result of the high current density through the nanowires, Joule heating may occur to such a significant extent where portions of the nanowire network become fragmented or melted and disrupt the conductive network. The corresponding temperature in a nanowire as a result of current flow can be modeled by:[100,101]

$$T_{increase} = \frac{Aj^2}{\pi\kappa\sigma}\operatorname{arcsinh}\left(\frac{2\sqrt{tk/\rho C}}{\alpha d}\right) \quad \text{(Eq. 3.1)}$$

where A is the cross sectional area of the nanowire, d is the diameter of the wire, j is the current density, $\sigma$ is the electrical conductivity, $\kappa$ is the thermal conductivity of the nanowire, k is the thermal conductivity of the underlying glass substrate, $\rho$ is the density of the substrate, C is the specific heat capacity of the substrate, and $\alpha$ is a model parameter constant. Using typical parameters for AgNWs and the underlying glass substrate, the temperature distribution through

the two-nanowire system can be approximated by correlating the current density shown in **Figure 1**. A temperature distribution through the nanowires can be seen in **Figure 3.2**. In the bulk of the silver nanowires away from the junction, the corresponding temperature approaches 200 °C, and at the regions of highest current density near the junctions, can surpass 300 °C. These temperatures can climb even higher with the use of a lower conductivity AgNW electrode with the same applied bias, as a lower conductivity signifies fewer wires to conduct electricity, and thus, a higher current density through the available wires. Though these temperatures are far below the melting temperature of bulk silver, nanoscale size effects lead to a large gradient of Gibbs-Thomson potential at the junction, and regions immediately adjacent to the junction.[102] This potential gradient is a driving force for diffusion of silver atoms into the junction,[60,102] resulting in the fragmentation of the nanowire network at a significantly lower temperature than the melting temperature of bulk silver.[48] At sufficiently high temperatures, the nanowires begin to melt, and due to the Plateau-Rayleigh instability, causes the AgNWs to reform into discrete, spherical droplets in an effort to minimize the surface energy of the nanowires.[103] This effect is further exasperated with increasing smaller dimensions of nanowires. According to the Gibbs-Thomson theory, $\Delta G = {}^{2\gamma\Omega}/_{r}$, where $\Delta G$ is the change in Gibbs Thomson potential, $\gamma$ is the surface energy, $\Omega$ is the volume per atom, and r is the radius, the Gibbs-Thomson potential is inversely related to the radius of the nanowire. Though the average diameter of nanowires used is 20 nm, significantly smaller dimension nanowires can be found within the percolation networks as well, and are comparatively less stable than their larger dimension counterparts, manifesting in a breakdown of these smaller nanowires first. At temperatures as low as 180 °C, the beginning of coalescence fragmented nanowires can be observed. As a result, the high temperatures

incurred in the sample through Joule heating will likely bring about the fragmentation and melting of AgNWs and the reformation into electrically disruptive, discrete nanoparticles.

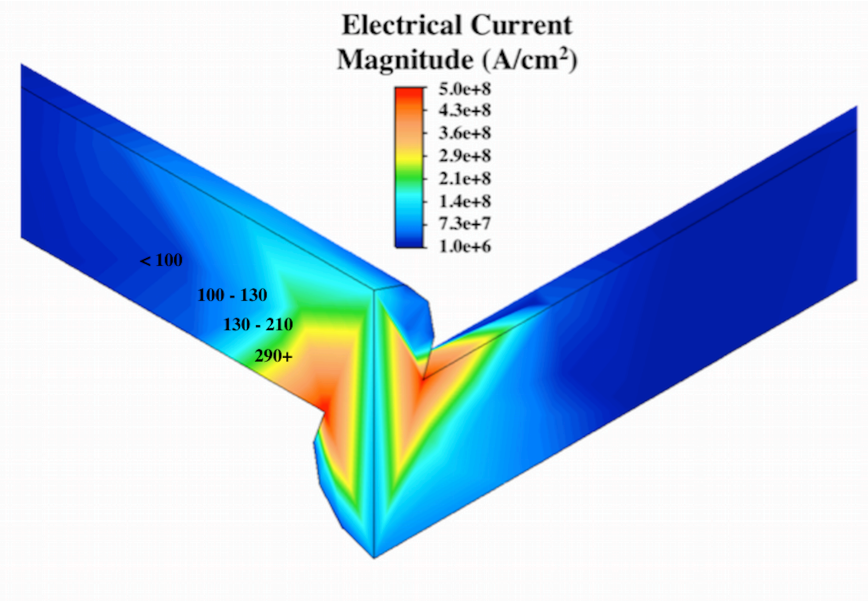


**Figure 3.2.** Finite element simulation of the current flow through a two nanowire network. Numbers shown indicate an increase in temperature (e.g. 100 – 130 means a 100 to 130 °C increase in temperature).

### 3.3.2. Empirical verification of the method of silver nanowire failure under current flow, and the use of ZnO to mitigate the failure

The above analysis was verified experimentally by fabricating both pristine AgNW and ZnO-AgNW electrodes on glass at a sheet resistance of 10 and 25 ohm/sq. Fabrication of the nanowire network on glass was achieved by drawing down a liquid solution of AgNW onto glass with a Mayer rod. Samples were post-treated by immersion in DI water to remove excess surfactant on the surface of the nanowire, and annealing to weld the junctions to lower the sheet resistance. A constant current was passed through the nanowire network to obtain a current density of 155 $mA/cm^2$, with the resulting electrically stressed samples of the low sheet resistance electrode shown in the scanning electron (SEM) image in **Figure 3.3a**, and the higher sheet resistance

sample shown in **Figure 3.3b**. After electrical stressing for the same duration, the 10 ohm/sq samples closely resembles nanowires annealed at 200 °C, while the 25 ohm/sq electrodes appear as AgNWs annealed at 250 °C as previously reported.[102] These two samples show the effect of Joule heating on samples of different resistivities, and serve as the basis of understanding the mechanism of electrical failure of AgNW networks under current flow. Because high current density will inevitably concentrate at the junctions due to the reduced volume available for current flow at the contact, these regions experience significant Joule heating. This is further exasperated by the higher resistance at the junctions, leading the contacts between nanowires to fail preferentially. With each failed junction, fewer nanowires are available to conduct electricity, inducing higher current in surrounding conducting paths if a constant current is applied to the sample. **Figure 3.3c** shows a local 'hotspot' in the nanowire percolation network, with several junctions broken within a small region. As current continues to pass through, these small hotspots force increased current in surrounding regions, elevating the local temperature, and in turn, enlarging the regions of broken and discrete nanowires, as seen in **Figure 3.3d**. This cascading process has an increasingly deleterious effect on the conduction path, with the hotspots amalgamating in large areas of complete current discontinuity (**Figure 3.3e**).

The electrical instability can be relieved in part by the conformal zinc oxide layer. Following AgNW coating, the solution-processed electrodes on glass substrate were brought into an ALD chamber. Because ALD is a self-limiting deposition technique relying on chemical reactions at the surface, a thin layer of aluminum oxide ($Al_2O_3$) was deposited to act as an adhesive layer prior to ZnO deposition. $Al_2O_3$ was selected as the adhesive layer as its precursor, trimethyl aluminum (TMA), reacts well with Ag, in addition to providing a hydroxylated surface[53,56] for

subsequent ZnO deposition, two important factors in light of the fact that hydroxylated surfaces are the most reactive with ALD precursors. Both $Al_2O_3$ and ZnO were deposited at low temperatures to prevent oxidation and melting of the AgNWs. Detailed procedures of the deposition process can be found in the Methods section. TEM images of both ZnO coated and pristine AgNW are provided in Chapter 2 in **Figure 2.2a**. Under the same current stressing conditions described above, both higher and lower resistance nanowire networks remained intact in a porous network with no evident degradation, as seen in the 20 ohm/sq. sample shown in **Figure 3.4a**. However, as temperature through the nanowire is proportional to the square of the current density as long as current can pass through intact, non-melted nanowires, progressively

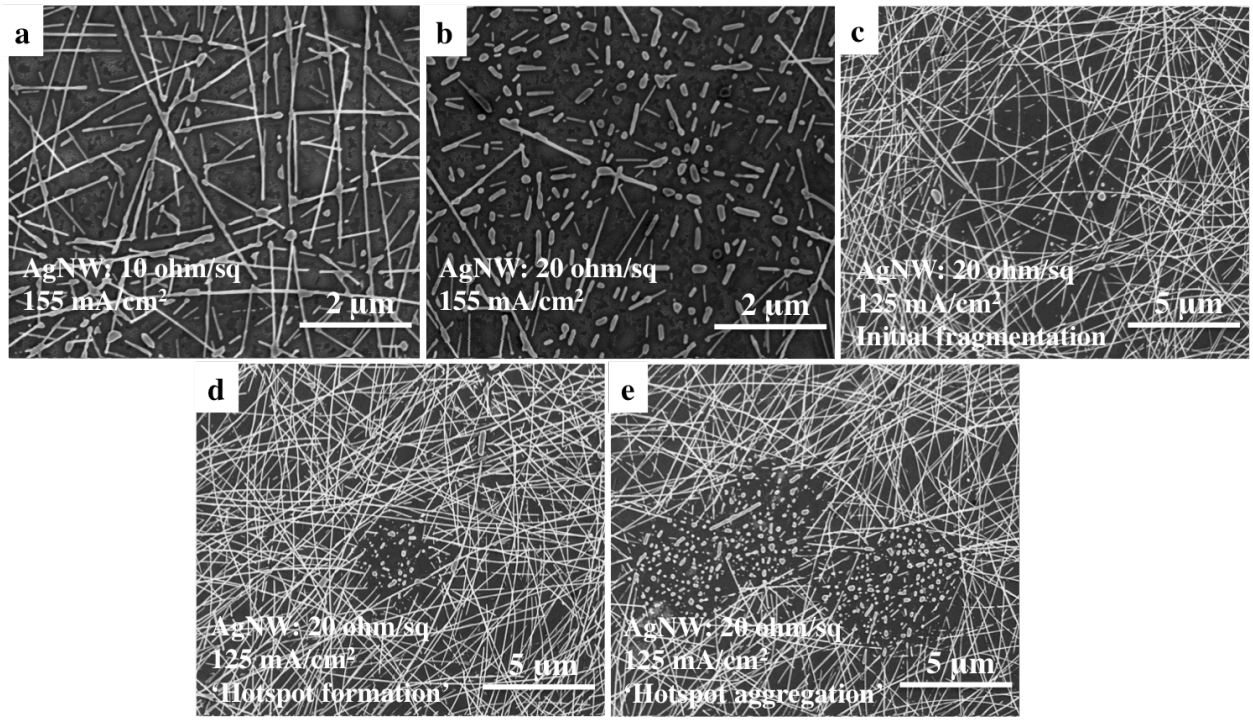


**Figure 3.3. | SEM images of electrically stressed AgNW networks.** a) SEM image of a 10 ohm/sq. pristine AgNW network electrically stressed at 155 mA/cm$^2$. b) Image of a 20 ohm/sq. AgNW network electrically stressed at 155 mA/cm$^2$. c) Image of a local fragmented nanowires after electrically stressing a 20 ohm/sq. AgNW network at 125 mA/cm$^2$. d) Enlarging of 'hotspot' after continued electrical stressing at 125 mA/cm$^2$. e) Amalgamation of 'hotspots' to form regions of electrical discontinuity after continued electrical stressing at 125 mA/cm$^2$.

higher current densities do begin to break down the ZnO protected nanowires. At a current density of 200 mA/cm$^2$, fragmentation of nanowires at the junctions was observed to occur in a 10 ohm/sq electrode, as seen in **Figure 3.4b.** However, the fragmentation remains confined to a few junctions, with the bulk majority of the network remaining intact. Furthermore, unlike the pristine AgNW sample, the ZnO-AgNW electrodes at higher current densities were able to conduct electricity without any abrupt increase in sheet resistance over six hours. Upon application of even higher current densities of 275 mA/cm$^2$, certain nanowires were observed to have melted (**Figure 3.4c**), but remained in a nanowire network instead of discrete nanoparticles. Zoomed out images corresponding on **Figure 3.4** are provide in **Figure 3.5a**, **3.5b**, and **3.5c**, respectively. Though the network is observed to degrade, it is important to note that these current densities are, for the most part, higher than those used for typical OLED applications.

The aforementioned empirical verification was conducted with a 2 Å layer of $Al_2O_3$, and a 4.5 nm thick ZnO layer. These thicknesses were selected due to it being the empirically observed minimum thickness of ZnO in which highly effective thermal protection was still observed, as demonstrate in a previous work.[102] In addition to the 4.5 nm ZnO layer, the same stressing conditions were also conducted on a 2 Å layer of $Al_2O_3$, with a 1.5, 3.0, and 7.5 nm ZnO layer. The samples with 3.0 and 7.5 nm thick ZnO layer when subjected to the same stressing conditions resemble the 4.5 nm coated sample after current stressing illustrated in **Figure 3.4a**. However, the 1.5 nm ZnO sample after stressing show some fragmentation at the junction, indicating inadequate protection. Though the 3.0 and 4.5 nm ZnO electrodes showed similar morphologies after current stressing, the 4.5 nm ZnO thickness was selected due to high temperature annealing for subsequent OLED fabrication.

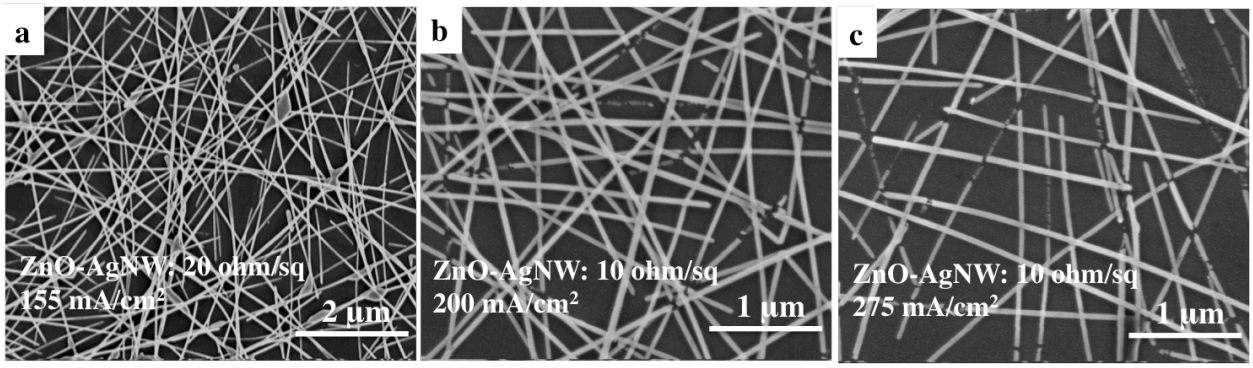


**Figure 3.4. | SEM images of electrically stressed ZnO-coated AgNW networks.** a) SEM image of a 20 ohm/sq. ZnO-coated AgNW network after electrical stressing at 155 mA/cm$^2$ for 1 hr. b) SEM image of a 20 ohm/sq. ZnO-coated AgNW network after electrical stressing at 200 mA/cm$^2$ for 1 hr. c) SEM image of a 20 ohm/sq. ZnO-coated AgNW network after electrical stressing at 275 mA/cm$^2$ for 1 hr.

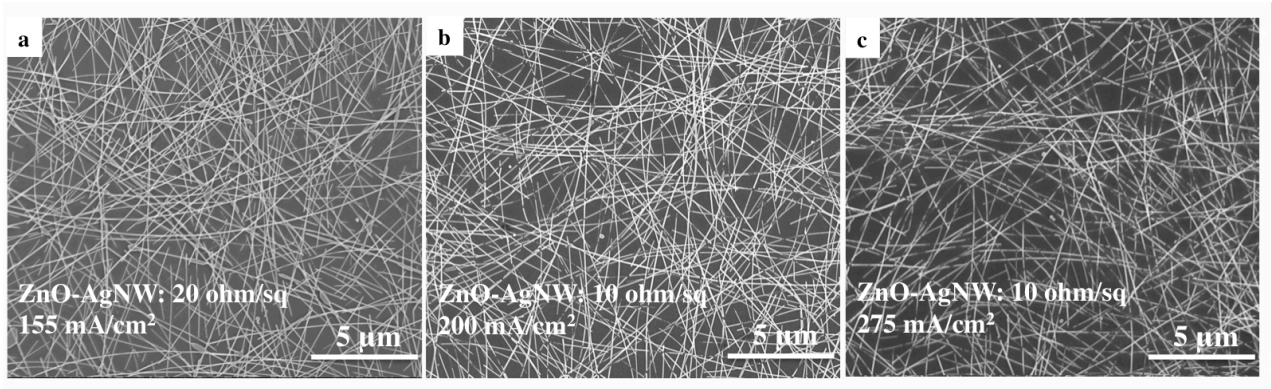


**Figure 3.5. | SEM images of electrically stressed ZnO-coated AgNW networks.** a) SEM image of a 20 ohm/sq. ZnO-coated AgNW network after electrical stressing at 155 mA/cm$^2$ for 1 hr. b) SEM image of a 20 ohm/sq. ZnO-coated AgNW network after electrical stressing at 200 mA/cm$^2$ for 1 hr. c) SEM image of a 20 ohm/sq. ZnO-coated AgNW network after electrical stressing at 275 mA/cm$^2$ for 1 hr.

### 3.3.3. Optoelectronic properties of pristine and ZnO-coated AgNW under current flow

To quantitatively analyze the electrical stability of the ALD coated AgNW film, the sheet resistance and transmittance were evaluated and compared with pristine AgNWs after current stressing. For electrical analysis, nanowires were coated on a glass slide to a sheet resistance of

10 ohm/sq, with silver paste coated on the edges for electrical contacts. The samples were connected to a Keithley 2400 source meter with a constant current density of 125 mA/cm$^2$ applied, and the resistance recorded *in situ*. **Figure 3.6a** illustrates the performance of the pristine AgNW and ZnO-AgNW during electrical stressing. The pristine AgNW sample is observed to increase linearly in sheet resistance over a span of approximately 9.5 hours, at which point a dramatic increase in sheet resistance is observed, indicating the formation of a line of virtual complete disconnect between the two electrical leads. In contrast, the zinc oxide enhanced sample maintains relatively same sheet resistance over the entire duration of 12 hours. The initial spike in resistance is due to the sudden increase in temperature upon application of current, while the subsequent drop in resistance up until two hours is attributed to the fusing of the junctions as a result of the thermal treatment brought about by current stressing. However, the fluctuation in sheet resistance of the ZnO-AgNW electrode is relatively minute, especially when contrasted to the pristine AgNW electrode.

In addition to electrical stability, optoelectronic devices such as OLEDs also require the maintenance of transparency throughout operational use. Though the effects of electrical stressing on the performance of subsequently fabricated devices are largely dependent on the electrical degradation, evidence of atmospheric corrosion is also evident, which further plays a role in optoelectronic performance. Following the procedure described above for electrical testing, a current density of 125 mA/cm$^2$ was applied to the AgNW electrode until electrical failure, with the same current density applied to the ZnO-AgNW electrode for the same duration of time. The transparency of both electrodes before and after electrical stressing was obtained, and displayed in **Figure 3.6b**. An 8% decrease in transparency is observed for the pristine

AgNW sample, whereas no evident optical degradation occurs for the ZnO-AgNW electrode. In both electrodes, an abrupt decrease in transparency at approximately 350 nm is observed. This commonly reported silver nanowire feature is attributed to the surface plasmon resonance absorption, and is located between 350-400 nm depending on the dimensions of the nanowires.[104,105]

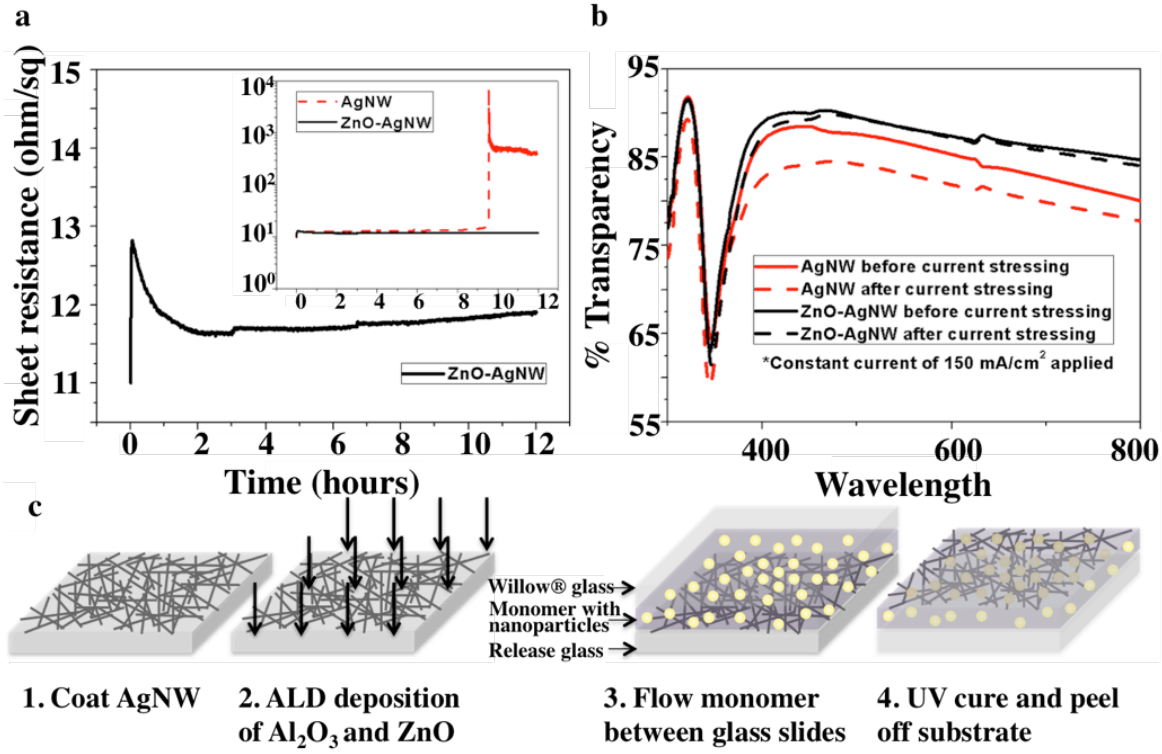


**Figure 3.6. | Optoelectronic performance of pristine AgNW and ZnO-coated AgNW networks and fabrication of OLED substrates.** a) Sheet resistance as a function of time under continuous current stressing at 125 mA/cm$^2$. b) Optical behavior of pristine AgNW and ZnO-coated AgNW electrodes after current stressing at 125 mA/cm$^2$. c) Schematic of the fabrication process of a freestanding ZnO-AgNW OLED substrate on glass.

## 3.3.4. OLED fabrication and analysis

OLED substrates were fabricated on the AgNW and ZnO-AgNW platform by embedding and transferring the nanowires from the release glass substrates following a similar method reported

in our previous publications, with a schematic flow chart shown in **Figure 3.6c**.[26,28,102] Briefly, a flexible Willow® glass substrate from Corning® was placed over the nanowire coated glass, and separated by a spacer layer to control the thickness between the two glass slides. An acrylate monomer admixed with barium strontium titante (BST) nanoparticles for enhanced light extraction was flowed in between the glass slides, and allowed to infiltrate the pores within the nanowire network. Following monomer infiltration, the resulting structure was exposed to ultraviolet radiation to convert the monomer into a solid cross-linked polymer film, and peeled off to obtain a freestanding substrate comprising the Willow® glass support, polymer layer, and embedded nanowires. Prior to substrate fabrication, the Willow® glass substrate was pretreated with 3-(Trichlorosilyl)propyl methacrylate to allow the polymer to covalently bond to the underlying glass slide. The adhesiveness of the polymer to the Willow® glass substrate was tested with the Scotch tape test and immersion in several solvents, with no delamination observed. Further in depth parameters and procedures of the substrate fabrication are detailed in the Methods section. The Willow® glass substrate was incorporated within the substrate process for expanded processing and manufacturing capabilities, and to provide an inherent hermetic barrier against moisture and oxygen on the anode side. Furthermore, devices fabricated utilizing the Willow glass-polymer composite substrate were observed to vastly outperform freestanding polymer substrates in terms of operational stability. **Figure 3.7** illustrates the performance of devices fabricated on freestanding polymer electrodes and ITO. Even when the devices fabricated on the polymer electrodes were driven at a lower current density and thus, lower luminance, the lifetime still lags significantly behind that of ITO, as can be seen in the driving voltage as a function of time in **Figure 3.7a**, luminance as a function of time in **Figure 3.7b**, and current and power efficiencies as a function of time in **Figure 3.7c** and **Figure 3.7d**,

respectively. It is hypothesized that the additional support provided by the Willow® glass substrate prevents mechanical deformation on both the macro and micro scale, which may quickly lead to device degradation for freestanding polymer films. Though the scale of the substrates and subsequent devices fabricated prevent a large bending radius, large-scale production of OLEDs fabricated upon the Willow® glass platform can be curved and flexible.

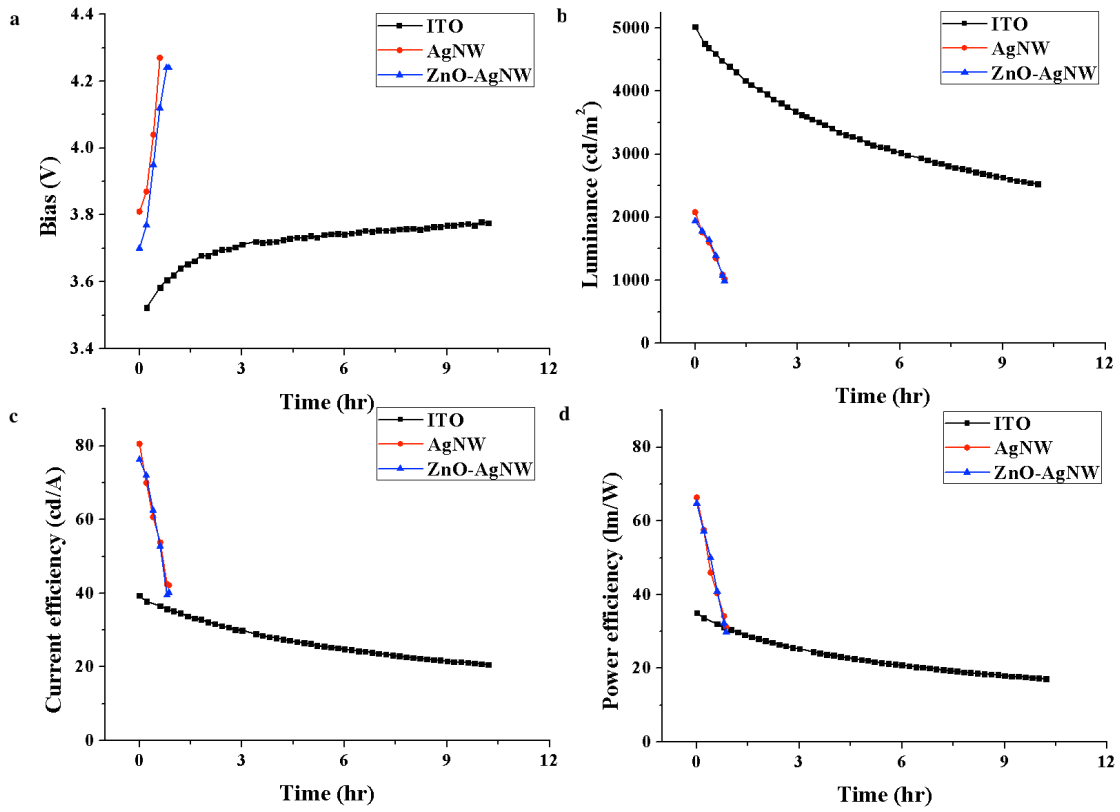


**Figure 3.7.** a) Driving voltage as a function of time for OLEDs fabricated on ITO/glass, pristine AgNW substrates, and ZnO-coated AgNW substrates under a constant current density. AgNW and ZnO-based substrates are freestanding polymer electrodes. b) Luminance as a function of time for. c) Current efficiency as a function of time. d) Power efficiency as a function of time.

Following substrate fabrication, white OLEDs were fabricated on the ZnO-AgNW/Willow® glass substrate, the AgNW/Willow® glass substrate, and ITO/glass, with the sandwich structure anode / poly(3,4-ethylenedioxythiophene) polystyrene sulfonate (PEDOT:PSS) as the hole

injection layer (HIL)/ 4,4'-Cyclohexylidenebis[N,N-bis(4-methylphenyl)benzenamine] (TAPC) as the hole transport layer (HTL) / N,N'(Di(naphthyl)-N,N'diphenyl-(1,1-biphenyl)-4.4'diamine (NPB): PO-01 (a thiopyridinyl-based iridium molecule) as a yellow emissive layer / 4,4′-Bis(*N*-carbazolyl)-1,1′-biphenyl (CBP) as an interlayer / Bis(2(2-hydroxypheyl)-pyridine)beryllium ($Bepp_2$) doped with 1-4-di-[4-(N,N-di-phenyl)amino]styryl-benzene (DSA-ph) as a blue emissive layer / $Bepp_2$ as the electron transport layer (ETL) / cesium fluoride (CsF) as the electron injection layer (EIL) / and aluminum (Al) as the cathode, as seen in the schematic in **Figure 3.8a**. An illustration of the materials is shown in **Figure 3.8b**, with the electroluminescence spectra shown in **Figure 3.9**. Both nanowire electrodes were fabricated with similar sheet resistance (10 ohm $sq^{-1}$) as ITO. Further experimental and processing details can be found in the Methods section.

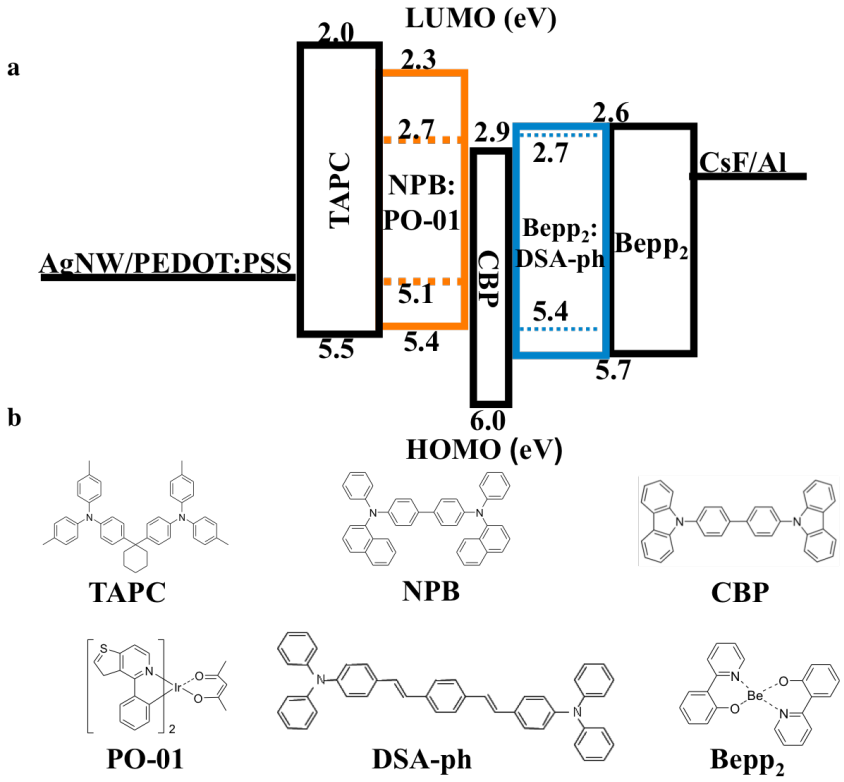


**Figure 3.8. | Illustration of the white OLED.** a) White OLED structure. b) Illustration of the materials used for the fabrication of white OLEDs.

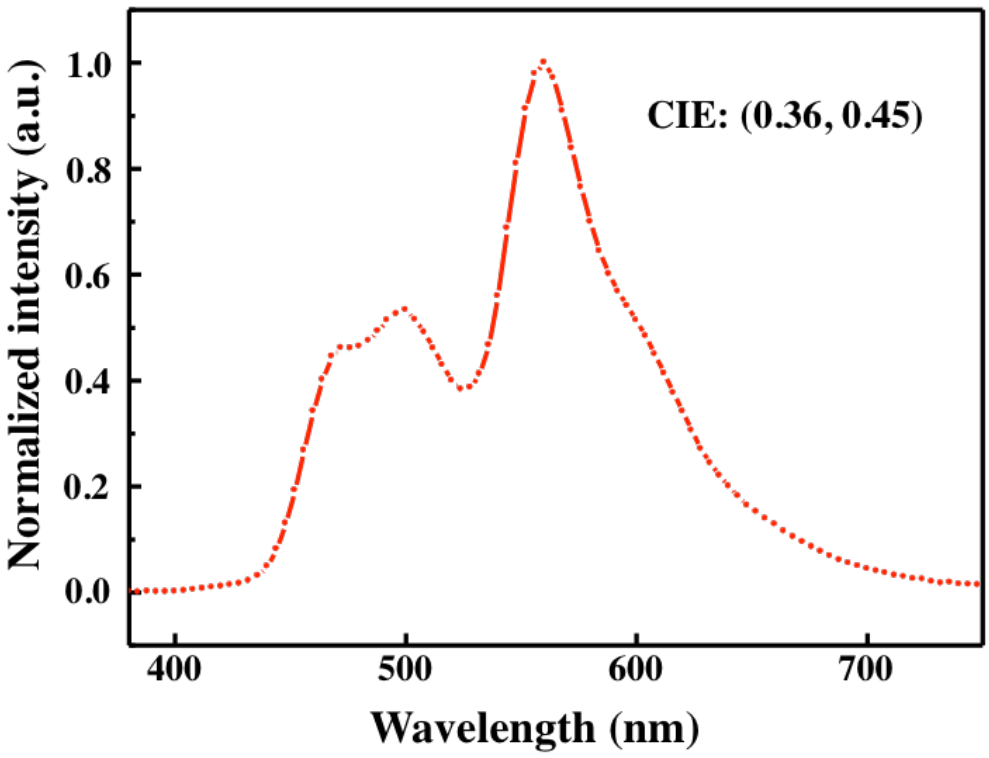


**Figure 3.9.** Electroluminescence spectrum at 1000 cd/m$^2$ of the white OLED fabricated.

## 3.3.5. OLED lifetime

The white OLEDs were tested at an initial luminance of 5000 cd/m$^2$ at a constant current, with the testing concluding when the luminance reached half of the original value ($t_{1/2}$). Representative performances of the devices fabricated on the three substrates are displayed in **Figure 3.10a – Figure 3.10d**. Evident from all of the images is the higher lifetime of both nanowire-based devices in contrast with ITO/glass, and the superior performance of ZnO-AgNW/Willow® substrates compared to pristine AgNW/Willow® electrodes. **Figure 3.10a** depicts the change in bias as a function of time. As all substrates used for device fabrication had roughly the same sheet resistance, the higher voltage required to drive the ITO based OLED is

indicative of the higher current density passing through the device compared to the nanowire based electrodes. Both AgNW and ZnO-AgNW OLEDs were driven at a current density of approximately 6 mA/cm$^2$, whereas ITO based OLEDs were driven at ~12.5 mA/cm$^2$ to reach the same luminance. Again, as the rate of degradation of the device is largely determined by the current density passing through,[76] **Figure 3.10a** is indicative of the longer lifetime, and thus, slower rate of decay, of OLEDs fabricated on the nanowire platforms. Figure **3.10b** justifies this assumption, with the exponential decay for the luminance of the ITO based OLED faster than that of the nanowire based substrates. Numerically, when fitted, the exponential decay constant was found to be 0.20 for OLEDs fabricated on ITO/glass, in contrast to 0.07 and 0.12 for ZnO-AgNW/Willow® glass and AgNW/Willow® glass based OLEDs. The earlier failure of the ITO based OLEDs is not expected to be due to degradation of the electrode, as in the case of AgNW based OLEDs as discussed in following paragraphs, due to the high electrical stability and robustness of ITO. To verify, AFM images showing ITO before and after electrical stressing the electrodes at 2x the operating current density of the OLED are depicted in **Figure 3.11a** and **Figure 3.11b**, with no morphological changes evident before and after stressing. Furthermore, sheet resistance measurements and optical characterization were taken before and after electrical stressing. The sheet resistances before and after stressing were measured to be 10.26 and 10.28 ohm/sq., respectively, and no decrease in transparency was observed after current stressing, as can be seen in **Figure 3.11c**. These factors indicate the degradation of the ITO based OLED is due to a higher current density passing through the device as opposed to an anode degradation. The current and power efficiencies are shown in **Figure 3.10c** and **Figure 3.10d**, respectively, and are approximately 100% higher than the respective values for ITO based OLEDs during operational use. The higher efficiencies are a result of the reduced waveguide and substrate mode

due to the elimination of ITO.

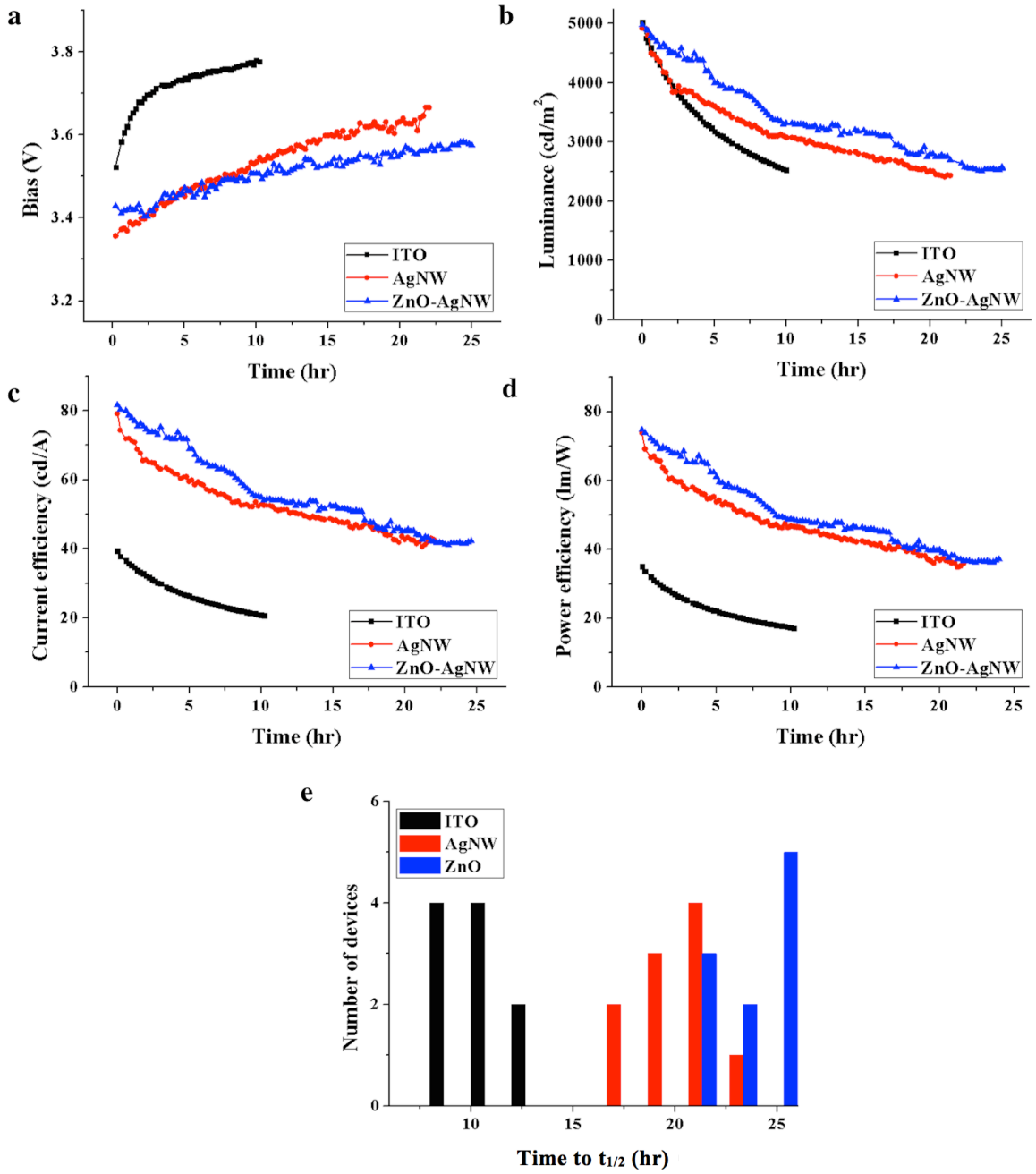


**Figure 3.10. | Device performance of OLEDs fabricated on ITO/glass, AgNW/Willow® glass, and ZnO-coated AgNW/Willow® glass.** a) Driving voltage as a function of time for OLEDs under a constant current density. b) Luminance as a function of time for. c) Current efficiency as a function of time. d) Power efficiency as a function of time. e) Histogram of the time to $t_{1/2}$ for OLEDs at an original luminance of 5000 cd/m$^2$.

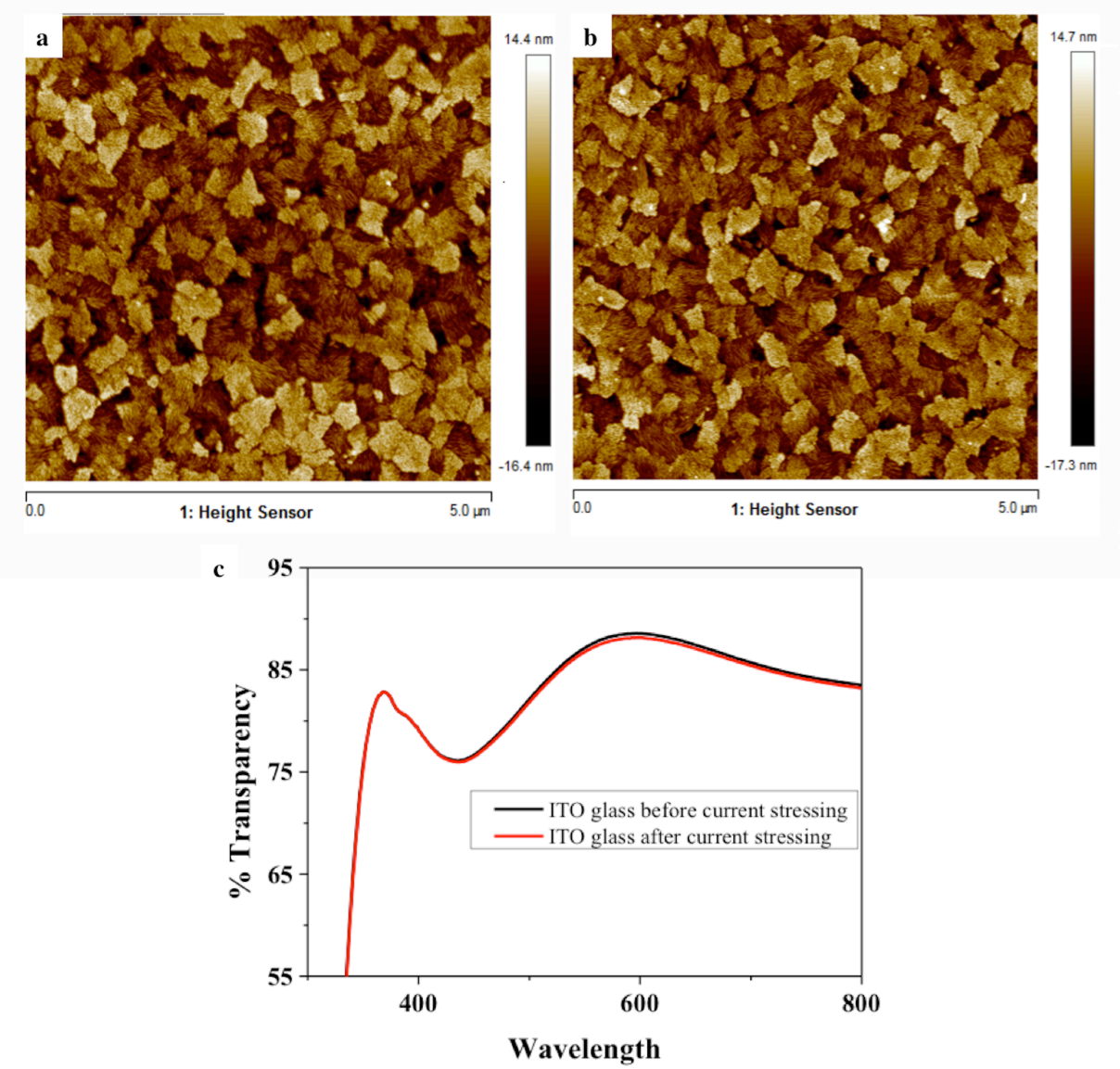


**Figure 3.11.** a) AFM image of ITO prior to electrical stressing. b) AFM image of ITO after electrical stressing at 2x the current density used for luminance testing. c) Transparency specta before and after electrical stressing.

**Figure 3.10f** illustrates a histogram of $t_{1/2}$ for devices fabricated on the three different substrates. On average, the AgNW and ZnO-AgNW/Willow® glass substrates lead to devices with approximately 2x and 2.4x longer lifetime than those on ITO/glass. The enhancement in lifetime using ZnO approaches the expected enhancement in lifetime when accounting for the difference in current density required to drive the device at a specific luminance. The ZnO

enhanced samples were also observed to last 18% longer than pristine AgNW based devices. To verify the statistical significance of the varying lifetimes of different samples, an unpaired Student's *t*-test was conducted, with statistical significance defined at the $P < 0.05$ level. Both nanowire based samples exhibited longer lifetime at a statistically significant level ($P < 0.01$), as did the ZnO based substrate when compared to AgNW ($P = 0.0005$).

### 3.3.6. Enhancement of lifetime for ZnO-AgNW based OLEDs in contrast to pristine AgNW based OLEDs

To examine the differences between the two different AgNW substrates, OLEDs were fabricated on both substrates and tested at a constant current of approximately 13 mA/cm$^2$ to reach an initial luminance of 10000 cd/m$^2$. Because of the similar initial resistance of the substrate, the differences in current density between the two devices were within 5% of each other. Both devices were electrically stressed for a period of 24 hours, at which point the layers on top of the substrate were washed away, as the use of the water soluble PEDOT:PSS allows for all subsequent layers evaporated on the surface to wash away along with the conductive polymer. Following the washing of the substrates, atomic force microscopy (AFM) was conducted to analyze any morphological changes that may have arisen as a result of the electrical stressing. **Figure 3.12a** illustrates a freestanding silver nanowire electrode on Willow® glass as a reference for subsequent samples. The white regions depicting areas of higher morphological features are attributed to localized regions of aggregated BST nanoparticles, as shown in **Figure 3.13**. **Figure 3.12b** shows the AgNW electrode after current stressing. In contrast to the non-stressed electrode, black regions within the image depicting areas where nanowires previously occupied form an 'empty network' at the surface of the substrate. Furthermore, several white features

appear on the image, as will be discussed further below. In **Figure 3.12c** the electrically stressed ZnO-AgNW electrode appears to be fairly intact. Though some evidence of morphological changes are present, most notably the higher features at certain junctions of nanowires, the network remains fairly intact, with no nanowires appearing to be missing from the top layer of the substrate.

The large white features in **Figure 3.12b** were hypothesized to be silver nanoparticles that reformed upon fragmentation or melting of the top surface of the nanowire electrode as a result of Joule heating and electromigration. To verify this hypothesis SEM-EDX analysis of the

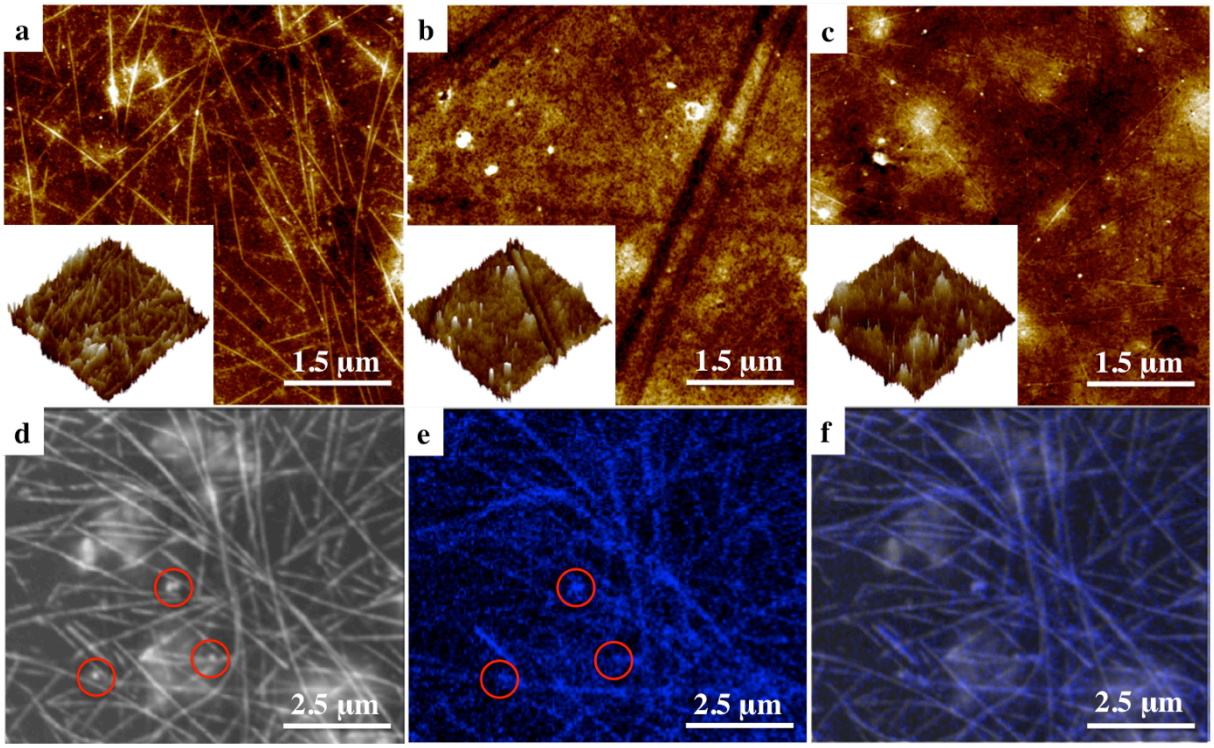


**Figure 3.12. | Characterization of the differences between AgNW and ZnO substrates.** a) AFM image of AgNWs embedded within a polymer matrix. b) AFM image of AgNWs embedded within a polymer matrix after electrical stressing for 24 hours. c) AFM image of ZnO-coated AgNWs embedded within a polymer matrix after electrical stressing for 24 hours. d) SEM image of embedded AgNW electrode after current stressing. e) EDX spectral image of silver of the corresponding SEM image shown in Figure 7d. f) Overland images of the SEM image in Figure 7d and the EDX spectral image in Figure 7e.

electrically stressed AgNW substrate was conducted. **Figure 3.12d** shows the SEM image of a region on the substrate with features similar to those observed in the AFM images, with **Figure 3.12e** depicting the spectral data of the same region for silver based on the energy transition of the valence electrons to the L orbital. When **Figure 3.12d and Figure 3.12e** are overlaid on top of each other, shown in **Figure 3.12f,** it is evident that those features correspond to silver nanoparticles that reformed from the melting of the nanowires. Though **Figure 3.12d** may appear to have intact nanowire networks, it is important to note that while AFM is a surface sensitive technique, the x-rays generated from EDX analysis originate within a five-micron depth, and the nanowire network seen in **Figure 3.12d** are largely embedded underneath the top surface of the substrate.

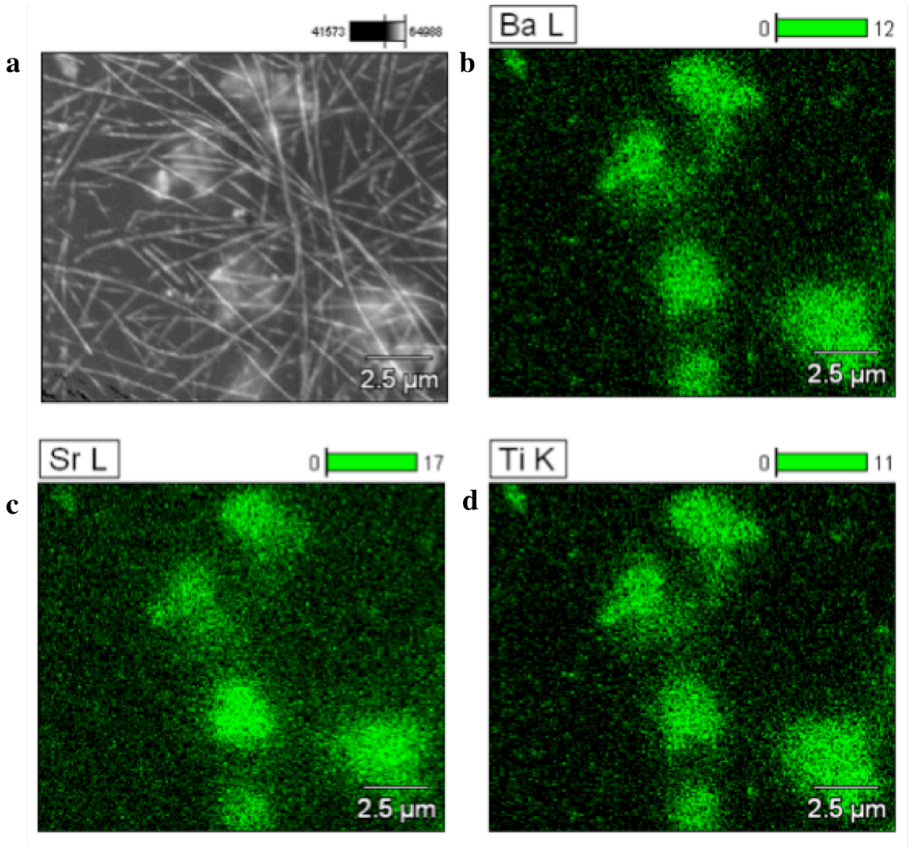


**Figure 3.13.** a) SEM image of embedded AgNWs in a polymer matrix. b) EDX spectral image of barium. c) EDX spectral image of strontium. d) EDX spectral image of titanium.

These remaining embedded nanowires explain why the enhancement in lifetime between OLEDs fabricated on ZnO-AgNW/Willow® and AgNW/Willow® substrates isn't greater, especially in light of the fact that the electrical stability test of pristine nanowires on glass was observed to lead to failure, whereas an intact network remained when ZnO was incorporated. Because the nanowire network comprises AgNWs stacked on top of each other, the top layer of nanowires accounts for a relatively small portion of the total nanowire network. The remaining embedded nanowires are protected in part from morphological changes from the surrounding, mechanically robust, cross-linked polymer matrix, in contrast to the nanowires on the surface in contact with the soft PEDOT:PSS. When these surface nanowires reform as nanoparticles at the surface, uneven and lower hole injection will occur, slowly increasing the driving voltage and decreasing the luminance of the OLED as time progresses.

Because of the ability of the ZnO-AgNW substrate to remain intact even under high current flow over extended periods of time, the newly developed substrate brings the transition away from ITO one step closer to reality. However, more effort will need to be put forth to truly realize the full potential of these alternative electrodes. Though the lifetime of OLEDs fabricated on both nanowire-based substrates was seen to significantly increase, the empirical lifetime still lags behind the theoretically expected lifetime, which scales proportional to $1/J^2$. This discrepancy may be due in part to the presence of localized shorts, even with the embedding of the nanowires within the polymer. Although the current efficiency remains high even with these shorts, these regions of rough morphology may induce localized high current flow that degrade the active material at a faster than expected rate. Methods such as the pre-biasing of electrodes prior to device fabrication,[4] or the utilization of a short reduction layer[106] may enable OLEDs

fabricated on these substrates to realize their full potential. Though at this point in time the stability and lifetime of AgNW based devices remain largely unstudied, this work demonstrates the potential for commercial viability of these alternative electrodes.

## 3.4. Conclusion

The electrical stability of silver nanowire electrodes was investigated for analysis of the application of these materials in OLED substrates. The failure mechanism for silver nanowire networks was observed to be an avalanche effect of steadily enlarging regions of broken nanowire networks as a result of Joule heating arising from electrical stressing, which could be ameliorated with a conformal layer of ZnO wrapped around the AgNW. An OLED substrate was fabricated comprising AgNWs coated with ZnO embedded within a polymer matrix covalently bonded to a flexible glass substrate. The lifetime of the OLED fabricated on the ZnO-AgNW/Willow® glass substrate was found to be 140% higher than those fabricated on ITO-glass, and 18% higher than those fabricated on AgNW/Willow® glass. With regards to the former, the lower current density required to drive the device was responsible for the enhancement of the lifetime, while the morphological stability in contrast with the AgNW/Willow® glass substrate was responsible for the latter. This newly developed OLED substrate shows great promise for replacing ITO as it demonstrates that devices fabricated on this platform can exhibit significantly better efficiency and lifetime, while remaining mechanically and morphologically robust.

# Chapter 4

# Highly flexible organometal halide perovskite quantum dot based light-emitting diodes on a silver nanowire-polymer composite electrode

## 4.1. Introduction

The rapid development of flexible electronics has been driven much in part by the development of innovative materials.[107,108] Organometal halide perovskites (denoted by $MAPbX_3$, where MA=$CH_3NH_3^+$, and X = Br, Cl, I) are one such development, and have been touted in recent years due to intriguing hybrid properties including the high charge-carrier mobility generally found in inorganic semiconductors, and the ability to be low-cost, solution-base processed, typically associated with organic semiconductors.[109–111] Due in part to this hybrid characteristic, these organometal halide perovskites are excellent candidates for high-performing flexible electronics.[112–114] As an example, high performance flexible solar cells utilizing these

materials on ITO-coated poly(ethylene terephthalate) (PET) or polyethylene naphthalate (PEN) polymer substrates have been widely reported.[115–117]

In addition to their utilization in solar cells, the photoluminescence (PL) properties of perovskites have been increasingly studied in recent years for their potential use as emissive materials for display and lighting applications due to desired characteristics of narrow spectral width and high color purity, high quantum yield (QY), and tunable emission (400-800 nm).[118–120] Organometal halide perovskite thin-film based light emitting diodes (LEDs) with comparable current efficiency to phosphorescent organic light-emitting diodes have been reported, signaling perovskites' attractiveness for electroluminescence (EL) applications.[121,122]

Perovskite based LEDs generally rely on a two-step deposition method in which perovskite precursor layers are sequentially deposited, followed by an annealing step to allow interdiffusion of the layers to achieve perovskite conversion, with the resulting layer manifesting in a thin film.[110] However, the development of high performance, flexible perovskite LEDs based on perovskite films remains a significant challenge due to several limitations. The $MAPbX_3$ films used for perovskite LEDs have a thickness of several hundred nanometers in addition to large grain sizes, rendering them unsuitable for highly flexible LEDs. Furthermore, the most commonly used solvents to process perovskite films are dimethyl formamide (DMF) and dimethyl sulfoxide (DMSO), which dissolve or partially dissolve several commonly used organic semiconductor materials including poly(2,3-dihydrothieno-1,4-dioxin)-poly(styrenesulfonate) (PEDOT:PSS), a ubiquitously used anode interfacial coating. This incompatibility of sequential layers from solvent attack limits device architectures for realizing efficient charge balance in the devices. Lastly, high quality perovskite films generally require a specified formula of precursor

solution and thermal treatment for the deposition of the perovskite layer to obtain a dense film with a small grain size. This processing is necessary to ensure the spatial confinement of excitons for radiative recombination,[123] but renders the device fabrication process both cumbersome and difficult to reproduce.

Several works have been reported discussing the previously mentioned issues, but a comprehensive solution has not yet been established. Bade *et al*. demonstrated flexible perovskite LEDs on a carbon nanotube (CNT) / polymer substrate, though the high sheet resistance of the CNT network led to lower performance than ITO based devices, and the device could only be bent to a 5 mm radius likely due to the thickness of the active layer.[124] Devices have been developed with structures such as single layer perovskite LEDs that avoid the use of PEDOT:PSS and other interfacial layers subject to solvent attack,[125] but more complicated structures are required for the realization of optimal charge injection, necessitating materials that can be compatible with commonly used process flows. Dense perovskite films have been reported by embedding perovskite within a polymer matrix,[125,126] yet the fabrication process is complicated and resulting devices have not been shown to be flexible.

As an alternative route to the fabrication of efficient perovskite LEDs, organometal halide perovskite quantum dots (QDs) can be utilized in replacement of perovskite films. Perovskite QDs can be processed into thin solid films in nonpolar solvents, and have shown enhanced PL properties, broadened scope of device architecture, and promising device performance.[124,126–129] Moreover, conventional inorganic QDs have been demonstrated to retain functionality upon mechanical deformation in flexible devices.[130,131] In this regard, colloidal perovskite QDs are well suited for application in flexible EL devices. Herein, we report on the use of colloidal

$CH_3NH_3PbBr_3$ QDs for the fabrication of efficient, flexible green LEDs. First, the use of colloidal perovskite QDs to ameliorate the aforementioned issues is elucidated upon, with the resulting device built on highly flexible composite silver nanowire (AgNW) / polymer anodes to realize highly flexible perovskite LEDs. Second, we report on the engineering of the hole transport layer (HTL) to enhance hole injection into the active perovskite QD layer for efficient charge transfer and high efficiency. The resulting devices exhibit current and power efficacies of 10.4 cd/A, and 8.1 lm/W, respectively, and an external quantum efficiency (EQE) of 2.6 % at 1000 cd/$m^2$. Moreover, with regards to mechanical performance, the devices could be bent to a maximum bending radius of 2.5 mm, or be subjected to 1000 cycles of bending and unbending at a radius of 4 mm while maintaining the performance metrics above. These results demonstrate the validity of the use of perovskite QDs for the fabrication of high performing perovskite LEDs, and its application for the future of flexible electronics.

# 4.2. Experimental Section

## 4.2.1. Materials

Colloidal $CH_3NH_3PbBr_3$ QDs were synthesized according to the emulsion synthesis described in our previous reports. AgNWs were purchased from Zhejiang Kechuang Advanced Materials Co. Ethoxylatedbisphenol-A dimethacrylate (SR540) and ethoxylated 6 trimethylolpropanetriacrylate (SR499) were supplied by Sartomer USA. PEDOT:PSS (Clevios™ P VP AI 4083) was purchased from Heraeus. PVK, TAPC and TmPyPB were purchased from Sigma-Aldrich.

## 4.2.2. Fabrication of AgNW-polymer composite electrode

AgNW solution in IPA was drawn down on a release glass substrate using a Meyer rod, followed by post-treatment processing comprising annealing at 150 °C for 3 min, soaking in DI water for 10 min, and a second annealing at 165 °C for 8 min. The AgNW coated glass slides were introduced in a Fiji ALD system from Cambridge NanoTech, where aluminum oxide ($Al_2O_3$) and zinc oxide (ZnO) were deposited conformally around the AgNWs from precursors of trimethylaluminum (TMA) and $H_20$ for $Al_2O_3$, and diethyl zinc (DEZ) and $H_20$ for ZnO. The pulse and purge times for the precursors of $Al_2O_3$ were 0.06 and 30 seconds, respectively, while the corresponding times for the precursors for ZnO were 0.06 / 45 seconds, and 0.06 / 60 seconds for DEZ and $H_20$, respectively. Following removal from the ALD chamber, a second release glass substrate was placed on top of the AgNW coated glass with a spacer layer introduced, wherein a monomer solution comprising SR540, SR499, and 2,2-dimethoxy- 2-phenylacetophenone (photoinitiator, Sigma-Aldrich, Inc. St. Louis, Missouri) at a weight ratio

1:2: 0.015 was flowed in between. The sandwich structure was exposed to UV irradiation of 365 nm, and the resulting freestanding AgNW composite film was peeled off the glass substrates.

### 4.2.3. Characterization of $CH_3NH_3PbBr_3$ QDs

Transmission electron microscopy (TEM) was performed using a FEI T12 Quick CryoEM and CryoET microscope operated at 120 eV. Scanning electron microscopy (SEM) images were taken on an S-4800 microscopy (Hitachi, Ltd., Japan). The PLQY of diluted QD solutions were determined using a fluorescence spectrometer with an integrated sphere (C9920-02, Hamamatsu Photonics, Japan) excited at a wavelength of 450 nm using a blue LED light source. Cyclic voltammetry (CV) measurements were recorded on a 660D electrochemical workstation, using glassy carbon as the working electrode and platinum as the counter electrode. The reference electrode was Ag/Ag+ (Ag wires with 0.01 M $AgNO_3$ in acetonitrile). $CH_3NH_3PbBr_3$ QDs in toluene were dropped on the working electrode to form a uniform film. The CV curve was obtained under a scanning rate of 10 mV/s. UV-vis absorption spectra of QDs dissolved in toluene was measured using a Shimadzu UV-1700 spectrophotometer, while photoluminescence spectra were taken with a F-380 fluorescence spectrometer from Photon Technology International.

### 4.2.4. Characterization of AgNW-polymer composite electrode

Atomic force microscopy (AFM) was carried out on a Dimension Icon Scanning Probe Microscope from Bruker. Transmittance spectra were obtained with a Shimadzu UV-1700 spectrophotometer. Bending tests were performed on a motorized linear stage with built-in controller (Zaber Technologies Inc.). A Keithley 2000 digital multimeter was used to monitor the resistance change.

### 4.2.5. Device fabrication

Substrates of either ITO/glass or AgNW-polymer composite electrode were sequentially washed with deionized water, acetone, and IPA. ITO/glass substrates were treated with UV ozone for 15 min. In a typical fabrication, PEDOT:PSS was spun onto the substrate at 4000 rpm, after a 30 min anneal at 120 °C, the solution processed devices were introduced into a nitrogen atmosphere glovebox. 10 mg/mL PVK:10wt% TAPC in 1,2-dichlorobenzene was sequentially spun at 4000 RPM for 1 min and annealed at 110 °C for 20 min. Following PVK: TAPC deposition, the active $CH_3NH_3PbBr_3$ QDs were dispersed in toluene (2.5 mg/mL), spun on the HTL, and annealed at 110 °C for 15 min. TmPyPB, CsF and Al were thermally evaporated at a pressure < $10^{-6}$ mbar with thicknesses of 40, 1, and 80 nm and a deposition rate of 1, 0.1, and 5 Å/s, respectively.

### 4.2.6. Characterizations of $CH_3NH_3PbBr_3$ QD-LED

Film thickness was measured with a Dektak Profilometer. Electroluminescence data was collected with a PR-655 spectrophotometer from Photo Research, Inc. Electrical measurements for the QD-LEDs were carried out in a nitrogen atmosphere glove box with a Keithley 2400 and Keithley 2000 SourceMeter unit connected to a calibrated silicon photodiode for L-V-J measurements. All characterization tests were carried out at room temperature.

# 4.3. Results and Discussion

## 4.3.1. $CH_3NH_3PbBr_3$ quantum dot characterization

Colloidal $CH_3NH_3PbBr_3$ QDs were synthesized according to a previously reported emulsion synthesis.[132] Perovskite precursors $PbBr_2$ and $CH_3NH_3$ were dissolved into dimethylformamide (DMF) along with coligands *n*-octylamine and oleic acid. Following precursor formation, the perovskite solution was dropped into a poor solvent such as toluene in a fixed ratio under vigorous stirring to aggregate the precursor into perovskite nanoparticles, evidenced by the formation of a yellow-green colloidal solution. Tert-butanol or acetone was used as a demulsifier to aid in the demulsion process. The colloidal solution was subsequently centrifuged to remove excessively large aggregations, and dried into powder for further use. The resulting $CH_3NH_3PbBr_3$ QDs have an average diameter of 7.2 ± 1.7 nm as illustrated in the transmission electron microscopy (TEM) image in **Figure 4.1a**, Quantum size confinement leads to discrete levels, and the optically allowed transitions between these levels give rise to discrete absorption bands in their UV−vis absorption spectrum, with the lowest energy excitonic band centered at 516 nm. The PL spectrum illustrates a sharp emission peak at 521 nm, with a narrow full width at half maximum (FWHM) of 21 nm. Both the absorbance and PL spectra are presented in **Figure 4.1b**. The absolute photoluminescence quantum yields (PLQY) of these $CH_3NH_3PbBr_3$ QDs in toluene was measured to be 78 ± 1 %, comparable to the traditionally used core-shell QDs.[23, 24]

The flexibility of thin films of $CH_3NH_3PbBr_3$ QDs was first investigated by spin-coating the QD dispersion in toluene onto flexible PET substrates. Scanning electron microscopy (SEM) images before and after ten cycles of repeated bending and unbending to a radius of 2.5 mm are

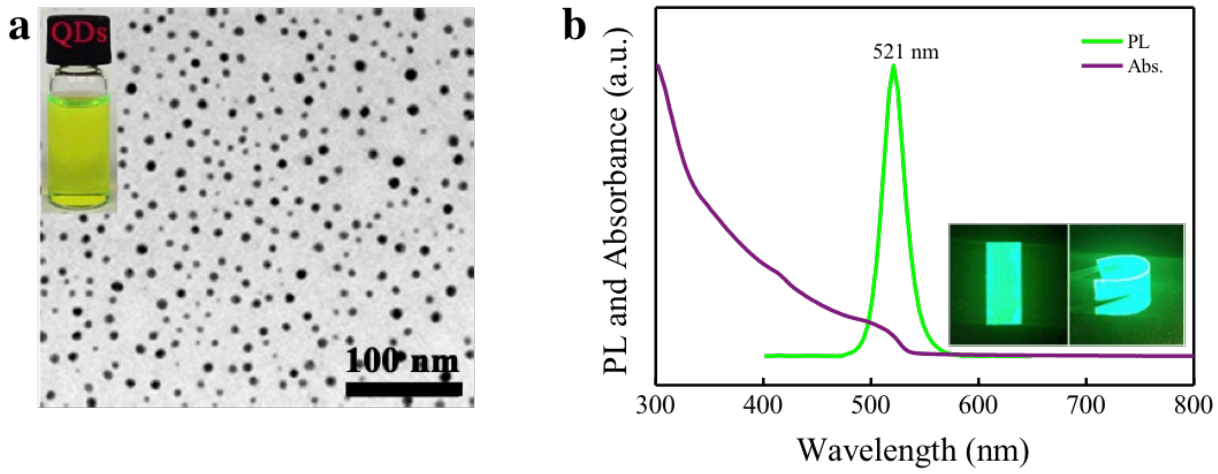


**Figure 4.1. | Characterization of $CH_3NH_3PbBr_3$ QDs.** a) Transmission electron microscopy (TEM) image of the $CH_3NH_3PbBr_3$ QDs, with an optical image of $CH_3NH_3PbBr_3$ QD solution in toluene shown in the inset. a) PL and absorbance spectra of the $CH_3NH_3PbBr_3$ QD film, with optical images of flexible $CH_3NH_3PbBr_3$ QD thin films under UV irradiation illustrated in the inset.

illustrated in **Figure 4.2a**. Before being subjected to mechanical deformation, the QDs form close-packed thin films, a requirement for high performing devices, as pinholes within the film lead to electrical leakage and degradation of EL performance. After cycles of repeated bending, the formation of only nanoscale cracks smaller than 10 nm is evident, signaling the capability of the QD films to retain high PL properties under mechanical deformation. In contrast, the bending of polycrystalline perovskite thin films on the same flexible substrate led to unrecoverable micrometer sized cracks (**Figure 4.2b**). This enhanced mechanical durability of perovskite QD-based flexible thin films over perovskite films can be attributed to the formation of thinner layers (on the order of tens of nanometers) due to the smaller particle size of the QDs. The perovskite films observed in **Figure 4.2a** are significantly thicker, on the order of hundreds of nanometers, due to their larger grain size (~ 50 nm).

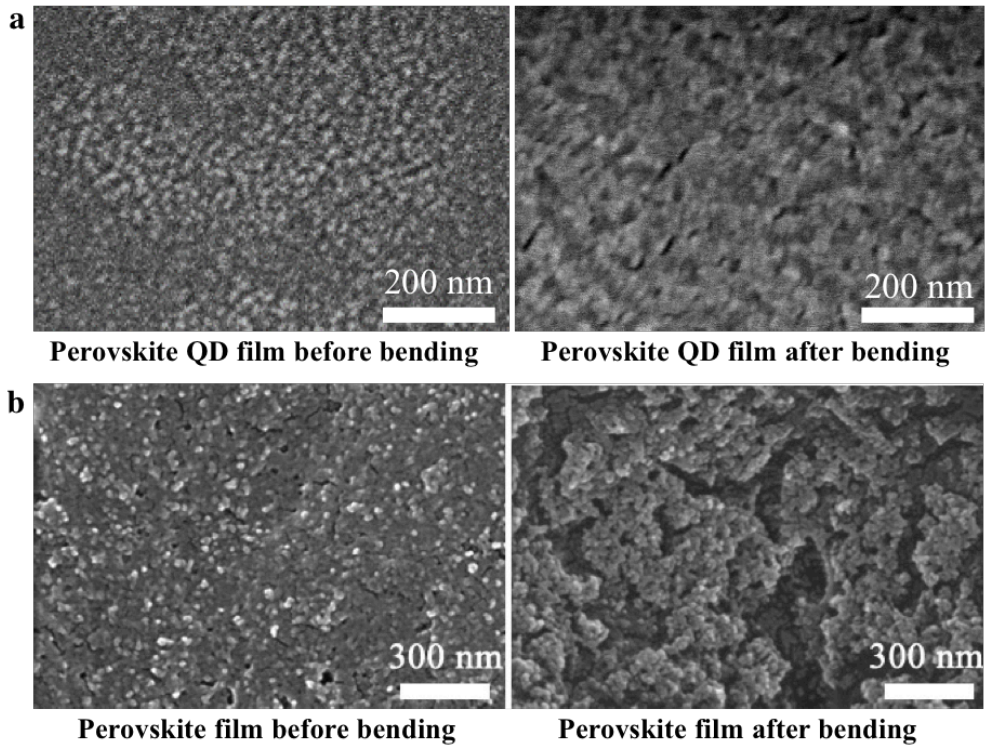


**Figure 4.2 | SEM images of perovskite thin films on PET before and after bending.** a) SEM images of flexible thin films of $CH_3NH_3PbBr_3$ QDs before (left) and after (right) bending. b) SEM images of polycrystalline perovskite thin films before (left) and after (right) bending.

## 4.3.2. Flexibility of AgNW substrate

In addition to the flexibility of the active layer, the substrate for flexible perovskite LEDs must also similarly be flexible, and ensure the capacity of all subsequent layers deposited on top to not degrade from various processing steps throughout the fabrication process. In contrast to the widely used indium tin oxide (ITO) coated PET substrates, AgNW-polymer composite electrode substrates have demonstrated enhanced flexibility to help realize high performing and mechanically durable flexible devices.[102,133] As such, the capacity of the $CH_3NH_3PbBr_3$ QDs for use in highly flexible devices was verified with the fabrication of green LEDs on AgNW

composite substrates. In depth discussion of the device performance and mechanical durability will be elucidated upon in further sections. The AgNW networks were embedded within the top surface of a polymer matrix to afford a smooth conductive surface to mitigate electrical shorting in a process similar to that described in Chapter 3. Briefly, AgNWs were coated on a release glass substrate, and brought into a Fiji ALD chamber for deposition of the adhesive $Al_2O_3$ layer and the protective ZnO layer. After removal from the deposition chamber, the resulting network of conformally coated, thermally and electrically stable nanowires forms a porous structure, which is subsequently infiltrated by a UV curable monomer. Upon UV irradiation, the monomer polymerizes allowing for a freestanding flexible electrode to be peeled off from the release substrate.

Electrodes fabricated based on this method exhibit low surface roughness on the order of ($R_a$) < 1 nm (as can be seen in AFM images of substrates fabricated in a similar manner in **Figure 2.5c** and **Figure 3.12a**), which is critical for minimization of leakage current and potential shorts for devices. Furthermore, the substrates also possess high optoelectronic properties, recording a low sheet resistance of 10 ohm per square at a transmittance of 86 % at 550 nm (**Figure 4.3a**). These optoelectronic properties for AgNW electrodes exceed the performance metrics of its ITO/glass counterpart, thus allowing for the AgNW composited electrode to serve as a platform for the fabrication of high performance, perovskite QD based LEDs. Most importantly for this work, in addition to the low surface roughness and superior optoelectronic properties when contrasted with ITO, the AgNW composite electrodes also exhibit significantly enhanced mechanical stability, with no resistance change observed after 1000 cycles of bending and

unbending to a radius of 4 mm (**Figure 4.3b**). This mechanical robustness is not observed in ITO, as the brittle and rigid material cracks lends itself to unrecoverable cracks.

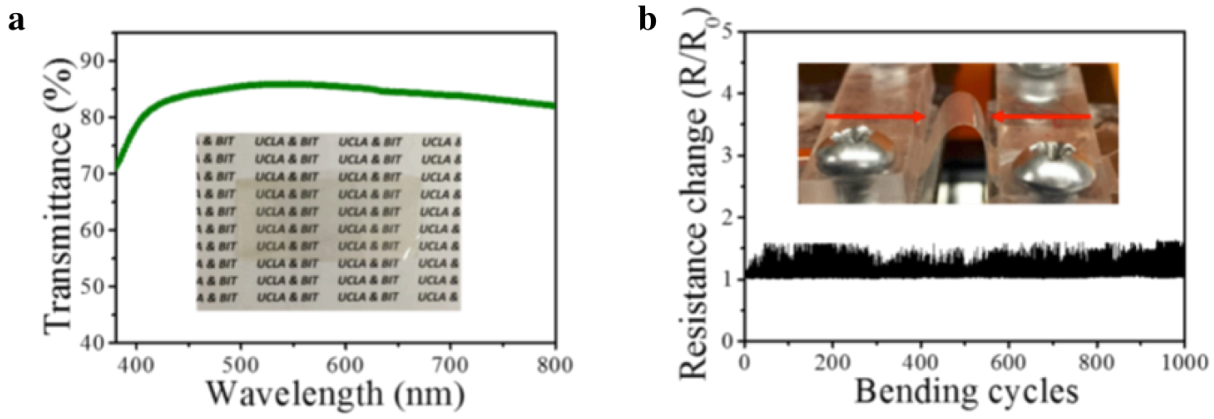


**Figure 4.3 | Characterization of a flexible AgNW substrate.** a) Transmittance spectrum of the AgNW-polymer based electrode, with an optical image of the flexible electrode with thickness of 90 microns shown in the inset. b) Normalized resistance change of the flexible AgNW-polymer composite substrate as a function of bending cycles to a bending radius of 4 mm. Mechanical bending apparatus shown in the inset.

## 4.3.3. Fabrication of flexible, green-emitting perovskite QD LEDs

In addition to the flexibility afforded to the LEDs by the flexible substrate and emissive layer, high electronic performance must also be realized through careful engineering to ensure the cohesive functionality of all other layers. This cohesive functionality ensures balanced and efficient charge carrier transport and injection, determinative factors of high device performance.[134] The $CH_3NH_3PbBr_3$ QDs were determined through cyclic voltammetry measurements (Figure S3) to have a deep highest occupied molecular orbital (HOMO) of -6.4 eV and lowest unoccupied molecular orbital (LUMO) of -3.7 eV. This deep lying HOMO level easily lends itself to charge imbalance in the $CH_3NH_3PbBr_3$ QD layer, as excess electron injection may occur due to the presence of a large hole injection barrier between the QD layer and common HTL materials. With consideration given to both the balance of carrier injection, in

addition to processing feasibility, green LEDs were designed and fabricated with a sandwich structure (Figure 2a) of AgNW-polymer composite substrate / poly(3,4-ethylenedioxythiophene) polystyrene sulfonate (PEDOT:PSS) (40 nm) / poly-(N-vinyl carbazole) (PVK):4,4'-Cyclohexylidenebis[N,N-bis(4-methylphenyl)benzenamine](TAPC) (40nm) / $CH_3NH_3PbBr_3$ QDs (20 nm) / 1,3,5-Tri(m-pyridin-3-ylphenyl)benzene (TmPyPB) (40 nm) / cesium fluoride (CsF) (1 nm) /aluminum (Al) (90 nm).. TmPyPB was selected as the ETL due to its high electron mobility ($10^{-4}$-$10^{-3}$ $cm^2/V$ s),[135] and barrier free injection to the $CH_3NH_3PbBr_3$ QDs, which can be realized due to the lower lying LUMO of TmPyPB (-2.7 eV) with respect to $CH_3NH_3PbBr_3$ QDs.[135] However, the deep lying HOMO of the QDs necessitates a similarly high HOMO of HTLs for efficient hole injection into the $CH_3NH_3PbBr_3$ QD layer. As such, PVK was selected from the subset of solution processable hole transport polymers for utilization as the HTL due to its deep lying HOMO of -5.8 eV.[136]

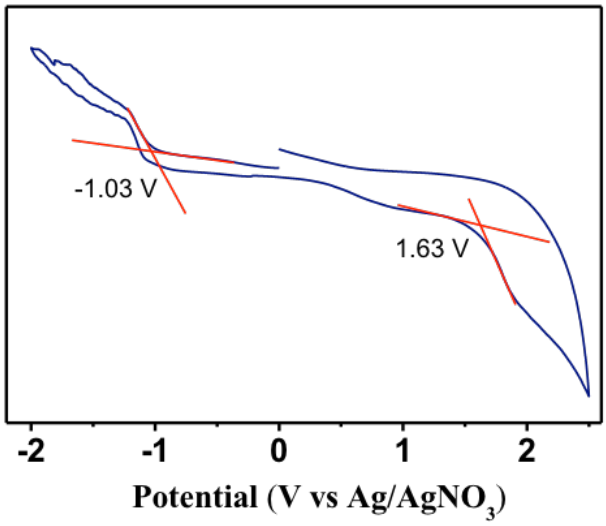


**Figure 4.4.** Cyclic voltammetry of a $CH_3NH_3PbBr_3$ QD film, with the dashed red lines drawn to determine the onset redox potentials.

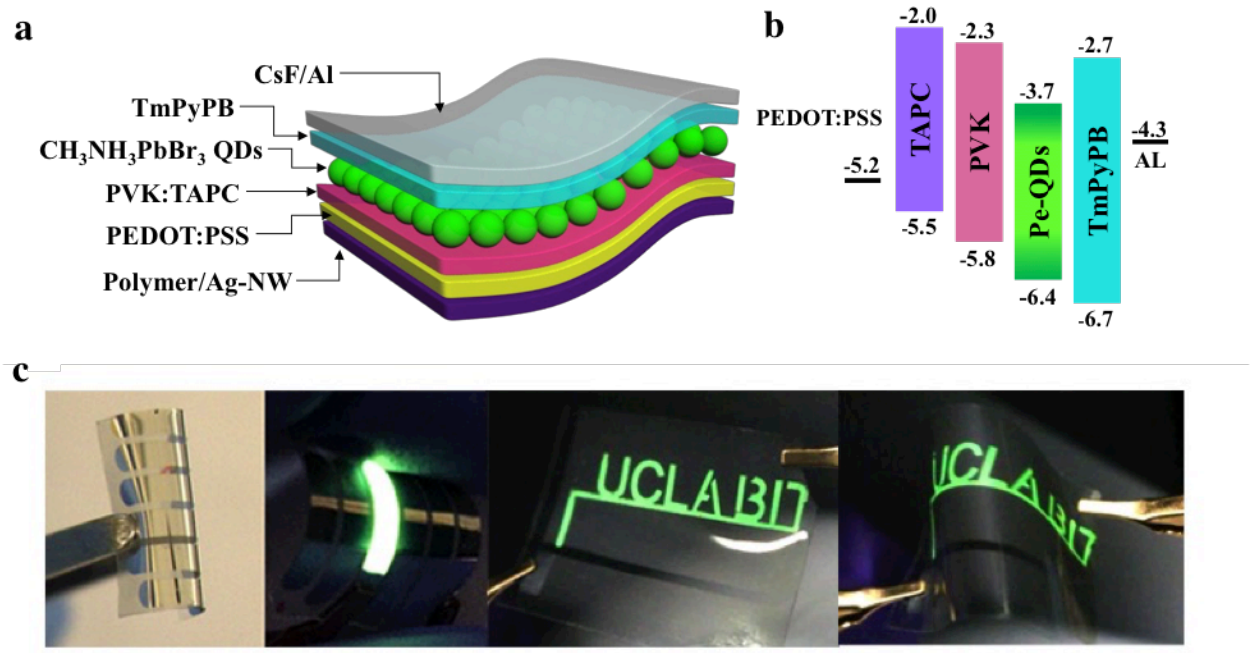


**Figure 4.5 | Flexible, green-emitting perovskite QD LEDs.** a) Cartoon of the sandwich structure used for the fabrication of flexible $CH_3NH_3PbBr_3$ QDs based LEDs. b) Schematic of the energy diagram of the sandwich structure used for the fabrication of QD LEDs. c) Optical images of the flexible $CH_3NH_3PbBr_3$ QDs based LEDs off and on (left) with active area of 0.12 $cm^2$ ; devices spelling out the abbreviations of UCLA and BIT when flat (center); and mechanically bent (right).

Though PVK was selected due to its relatively high HOMO, an inherent drawback of the material is its low hole mobility, on the order of $10^{-6}$ $cm^2/Vs$.[134] Furthermore, even with its relatively high HOMO, a hole injection barrier of 0.6 eV from PEDOT:PSS into PVK is still present with this structure. To ameliorate these issues, 4,4'-Cyclohexylidenebis[N,N-bis(4-methylphenyl) benzenamine] (TAPC) was admixed in PVK. Because TAPC possesses a very high hole mobility of ~ $10^{-2}$ $cm^2/Vs$,[137] hole transport in the PVK-TAPC blended system can occur via hopping amongst sites associated with the TAPC molecules.[138] In addition, as illustrated in the energy diagram of the sandwich structure in **Figure 2b**, the incorporation of TAPC in the HTL results in energy barriers between the HOMOs of PEDOT:PSS and TAPC,

TAPC and PVK, and PVK and $CH_3NH_3PbBr_3$ QDs of 0.3 eV, 0.3 eV and 0.6 eV, respectively, significantly reducing the barrier for hole injection into the QD layer. As a result, the molecularly doped polymer hole transport layer of PVK:TAPC simultaneously reduces the hole injection barrier and improves hole transport mobility for balanced charge carriers in the device. **Figure 2c** illustrates various green LEDs in the on and off state using this structure.

## 4.3.4. Optimization of PVK:TAPC concentration

Because of each material's inherent benefits and drawbacks, the optimization of the concentration between TAPC and PVK is critical for device performance. To optimize this concentration, hole-only devices were fabricated with the sandwich structure AgNW composite electrode / PEDOT:PSS (40 nm) / PVK: x% TAPC (40 nm), where x = 0, 10, 20) / $CH_3NH_3PbBr_3$ QDs (20 nm) /$MoO_3$ (5 nm) / Al. Electron-only devices were also fabricated with the sandwich structure Al / $CH_3NH_3PbBr_3$ QDs (20 nm) / TmPyPB (40 nm) / CsF (1 nm) / Al. The schematics of these hole-only and electron-only devices are depicted in **Figure 4.6a**, with **Figure 4.6b** illustrating the *J-V* curve of these devices. It is evident from the *J-V* curves that the hole-only devices without TAPC exhibit approximately a two order of magnitude lower current density than that observed in electron-only devices. This discrepancy in current density implies that electrons are the dominant carrier in Pe-QD-LEDs utilizing pristine PVK as the HTL and TmPyPB as the ETL.

With the addition of increasing concentrations up to 10% of TAPC into PVK, the hole current density is observed to increase as a result of the reduced barrier for injection and enhanced hole mobility. At a ratio of PVK:10%TAPC, a comparable current density is observed in the hole-only device and the electron-only device, signifying a balance between carrier injection in the

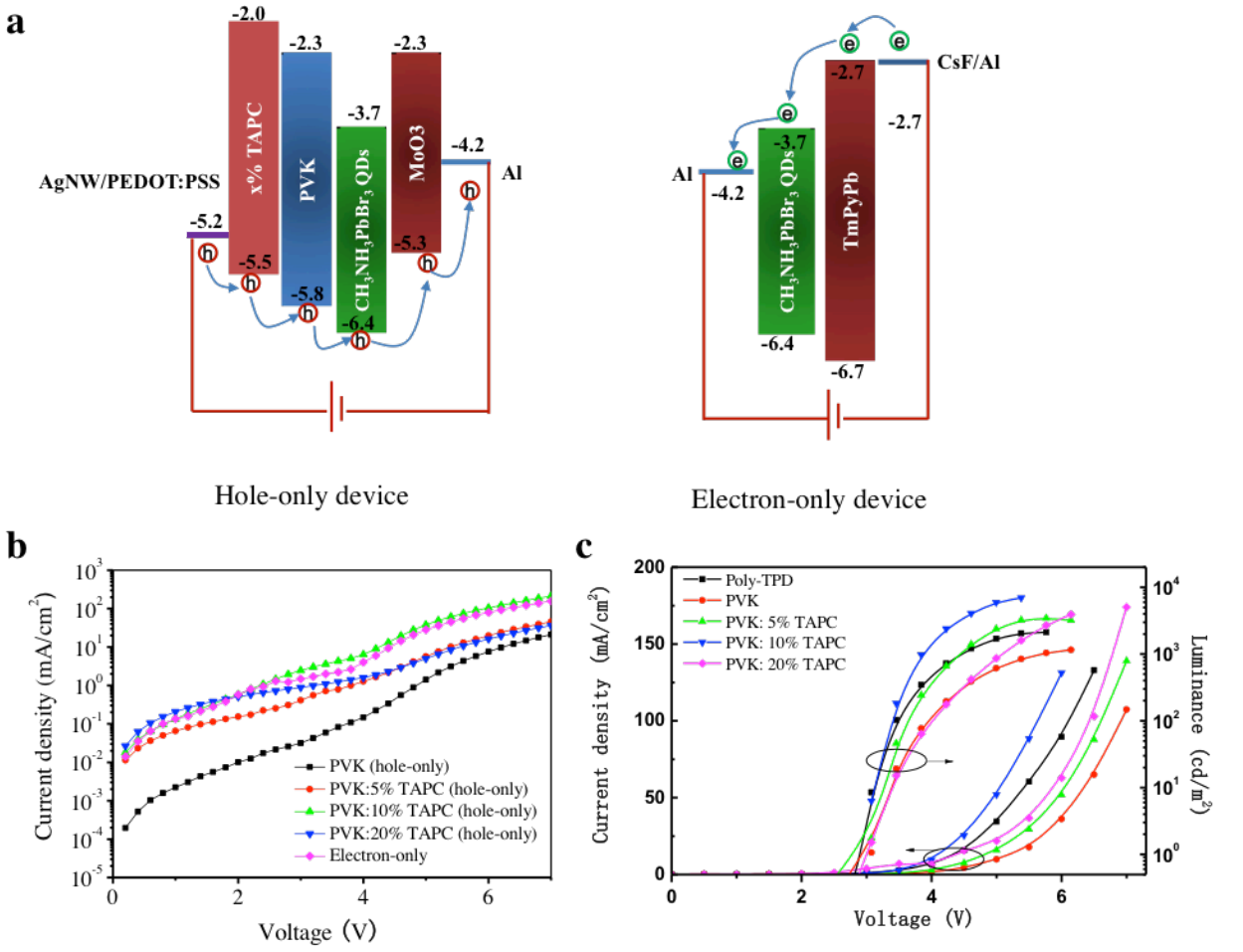


**Figure 4.6 | Optimization of the PVK:TAPC concentration.** a) Schematics of the energy diagram for hole-only (left) and electron-only (right) device structures designed for determination of balanced charge injection into the $CH_3NH_3PbBr_3$ QD layer. b. *J-V* curve for hole-only and electron-only devices. c. *L-V-J* characteristics of Pe-QD-LEDs with poly-TPD, PVK and PVK:x% TAPC (x = 5, 10, 20) as the HTL on ITO glass.

Pe-LEDs. However, with further increase in TAPC concentration, a sharp decrease in current density was observed due to morphological issues brought about due to the well-known poor film quality of TAPC.[139] As a validation of the improved ability of the bi-material HTL to realize efficient and balanced hole injection, $CH_3NH_3PbBr_3$ QD based LEDs were fabricated with PVK: x% TAPC (x= 0, 5, 10, 20) as the HTL on the flexible AgNW-polymer composite electrode. In addition, poly(4-butylphenyl-diphenyl-amine) (Poly-TPD), a widely used hole transport polymer

with a HOMO of -5.1 eV[140] was also investigated as a HTL as an illustration of typical device performance when using a higher lying HOMO HTL. The Luminance (*L*)-Voltage (*V*)-Current density (*J*) characteristics of these devices are illustrated in **Figure 4.6c**. As a result of the increased mobility and hole injection, devices using the bi-material HTL with PVK:10% TAPC exhibit the highest luminance and lowest driving voltage compared to devices with other concentrations of TAPC, PVK-only or Poly-TPD-only as the HTL. Because of this simultaneous increase in luminance and decrease in driving voltage, the 10% TAPC bi-material HTL exhibits the highest current, power and external quantum efficiency (**Figure 4.7)**.

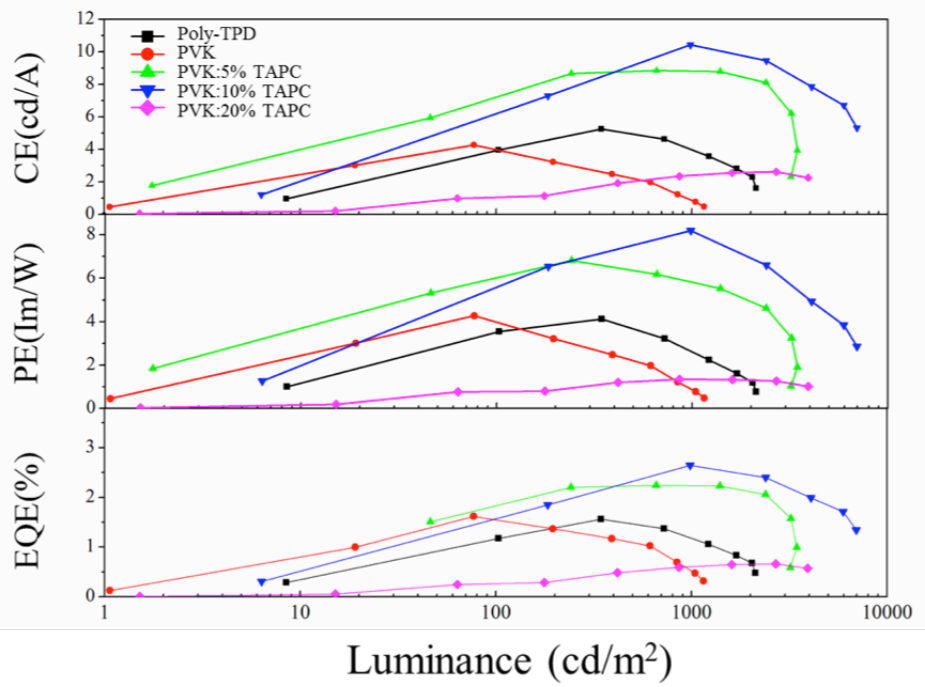


**Figure 4.7.** Current effieciency (CE), power efficiecy (PE) and EQE of the QD LEDs utilizing different Poly-TPD, PVK, and PVK:x% TAPC (x = 5, 10, 20%).

## 4.3.5. Device performance using PVK:10% TAPC as the HTL

After determination of the ideal PVK:TAPC concentration for optimal charge balance, all

subsequent devices were fabricated with the sandwich structure AgNW-polymer composite substrate / PEDOT:PSS / PVK:10% TAPC / CH3NH3PbBr3 QDs / TmPyPB / CsF / Al. The EL spectrum of the device (**Figure 4.8a**) validates the emission as an ideal color-saturated green peaking at 524 nm with Commission Internationale de l'Eclairage (CIE) color coordinates of (0.14, 0.77), and a narrow FWHM of ~24 nm, consistent with the QD's PL spectrum with luminescent peak centered at 521 nm and FWHM of 21 nm (**Figure 4.8a**). The L-J-V characteristics of the green LEDs are shown in Figure 4.9b. These devices exhibit good diode characteristics with a turn-on voltage of 2.9 eV and maximum luminance of 6960 cd/m2. When

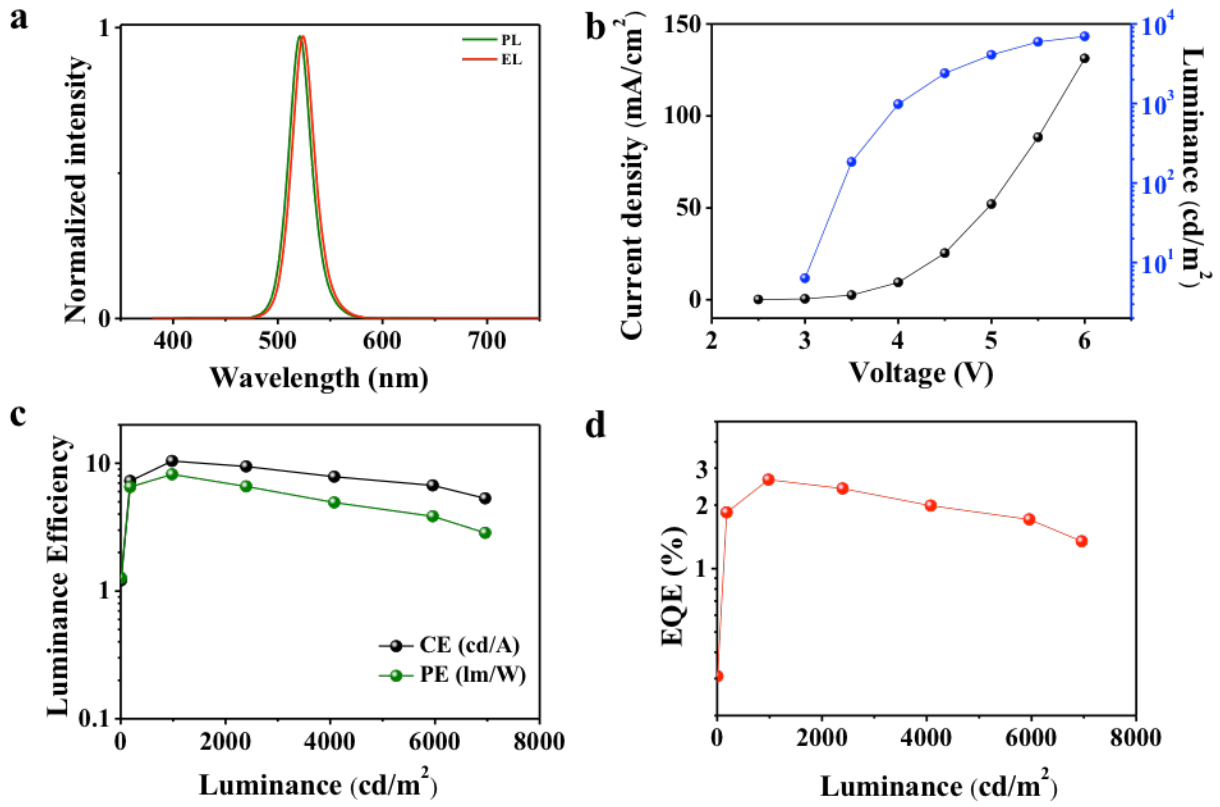


**Figure 4.8 | EL performance of the flexible $CH_3NH_3PbBr_3$ QDs based LED.** a) PL spectrum of $CH_3NH_3PbBr_3$ QDs in toluene and. EL spectrum of the flexible $CH_3NH_3PbBr_3$ QDs based LED. b) *L-V-J* characteristics of a representative flexible $CH_3NH_3PbBr_3$ QD LED. (c) Current and power efficiency of a representative flexible $CH_3NH_3PbBr_3$ QD LED. d) EQE of a representative flexible $CH_3NH_3PbBr_3$ QD LED.

compared to the control device on ITO/glass, the flexible LED based on the AgNW composite substrate has a similar luminance at the same driving voltage, but a lower current density, indicative of higher luminescent efficiency (**Figure 4.9a**). **Figure 4.8c** and **Figure 4.8d** illustrates a representative example of the luminance efficiency and EQE of the flexible green $CH_3NH_3PbBr_3$ QDs LED, quantified by current efficiency (CE), power efficiency (PE), and EQE at 1000 cd/m$^2$ of 10.5 cd/A, 8.2 lm/W, and 2.7%, respectively. These values represent a 46, 42, and 44% enhancement when compared to the performance metrics obtained for control device fabricated on ITO coated glasses (**Figure 4.9b**). This enhancement in efficiency can be attributed to the reduction of the waveguide mode trapping light due to total internal reflection at the ITO/glass and glass/air interfaces. With the AgNW substrate, light rays originating from low angles of incidence can potentially scatter off of the AgNWs, changing their trajectory to eventually escape the substrate. The increased light escaping through the substrate at the same driving voltage thus increases the luminance efficacy and EQE of the devices.

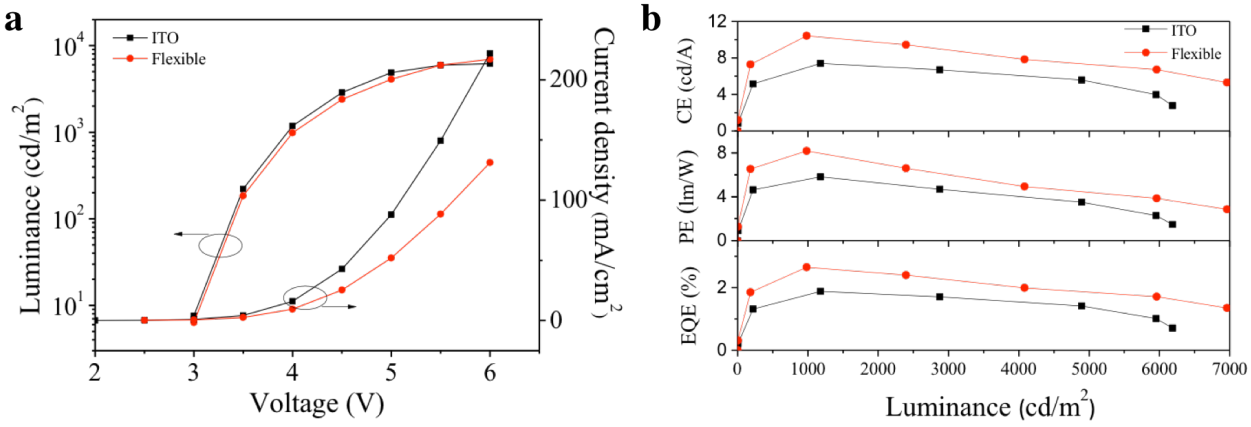


**Figure 4.9 | EL comparison of the perovskite QD LEDs on flexible AgNW substrates and on ITO/glass.** a) *L-V-J* characteristics. b) Current efficiency, power efficiency and EQE.

## 4.3.6. Flexibility of the green-emitting, perovskite QD LED

Though the validity of the use of the active layer and substrate in flexible devices was touched upon previously, the limits to the mechanical robustness of the green LEDs was quantified by measuring the luminance of the flexible $CH_3NH_3PbBr_3$ QDs based LED under different bending radii when driven at a driving voltage of 3.5 V. The flexible devices were bent using the clamps of a sample holder, while luminance detection was conducted using a PR-655 Spectra Scan Spectroradiometer with detection spot size of 0.89 mm in diameter (MS-75 and SL-1X lens) vertically positioned above the bent device. As seen in **Figure 4.10a**, the luminance of the device decreased slightly from the initial 184 cd/m$^2$ to 157, 154 and 147 cd/m$^2$ at a bending radius of 5.5 mm, 4 mm and 2.5 mm, respectively, representing a decrease of 15%, 16% and 20%. When relaxed to its equilibrium flat shape, the measured luminance was 178 cd/m$^2$, achieving a recovery of 97% of its original luminance. The decline in luminance with bending and subsequent restoration upon relaxation is attributed to the reduced current density at the same bias voltage (**Figure 4.10b**). This reduced current density is a result of the increased sheet resistance of the AgNW-polymer composite electrode substrates when subjected to bending due to loss of interconnection between nanowires, especially in regions of high local strain. (**Figure 4.3b**). As **Figure 4.3b** additionally shows the restoration of the sheet resistance upon relaxation, the corresponding recovery of luminance highlights the mechanical durability of the perovskite QD film, as is pictorially evident in **Figure 4.2a**. A cycling test of 1000 bending and unbending cycles to a radius of 4 mm was also conducted, with the results shown in **Figure 4.10c**. At a bias voltage of 3.5 V, the device luminance exhibits a steady luminance of 170±4 cd/m$^2$, indicating both high flexibility and bending stability for the perovskite QDs based LED device on the

flexible AgNW composite electrodes.

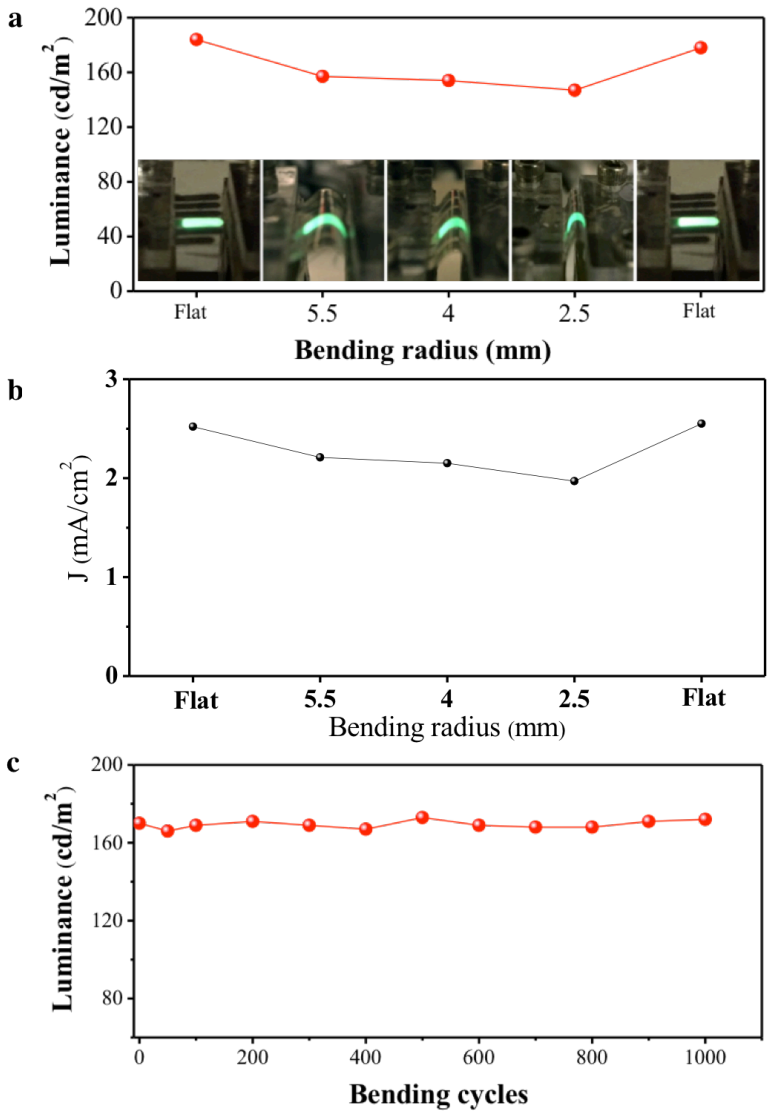


**Figure 4.10 | Bending characteristics of the flexible $CH_3NH_3PbBr_3$ QDs based LED.** a) Luminance of the flexible $CH_3NH_3PbBr_3$ QDs based LED when driven at 3.5 V and bent to a bending radius of ∞ (flat), 5.5 mm, 4 mm, 2.5 mm and ∞, respectively. b) Current density (*J*) of the flexible perovskite QD-LEDs operated at 3.5 V with bending radius of ∞ (flat), 5.5 mm, 4 mm, 2.5 mm and ∞, respectively. c) Luminance of the perovskite QD-LED as a function of bending and unbending cycles to a radius of 4 mm.

# 4.4. Conclusion

Highly flexible $CH_3NH_3PbBr_3$ QDs based LEDs have been fabricated on AgNW composite substrates. The development of perovskite LEDs based on these QDs mitigates issues commonly found in LEDs based on perovskite films: low flexibility due to thick active layers and large grain sizes, limited device architecture due to very polar aprotic solvents used for deposition of the active layer, and a cumbersome fabrication process. Upon fabrication of perovskite QDs into a green LED, high flexibility and bending stability was observed, enabled by the ultra-thin QD layer. The dispersion of the $CH_3NH_3PbBr_3$ QDs in a non-polar solvent allows the employment of a molecularly doped HTL to enhance hole injection into the deep HOMO level of the QDs. The HTL was further engineered by admixing PVK with TAPC to take advantage of the deep HOMO of PVK and the high hole mobility of TAPC. The flexible QDs based LED utilizing this bi-material HTL exhibit high current and power efficiencies of 10.4 cd/A, 8.1 lm/W, respectively, and an EQE of 2.6 % at a brightness of 1000 cd/m$^2$. These performance metrics are recoverable after being bent to a bending radius of 2.5 mm, or after repeated cycles of cyclical testing at 4 mm. To our knowledge, this is the first report of highly flexible and efficient $CH_3NH_3PbBr_3$ QDs based LEDs. This study paves a fundamental path for material and device design towards highly flexible and efficient perovskite LEDs.

# Chapter 5

# Summary and outlook

## 5.1. Conclusions

The previous chapters in this dissertation detail work done in improving the stability of AgNWs, and the utilization of these enhanced AgNWs for various lighting applications. In Chapter 2, the use of atomic layer deposition for the conformal deposition of a metal oxide around the AgNWs was first presented as a technique to improve the thermal stability of silver nanowires. Prior to the publication of this work, no solutions existed for flexible electrodes which simultaneously protect both the polymer and the conductive portion, while retaining a porous conductive network to allow for the smooth surface required for OLED fabrication. In addition, the highest reports of thermal stability of flexible AgNW electrodes at the time of publication was 230 °C for under ten minutes. With this novel technique, silver nanowires were able to withstand an annealing temperature up to 500 °C while showing only increases in resistance attributed to the temperature dependence of resistivity, and no change in optical performance. This temperature represents a 320 °C increase from the initial onset of thermal

degradation of silver nanowires typically observed. Furthermore, when these thermally stable AgNWs were used in conjunction with a thermally stable, transparent polymer matrix, the freestanding electrodes were able to withstand a temperature of 300 °C for six hours, higher than any previously reports of thermally stable flexible silver nanowires at the time of publications. As a proof of concept, the thermally stable electrode was utilized in a PLED fabrication requiring high temperature processing. Due to the thermal stability afforded by the newly developed technique, the PLEDs using the flexible substrate exhibited comparable performance to those fabricated on ITO/glass. Control devices fabricated on non-thermally stable flexible substrates were non functional as the anodes degraded to a substantial degree during the heat extensive fabrication process.

Using the same concept, these AgNWs were also shown to be electrically stable. The demonstration of electrically stable silver nanowires had been, at the time of publication, not reported, with the only works focusing on silver nanowires under current flow the description of the failure of silver nanowires under operating conditions less stressful than standard operating conditions of various optoelectronic devices. In Chapter 3, discussions first proceeded with the failure mechanism of AgNWs under current flow, where a cascading breakdown of silver nanowires as elevated current densities with progressively more failed nanowires induced electrical breakdown over time. The ability of the conformally coated metal oxide to mitigate electrical failure under typical operating conditions of OLEDs represents one avenue towards electrically stable silver nanowires, which is integral for the adoption of this technology for commercial applications. As a proof of concept, these electrically stable AgNWs were integrated in a new OLED substrate to highlight the differences in lifetime with and without the electrically

stable component.. The OLEDs fabricated on the newly developed substrate exhibited a 140% increase in lifetime when compared to the same OLED structure fabricated on ITO/glass, and a 20% increase when compared to OLEDs fabricated on the newly developed substrate with no conformal metal oxide layer. The 20% discrepancy between OLEDs fabricated on these two substrates was shown to be morphological stability in response to current stressing of the electrically stable substrate.

Chapter 4 presents a flexible light emitting diode based on flexible organometal halide perovskite quantum dots on a silver nanowire based composite electrode. In contrast to the typical thick perovskite films formed from the deposition of perovskite precursors and subsequent post treatment processing, the utilization of perovskite quantum dots as a thin film allows for several improvements. First, as perovskite precursors typically require highly polar solvents for deposition, the elimination of these solvents from the process flow opens up the range of materials to select from, allowing more efficient devices to be engineered. Furthermore, perovskite films are thicker in scale, preventing highly flexible films due to cracking of the active layer. This work demonstrates the use of perovskite quantum dots to prevent prohibitively large, irreversible cracks to form upon mechanical deformation. Furthermore, the performance metrics approach top reported devices based on perovskite films due in part to efficient charge balancing through hole-injection enhancement with a PVK:10% TAPC HTL. The resulting green-emission device exhibits a current efficacy of 10.4 cd/A, power efficacy of 8.1 lm/W, and EQE of 2.6% at a brightness of 1000 cd/m$^2$. These performance metrics were virtually fully recoverable after being bent to a maximum bending radius of 2.5 mm, or 1000 repeated cycles of

bending and unbending to a 4 mm bending radius. At the time of preparation of this dissertation, this is the first report of highly flexible, efficient perovskite LEDs based on $CH_3NH_3PbBr_3$ QDs.

## 5.2. Outlook and future work

The field of lighting, and more broadly, electronics, is poised to make a radical change in upcoming years. These changes and continual progress in improving and developing new materials and structures has the potential to realize a myriad of new applications for a host of different industries by enabling a whole new generation of devices previously only imaged as futuristic, radical extensions of science fiction, or pie in the sky conceptual ideas. More specifically to the scope of this dissertation, future continuation of this work towards the future of next generation electronics can proceed generally in two broad directions.

Though significant strides have been made in improving the stability of AgNWs for use in practical applications, there is still much work to be done. Because the cost of ALD may be prohibitive for large-scale applications, progress into more cost effective solutions must be made. One potential solution is sol-gel processing metal oxide films on the silver nanowires,[141,142] though challenges exist in developing ways to conformally coat the metal oxide around only the AgNW, in addition to mitigating potential damage done to the nanowires during the sol-gel conversion process typically requiring in excess of 200 °C. Furthermore, though elevated thermal and stability have been presented throughout this dissertation, the long-term stability of these nanowires with regards to optoelectronic performance, and the parameters related to that performance should be investigated. In particular, because AgNWs have demonstrated their use in a wide array of applications, ranging from the source-drain electrodes in stretchable TFTs,[30]

the sensing layer in temperatures sensors, and of course, transparent electrodes for a plurality of varying devices,[14,144] the lifetime of these devices with regard to the nanowire component should be examined in stressing conditions equal or exceeding the operating conditions of the device. By developing low-cost, executable methods for the integration of silver nanowires into next generation devices, and demonstrating the validity of their use with regards to performance, stability, and lifetime, huge markets and widespread commercialization become not only possible, but plausible as well.

Pivoting towards the second direction, improvements on the substrate alone can only improve OLED efficiency, lifetime, and overall performance up to a certain degree. As such, continual breakthroughs in the other layers of the OLED stack will need to be achieved. Though significant progress have been made in developing new materials for high performing OLEDs, the lifetime of blue materials still lags behind other materials, anchoring the overall performance of white OLEDs. Thermally activated delayed fluorescence (TADF) emitting materials have emerged as the most likely candidate for blue emitters due to their high efficiency and relatively higher stability.[145,146] However, the wide emission spectra associated with TADF materials, efficiency roll-off at high luminance, and lifetime still remain problems to solve. Looking at modes of light loss within the OLED stack, the approximately 45% of light coupled to the surface plasmon polariton (SPP) mode[147] drives significant research in developing new layers and methods to extract this lost light. With new developments in the materials and layers, device design becomes absolutely critical as well, as strategies such as effective charge / exciton confined emissive layer (EML) structures, and bipolar transportation in the (EML) have proved beneficial in resolving efficiency and stability issues. Unlimited combinations are possible with different materials,

different layers, different thicknesses, and different structures. The optimization of all these different components is no easy task, but steady progress will drive the realization of long lifetime, high color purity, cost effective devices.

The work presented in this dissertation represents but a sliver of what the next generation of electronics may have in store for us. Though the preceding chapters focused on the use of silver nanowires for next generation lighting applications, they also provide a glimpse into the future of flexible and stretchable electronics. The amalgamation of some of the devices discussed within these pages into integrated systems promises a future of electronic skins, consumer tunable electronics, conformal and stretchable energy storing and generating devices, and self-aware autonomous robots. These developments have unparalleled significance in fields of medicine and diagnostics, law enforcement and manufacturing, to name a few. The future of electronics is here, and with innovations such as this next generation of lighting, it promises to be a bright one.

# References


(1) Kumar, A.; Zhou, C. The Race to Replace Tin-Doped Indium Oxide: Which Material Will Win? *ACS Nano* **2010**, *4*, 11–14.

(2) Zeng, X. Y.; Zhang, Q. K.; Yu, R. M.; Lu, C. Z. A New Transparent Conductor: Silver Nanowire Film Buried at the Surface of a Transparent Polymer. *Adv. Mater.* **2010**, *22*, 4484–4488.

(3) Langley, D.; Giusti, G.; Mayousse, C.; Celle, C.; Bellet, D.; Simonato, J.-P. Flexible Transparent Conductive Materials Based on Silver Nanowire Networks: A Review. *Nanotechnology* **2013**, *24*, 452001.

(4) Lee, Y.; Suh, M.; Kim, D.; Lee, D.; Chang, H.; Lee, H. S.; Kim, Y. W.; Kim, T.; Suh, K. S.; Jeon, D. Y. Improved Operational Stability of Polymer Light-Emitting Diodes Based on Silver Nanowire Electrode Through Pre-Bias Conditioning Treatment. *Adv. Funct. Mater.* **2014**, *24*, 6465–6472.

(5) Song, M.; Park, J. H.; Kim, C. S.; Kim, D.-H.; Kang, Y.-C.; Jin, S.-H.; Jin, W.-Y.; Kang, J.-W. Highly Flexible and Transparent Conducting Silver nanowire/ZnO Composite Film for Organic Solar Cells. *Nano Res.* **2014**, *7*, 1370–1379.

(6) Jin, J.; Lee, J.; Jeong, S.; Yang, S.; Ko, J.-H.; Im, H.-G.; Baek, S.-W.; Lee, J.-Y.; Bae, B.-S. High-Performance Hybrid Plastic Films: A Robust Electrode Platform for Thin-Film Optoelectronics. *Energy Environ. Sci.* **2013**, *6*, 1811.

(7) Zhang, X.; Yan, X.; Chen, J.; Zhao, J. Large-Size Graphene Microsheets as a Protective Layer for Transparent Conductive Silver Nanowire Film Heaters. *Carbon N. Y.* **2014**, *69*, 437–443.

(8) Yu, C.; Wu, H.; Chien, C. Effect of Passivation Layer on InGaZnO Thin-Film Transistors

with Hybrid Silver Nanowires as Source and Drain Electrodes as Source and Drain Electrodes. *81101*.

(9) Liu, H.-C.; Lai, Y.-C.; Lai, C.-C.; Wu, B.-S.; Zan, H.-W.; Yu, P.; Chueh, Y.-L.; Tsai, C.-C. Highly Effective Field-Effect Mobility Amorphous InGaZnO TFT Mediated by Directional Silver Nanowire Arrays. *ACS Appl. Mater. Interfaces* **2015**, *7*, 232–240.

(10) Huang, G.-W.; Xiao, H.-M.; Fu, S.-Y. Paper-Based Silver-Nanowire Electronic Circuits with Outstanding Electrical Conductivity and Extreme Bending Stability. *Nanoscale* **2014**, *6*, 8495–8502.

(11) Wu, J.; Agrawal, M.; Becerril, A.; Bao, Z.; Liu, Z.; Chen, Ḱ. Y.; Peumans, P. Organic Light-Emitting Diodes on. *ACS Nano* **2010**, *4*, 43–48.

(12) Kim, K. S.; Zhao, Y.; Jang, H.; Lee, S. Y.; Kim, J. M.; Kim, K. S.; Ahn, J.-H.; Kim, P.; Choi, J.-Y.; Hong, B. H. Large-Scale Pattern Growth of Graphene Films for Stretchable Transparent Electrodes. *Nature* **2009**, *457*, 706–710.

(13) Bae, S.; Kim, H.; Lee, Y.; Xu, X.; Park, J.-S.; Zheng, Y.; Balakrishnan, J.; Lei, T.; Kim, H. R.; Song, Y. Il; *et al.* Roll-to-Roll Production of 30-Inch Graphene Films for Transparent Electrodes. *Nat. Nanotechnol.* **2010**, *5*, 574–578.

(14) Yu, Z.; Li, L.; Zhang, Q.; Hu, W.; Pei, Q. Silver Nanowire-Polymer Composite Electrodes for Efficient Polymer Solar Cells. *Adv. Mater.* **2011**, *23*, 4453–4457.

(15) Li, L.; Yu, Z.; Hu, W.; Chang, C. H.; Chen, Q.; Pei, Q. Efficient Flexible Phosphorescent Polymer Light-Emitting Diodes Based on Silver Nanowire-Polymer Composite Electrode. *Adv. Mater.* **2011**, *23*, 5563–5567.

(16) Yu, Z.; Zhang, Q.; Li, L.; Chen, Q.; Niu, X.; Liu, J.; Pei, Q. Highly Flexible Silver Nanowire Electrodes for Shape-Memory Polymer Light-Emitting Diodes. *Adv. Mater.*

**2011**, *23*, 664–668.

(17) Li, J.; Liang, J.; Jian, X.; Hu, W.; Li, J.; Pei, Q. A Flexible and Transparent Thin Film Heater Based on a Silver Nanowire/Heat-Resistant Polymer Composite. *Macromol. Mater. Eng.* **2014**, *299*, 1403–1409.

(18) Hu, W.; Niu, X.; Li, L.; Yun, S.; Yu, Z.; Pei, Q. Intrinsically Stretchable Transparent Electrodes Based on Silver-Nanowire–crosslinked-Polyacrylate Composites. *Nanotechnology* **2012**, *23*, 344002.

(19) Yun, S.; Niu, X.; Yu, Z.; Hu, W.; Brochu, P.; Pei, Q. Compliant Silver Nanowire-Polymer Composite Electrodes for Bistable Large Strain Actuation. *Adv. Mater.* **2012**, *24*, 1321–1327.

(20) Hu, W.; Niu, X.; Zhao, R.; Pei, Q. Elastomeric Transparent Capacitive Sensors Based on an Interpenetrating Composite of Silver Nanowires and Polyurethane. *Appl. Phys. Lett.* **2013**, *102*.

(21) Liang, J.; Li, L.; Niu, X.; Yu, Z.; Pei, Q. Elastomeric Polymer Light-Emitting Devices and Displays. *Nat. Photonics* **2013**, *7*, 817–824.

(22) Liang, J.; Li, L.; Tong, K.; Ren, Z.; Hu, W.; Niu, X.; Chen, Y.; Pei, Q. Silver Nanowire Percolation Network Soldered with Graphene Oxide at Room Temperature and Its Application for Fully Stretchable Polymer Light-Emitting Diodes. *ACS Nano* **2014**, *8*, 1590–1600.

(23) Yu, Z.; Sun, M.; Pei, Q. Electrochemical Formation of Stable P-I-N Junction in Conjugated Polymer Thin Films. **2009**, 8481–8486.

(24) Yu, Z.; Wang, M.; Lei, G.; Liu, J.; Li, L.; Pei, Q. Stabilizing the Dynamic P - I - N Junction in Polymer Light-Emitting. **2011**, 367–372.

(25) Yu, Z.; Hu, L.; Liu, Z.; Sun, M.; Wang, M.; Grüner, G.; Pei, Q. Fully Bendable Polymer Light Emitting Devices with Carbon Nanotubes as Cathode and Anode. *Appl. Phys. Lett.* **2009**, *95*, 2007–2010.

(26) Liang, J.; Li, L.; Niu, X.; Yu, Z.; Pei, Q. Fully Solution-Based Fabrication of Flexible Light-Emitting Device at Ambient Conditions. *J. Phys. Chem. C* **2013**, *117*, 16632–16639.

(27) Li, L.; Yu, Z.; Chang, C.; Hu, W.; Niu, X.; Chen, Q.; Pei, Q. Efficient White Polymer Light-Emitting Diodes Employing a Silver Nanowire–polymer Composite Electrode. *Phys. Chem. Chem. Phys.* **2012**, *14*, 14249.

(28) Li, L.; Liang, J.; Chou, S.-Y.; Zhu, X.; Niu, X.; ZhibinYu; Pei, Q. A Solution Processed Flexible Nanocomposite Electrode with Efficient Light Extraction for Organic Light Emitting Diodes. *Sci. Rep.* **2014**, *4*, 4307.

(29) Yu, Z.; Niu, X.; Liu, Z.; Pei, Q. Intrinsically Stretchable Polymer Light-Emitting Devices Using Carbon Nanotube-Polymer Composite Electrodes. *Adv. Mater.* **2011**, *23*, 3989–3994.

(30) Liang, J.; Li, L.; Chen, D.; Hajagos, T.; Ren, Z.; Chou, S.-Y.; Hu, W.; Pei, Q. Intrinsically Stretchable and Transparent Thin-Film Transistors Based on Printable Silver Nanowires, Carbon Nanotubes and an Elastomeric Dielectric. *Nat. Commun.* **2015**, *6*, 7647.

(31) Emmott, C. J. M.; Urbina, A.; Nelson, J. Environmental and Economic Assessment of ITO-Free Electrodes for Organic Solar Cells. *Sol. Energy Mater. Sol. Cells* **2012**, *97*, 14–21.

(32) Thejo Kalyani, N.; Dhoble, S. J. Organic Light Emitting Diodes: Energy Saving Lighting Technology - A Review. *Renew. Sustain. Energy Rev.* **2012**, *16*, 2696–2723.

(33) Geffroy, B.; le Roy, P.; Prat, C. Organic Light-Emitting Diode (OLED) Technology:

Materials, Devices and Display Technologies. *Polym. Int.* **2006**, *55*, 572–582.

(34) Reineke, S.; Thomschke, M.; Lussem, B.; Leo, K. White Organic Light-Emitting Diodes: Status and Perspective. *Rev. Mod. Phys.* **2013**, *85*, 1245–1293.

(35) Zmija, J.; Małachowski, M. J. Organic Light Emitting Diodes Operation and Application in Displays. *Arch. Mater. Sci. Eng.* **2009**, *40*, 5–12.

(36) Gather, M. C.; Köhnen, A.; Meerholz, K. White Organic Light-Emitting Diodes. *Adv. Mater.* **2011**, *23*, 233–248.

(37) Hu, L.; Wu, H.; Cui, Y. Metal Nanogrids, Nanowires, and Nanofibers for Transparent Electrodes. *MRS Bull.* **2011**, *36*, 760–765.

(38) Hamaguchi, T.; Omae, K.; Takebayashi, T.; Kikuchi, Y.; Yoshioka, N.; Nishiwaki, Y.; Tanaka, a; Hirata, M.; Taguchi, O.; Chonan, T. Exposure to Hardly Soluble Indium Compounds in ITO Production and Recycling Plants Is a New Risk for Interstitial Lung Damage. *Occup. Environ. Med.* **2008**, *65*, 51–55.

(39) Chen, Z. A Mechanical Assessment of Flexible Optoelectronic Devices. *Thin Solid Films* **2001**, *394*, 201–205.

(40) Ellmer, K. Past Achievements and Future Challenges in the Development of Optically Transparent Electrodes. *Nat. Photonics* **2012**, *6*, 808–816.

(41) Rowell, M. W.; Topinka, M. a.; McGehee, M. D.; Prall, H. J.; Dennler, G.; Sariciftci, N. S.; Hu, L.; Gruner, G. Organic Solar Cells with Carbon Nanotube Network Electrodes. *Appl. Phys. Lett.* **2006**, *88*, 86–89.

(42) Zhang, D.; Ryu, K.; Liu, X.; Polikarpov, E.; Ly, J.; Tompson, M. E.; Zhou, C. Transparent, Conductive, and Flexible Carbon Nanotube Films and Their Application in Organic Light-Emitting Diodes. *Nano Lett.* **2006**, *6*, 1880–1886.

(43) Zou, J.; Yip, H. L.; Hau, S. K.; Jen, A. K. Y. Metal Grid/conducting Polymer Hybrid Transparent Electrode for Inverted Polymer Solar Cells. *Appl. Phys. Lett.* **2010**, *96*, 3–6.

(44) Im, H.-G.; Jin, J.; Ko, J.-H.; Lee, J.; Lee, J.-Y.; Bae, B.-S. Flexible Transparent Conducting Composite Films Using a Monolithically Embedded AgNW Electrode with Robust Performance Stability. *Nanoscale* **2014**, *6*, 711–715.

(45) Im, H.; Jung, S.; Jin, J.; Lee, D.; Lee, J.; Lee, D.; Lee, J. Hybrid Film Using a Surface-Embedded Copper Nanowire Network : A Highly Oxidation-Resistant Copper Nanowire Electrode for Flexible. *ACS Nano* **2014**, *8*, 10973–10979.

(46) Huang, Q.; Shen, W.; Fang, X.; Chen, G.; Yang, Y.; Huang, J.; Tan, R.; Song, W. Highly Thermostable, Flexible, Transparent, and Conductive Films on Polyimide Substrate with an AZO/AgNW/AZO Structure. *ACS Appl. Mater. Interfaces* **2015**, 150210103909000.

(47) Lee, J. Y.; Connor, S. T.; Cui, Y.; Peumans, P. Solution-Processed Metal Nanowire Mesh Transparent Electrodes. *Nano Lett.* **2008**, *8*, 689–692.

(48) Chen, J.; Ahn, H.; Yen, S.; Tsai, Y. Thermally Induced Percolational Transition and Thermal Stability of Silver Nanowire Networks Studied by THz Spectroscopy. *ACS Appl. Mater. Interfaces* **2014**, *6*, 20995–20999.

(49) Kim, A.; Won, Y.; Woo, K.; Kim, C. H.; Moon, J. Highly Transparent Low Resistance ZnO/Ag nanowire/ZnO Composite Electrode for Thin Film Solar Cells. *ACS Nano* **2013**, *7*, 1081–1091.

(50) Xu, Q.; Shen, W.; Huang, Q.; Yang, Y.; Tan, R.; Zhu, K.; Dai, N.; Song, W. Flexible Transparent Conductive Films on PET Substrates with an AZO/AgNW/AZO Sandwich Structure. *J. Mater. Chem. C* **2014**, *2*, 3750.

(51) Chen, S.; Song, L.; Tao, Z.; Shao, X.; Huang, Y.; Cui, Q.; Guo, X. Neutral-pH

PEDOT:PSS as over-Coating Layer for Stable Silver Nanowire Flexible Transparent Conductive Films. *Org. Electron.* **2014**, *15*, 3654–3659.

(52) Göbelt, M.; Keding, R.; Schmitt, S. W.; Hoffmann, B.; Jäckle, S.; Latzel, M.; Radmilović, V. V.; Radmilović, V. R.; Spiecker, E.; Christiansen, S. Encapsulation of Silver Nanowire Networks by Atomic Layer Deposition for Indium-Free Transparent Electrodes. *Nano Energy* **2015**.

(53) Standridge, S. D.; Schatz, G. C.; Hupp, J. T. Toward Plasmonic Solar Cells: Protection of Silver Nanoparticles via Atomic Layer Deposition of TiO2. *Langmuir* **2009**, *25*, 2596–2600.

(54) Dikin, D. a; Stankovich, S.; Zimney, E. J.; Piner, R. D.; Dommett, G. H. B.; Evmenenko, G.; Nguyen, S. T.; Ruoff, R. S. Preparation and Characterization of Graphene Oxide Paper. *Nature* **2007**, *448*, 457–460.

(55) Ji, Z.; Shen, X.; Li, M.; Zhou, H.; Zhu, G.; Chen, K. Synthesis of Reduced Graphene oxide/CeO2 Nanocomposites and Their Photocatalytic Properties. *Nanotechnology* **2013**, *24*, 115603.

(56) Whitney, A. V.; Elam, J. W.; Stair, P. C.; Van Duyne, R. P. Toward a Thermally Robust Operando Surface-Enhanced Raman Spectroscopy Substrate. *J. Phys. Chem. C* **2007**, *111*, 16827–16832.

(57) Guisbiers, G.; Pereira, S. Theoretical Investigation of Size and Shape Effects on the Melting Temperature of ZnO Nanostructures. *Nanotechnology* **2007**, *18*, 435710–435716.

(58) Perez, I.; Robertson, E.; Banerjee, P.; Henn-Lecordier, L.; Son, S. J.; Lee, S. B.; Rubloff, G. W. TEM-Based Metrology for HfO2 Layers and Nanotubes Formed in Anodic Aluminum Oxide Nanopore Structures. *Small* **2008**, *4*, 1223–1232.

(59) Lee, H. Y.; An, C. J.; Piao, S. J.; Ahn, D. Y.; Kim, M. T.; Min, Y. S. Shrinking Core Model for Knudsen Diffusion-Limited Atomic Layer Deposition on a Nanoporous Monolith with an Ultrahigh Aspect Ratio. *J. Phys. Chem. C* **2010**, *114*, 18601–18606.

(60) Song, T. Bin; Chen, Y.; Chung, C. H.; Yang, Y.; Bob, B.; Duan, H. S.; Li, G.; Tu, K. N.; Huang, Y. Nanoscale Joule Heating and Electromigration Enhanced Ripening of Silver Nanowire Contacts. *ACS Nano* **2014**, *8*, 2804–2811.

(61) Zhao, M.; Zhou, X. H.; Jiang, Q. Comparison of Different Models for Melting Point Change of Metallic Nanocrystals. *J. Mater. Res.* **2001**, *16*, 3304–3308.

(62) Elechiguerra, J. L.; Larios-Lopez, L.; Liu, C.; Garcia-Gutierrez, D.; Camacho-Bragado, A.; Yacaman, M. J. Corrosion at the Nanoscale: The Case of Silver Nanowires and Nanoparticles. *Chem. Mater.* **2005**, *17*, 6042–6052.

(63) Sorel, S.; Lyons, P. E.; De, S.; Dickerson, J. C.; Coleman, J. N. The Dependence of the Optoelectrical Properties of Silver Nanowire Networks on Nanowire Length and Diameter. *Nanotechnology* **2012**, *23*, 185201.

(64) Ennis, C. P.; Kaiser, R. I. Mechanistical Studies on the Electron-Induced Degradation of Polymers: Polyethylene, Polytetrafluoroethylene, and Polystyrene. *Phys. Chem. Chem. Phys.* **2010**, *12*, 14884–14901.

(65) Yang, S.; Kwak, S.-Y.; Jin, J.; Kim, J.-S.; Choi, Y.; Paik, K.-W.; Bae, B.-S. Thermally Resistant UV-Curable Epoxy–siloxane Hybrid Materials for Light Emitting Diode (LED) Encapsulation. *J. Mater. Chem.* **2012**, *22*, 8874.

(66) Zilberberg, K.; Gharbi, H.; Behrendt, A.; Trost, S.; Riedl, T. Low-Temperature, Solution-Processed MoO. **2012**.

(67) Takayama, M.; Naka, S.; Okada, H. Organic Light-Emitting Diode with Solution-

Processed Molybdenum Trioxide from Dilute Aqueous Solution. *Jpn. J. Appl. Phys.* **2013**, *52*, 1–4.

(68) Ghaffarzadeh, K.; Bardsley, N. OLED Lighting Opportunities 2015-2025: Forecasts, Technologies, Players: IDTechEx http://www.idtechex.com/research/reports/oled-lighting-opportunities-2015-2025-forecasts-technologies-players-000406.asp (accessed Mar 9, 2016).

(69) Hösel, M.; Angmo, D.; Søndergaard, R. R.; dos Reis Benatto, G. a.; Carlé, J. E.; Jørgensen, M.; Krebs, F. C. High-Volume Processed, ITO-Free Superstrates and Substrates for Roll-to-Roll Development of Organic Electronics. *Adv. Sci.* **2014**, 1–12.

(70) Angmo, D.; Andersen, T. R.; Bentzen, J. J.; Helgesen, M.; Søndergaard, R. R.; Jørgensen, M.; Carlé, J. E.; Bundgaard, E.; Krebs, F. C. Roll-to-Roll Printed Silver Nanowire Semitransparent Electrodes for Fully Ambient Solution-Processed Tandem Polymer Solar Cells. *Adv. Funct. Mater.* **2015**, *25*, 4539–4547.

(71) Dos Reis Benatto, G. a; Roth, B.; Corazza, M.; Søndergaard, R. R.; Gevorgyan, S. a; Jørgensen, M.; Krebs, F. C. Roll-to-Roll Printed Silver Nanowires for Increased Stability of Flexible ITO-Free Organic Solar Cell Modules. *Nanoscale* **2015**, *8*, 318–326.

(72) Yu, Z.; Liu, Z.; Wang, M.; Sun, M.; Lei, G.; Pei, Q. Highly Flexible Polymer Light-Emitting Devices Using Carbon Nanotubes as Both Anodes and Cathodes. *J. Photonics Energy* **2011**, *1*, 11003.

(73) Morales-Masis, M.; Dauzou, F.; Jeangros, Q.; Dabirian, A.; Lifka, H.; Gierth, R.; Ruske, M.; Moet, D.; Hessler-Wyser, A.; Ballif, C. An Indium-Free Anode for Large-Area Flexible OLEDs: Defect-Free Transparent Conductive Zinc Tin Oxide. *Adv. Funct. Mater.* **2016**, *26*, 384–392.

(74) Madaria, A. R.; Kumar, A.; Zhou, C. Large Scale, Highly Conductive and Patterned Transparent Films of Silver Nanowires on Arbitrary Substrates and Their Application in Touch Screens. *Nanotechnology* **2011**, *22*, 245201.

(75) Wang, L.; Matson, D. W.; Polikarpov, E.; Swensen, J. S.; Bonham, C. C.; Cosimbescu, L.; Berry, J. J.; Ginley, D. S.; Gaspar, D. J.; Padmaperuma, A. B. Highly Efficient Blue Organic Light Emitting Device Using Indium-Free Transparent Anode Ga:ZnO with Scalability for Large Area Coating. *J. Appl. Phys.* **2010**, *107*.

(76) Kondakov, D. Y. Device Degradation. In *OLED Fundamentals: Materials, Devices, and Processing of Organic Light-Emitting Diodes*; Gaspar, D. J.; Polikarpov, E., Eds.; CRC Press, 2015; pp. 339–364.

(77) Hsu, S.-Y.; Lee, M.-C.; Lee, K.-L.; Wei, P.-K. Extraction Enhancement in Organic Light Emitting Devices by Using Metallic Nanowire Arrays. *Appl. Phys. Lett.* **2008**, *92*, 13303.

(78) Zhou, L.; Xiang, H.-Y.; Shen, S.; Li, Y.-Q.; Chen, J.-D.; Xie, H.-J.; Goldthorpe, I. a; Chen, L.-S.; Lee, S.-T.; Tang, J.-X. High-Performance Flexible Organic Light-Emitting Diodes Using Embedded Silver Network Transparent Electrodes. *ACS Nano* **2014**, *8*, 12796–12805.

(79) Chang, H.-W.; Tien, K.-C.; Hsu, M.-H.; Huang, Y.-H.; Lin, M.-S.; Tsai, C.-H.; Tsai, Y.-T.; Wu, C.-C. Organic Light‐emitting Devices Integrated with Internal Scattering Layers for Enhancing Optical Out‐coupling. *J. SID* **2011**, *19*, 196–201.

(80) Chang, H. W.; Lee, J.; Hofmann, S.; Hyun Kim, Y.; M??ller-Meskamp, L.; L??ssem, B.; Wu, C. C.; Leo, K.; Gather, M. C. Nano-Particle Based Scattering Layers for Optical Efficiency Enhancement of Organic Light-Emitting Diodes and Organic Solar Cells. *J. Appl. Phys.* **2013**, *113*.

(81) Chen, S.; Qin, W.; Zhao, Z.; Tang, B. Z.; Kwok, H.-S. One-Step Fabrication of Organic Nanoparticles as Scattering Media for Extracting Substrate Waveguide Light from Organic Light-Emitting Diodes. *J. Mater. Chem.* **2012**, *22*, 13386–13390.

(82) Tsujioka, T. T.; Ujii, H. F.; Amada, Y. H.; Akahashi, H. T. Driving Duty Ratio Dependence of Lifetime of Tris ( 8-Hydroxy-Quinolinate ) Aluminum-Based Organic Light-Emitting Diodes. *Jpn. J. Appl. Phys.* **2001**, *40*, 2523–2526.

(83) McCarthy, M. A.; Liu, B.; Donoghue, E. P.; Kravchenko, I.; Kim, D. Y.; So, F.; Rinzler, A. G. Low-Voltage, Low-Power, Organic Light-Emitting Transistors for Active Matrix Displays. *Science (80-. ).* **2011**, *332*, 570–573.

(84) Zhao, J.; Sun, H.; Dai, S.; Wang, Y.; Zhu, J. Electrical Breakdown of Nanowires. *Nano Lett.* **2011**, *11*, 4647–4651.

(85) Khaligh, H. H.; Goldthorpe, I. a. Failure of Silver Nanowire Transparent Electrodes under Current Flow. *Nanoscale Res. Lett.* **2013**, *8*, 235.

(86) Mayousse, C.; Celle, C.; Fraczkiewicz, A.; Simonato, J. Stability of Silver Nanowire Based Electrodes under Environmental and Electrical Stresses. *Nanoscale* **2015**, *7*, 2107–2115.

(87) Spechler, J. a.; Nagamatsu, K. a.; Sturm, J. C.; Arnold, C. B. Improved Efficiency of Hybrid Organic Photovoltaics by Pulsed Laser Sintering of Silver Nanowire Network Transparent Electrode. *ACS Appl. Mater. Interfaces* **2015**, 150508102926006.

(88) Lu, H.; Zhang, D.; Cheng, J.; Liu, J.; Mao, J.; Choy, W. C. H. Locally Welded Silver Nano-Network Transparent Electrodes with High Operational Stability by a Simple Alcohol-Based Chemical Approach. *Adv. Funct. Mater.* **2015**, n/a-n/a.

(89) Chalh, M.; Vedraine, S.; Lucas, B.; Ratier, B. Plasmonic Ag Nanowire Network

Embedded in Zinc Oxide Nanoparticles for Inverted Organic Solar Cells Electrode. *Sol. Energy Mater. Sol. Cells* **2016**, *152*, 34–41.

(90) Sekitani, T.; Zschieschang, U.; Klauk, H.; Someya, T. Flexible Organic Transistors and Circuits with Extreme Bending Stability. *Nat. Mater.* **2010**, *9*, 1015–1022.

(91) Lee, S. K.; Kim, B. J.; Jang, H.; Yoon, S. C.; Lee, C.; Hong, B. H.; Rogers, J. a.; Cho, J. H.; Ahn, J. H. Stretchable Graphene Transistors with Printed Dielectrics and Gate Electrodes. *Nano Lett.* **2011**, *11*, 4642–4646.

(92) Wu, M. Y.; Zhao, J.; Xu, F.; Chang, T. H.; Jacobberger, R. M.; Ma, Z.; Arnold, M. S. Highly Stretchable Carbon Nanotube Transistors Enabled by Buckled Ion Gel Gate Dielectrics. *Appl. Phys. Lett.* **2015**, *107*, 53301-1-053301–053305.

(93) Lipomi, D. J.; Bao, Z. Stretchable, Elastic Materials and Devices for Solar Energy Conversion. *Energy Environ. Sci.* **2011**, *4*, 3314.

(94) Lipomi, D. J.; Vosgueritchian, M.; Tee, B. C.-K.; Hellstrom, S. L.; Lee, J. a; Fox, C. H.; Bao, Z. Skin-like Pressure and Strain Sensors Based on Transparent Elastic Films of Carbon Nanotubes. *Nat. Nanotechnol.* **2011**, *6*, 788–792.

(95) Benight, S. J.; Wang, C.; Tok, J. B. H.; Bao, Z. Stretchable and Self-Healing Polymers and Devices for Electronic Skin. *Prog. Polym. Sci.* **2013**, *38*, 1961–1977.

(96) Cui, Z.; Poblete, F. R.; Cheng, G.; Yao, S.; Jiang, X.; Zhu, Y. Design and Operation of Silver Nanowire Based Flexible and Stretchable Touch Sensors. *J. Mater. Res.* **2014**, *30*, 79–85.

(97) Ge, J.; Sun, L.; Zhang, F. R.; Zhang, Y.; Shi, L. A.; Zhao, H. Y.; Zhu, H. W.; Jiang, H. L.; Yu, S. H. A Stretchable Electronic Fabric Artificial Skin with Pressure-, Lateral Strain-, and Flexion-Sensitive Properties. *Adv. Mater.* **2015**, 722–728.

(98) Wiley, B. J.; Wang, Z.; Wei, J.; Yin, Y.; Cobden, D. H.; Xia, Y. Synthesis and Electrical Characterization of Silver Nanobeams. *Nano Lett.* **2006**, *6*, 2273–2278.

(99) De, S.; Higgins, T. M.; Lyons, P. E.; Doherty, E. M.; Nirmalraj, P. N.; Blau, W. J.; Boland, J. J.; Coleman, J. N. Silver Nanowire Networks as Flexible, Transparent, Conducting Films: Extremely High DC to Optical Conductivity Ratios. *ACS Nano* **2009**, *3*, 1767–1774.

(100) Fangohr, H.; Chernyshenko, D. S.; Franchin, M.; Fischbacher, T.; Meier, G. Joule Heating in Nanowires. *Phys. Rev. B - Condens. Matter Mater. Phys.* **2011**, *84*, 1–14.

(101) You, C.-Y.; Sung, I. M.; Joe, B.-K. Analytic Expression for the Temperature of the Current-Heated Nanowire for the Current-Induced Domain Wall Motion. *Appl. Phys. Lett.* **2006**, *89*, 222513.

(102) Chen, D.; Liang, J.; Liu, C.; Saldanha, G.; Zhao, F.; Tong, K.; Liu, J.; Pei, Q. Thermally Stable Silver Nanowire-Polyimide Transparent Electrode Based on Atomic Layer Deposition of Zinc Oxide on Silver Nanowires. *Adv. Funct. Mater.* **2015**, 7512–7520.

(103) Rayleigh, Lord. On the Instability of Jets. *Proc. London Math. Soc.* **1878**, *10*, 4–13.

(104) Xie, S.; Ouyang, Z.; Jia, B.; Gu, M. Nanowire Networks As Transparent Electrodes for Crystalline Silicon Wafer Solar Cells. *Opt. Express* **2013**, *21*, 1276–1279.

(105) van de Groep, J. V; Spinelli, P.; Polman, A. Transparent Conducting Silver Nanowire Networks. *Nano Lett.* **2012**, *12*, 3138–3144.

(106) Lee, H.; Lee, D.; Ahn, Y.; Lee, E.-W.; Park, L. S.; Lee, Y. Highly Efficient and Low Voltage Silver Nanowire-Based OLEDs Employing a N-Type Hole Injection Layer. *Nanoscale* **2014**, *6*, 8565–8570.

(107) Liu, Y.; Zhou, H.; Cheng, R.; Yu, W.; Huang, Y.; Duan, X. Highly Flexible Electronics

from Scalable Vertical Thin Film Transistors TL - 14. *Nano Lett.* **2014**, *14 VN-r*, 14131418.

(108) Lee, M.-S.; Lee, K.; Kim, S.-Y.; Lee, H.; Park, J.; Choi, K.-H.; Kim, H.-K.; Kim, D.-G.; Lee, D.-Y.; Nam, S.; *et al.* High-Performance, Transparent, and Stretchable Electrodes Using Graphene–Metal Nanowire Hybrid Structures. *Nano Lett.* **2013**, *13*, 2814–2821.

(109) Dong, Q.; Fang, Y.; Shao, Y.; Mulligan, P.; Qiu, J.; Cao, L.; Huang, J. Electron-Hole Diffusion Lengths > 175 Um in Solution-Grown CH 3 NH 3 PbI 3 Single Crystals. *Science* **2015**, *347*, 967–970.

(110) Stranks, S. D.; Snaith, H. J. Metal-Halide Perovskites for Photovoltaic and Light-Emitting Devices. *Nat. Nanotechnol.* **2015**, *10*, 391–402.

(111) Manser, J. S.; Kamat, P. V. Band Filling with Free Charge Carriers in Organometal Halide Perovskites. *Nat. Photonics* **2014**, *8*, 737–743.

(112) Docampo, P.; Ball, J. M.; Darwich, M.; Eperon, G. E.; Snaith, H. J. Efficient Organometal Trihalide Perovskite Planar-Heterojunction Solar Cells on Flexible Polymer Substrates. *Nat. Commun.* **2013**, *4*, 2761.

(113) Hu, X.; Zhang, X.; Liang, L.; Bao, J.; Li, S.; Yang, W.; Xie, Y. High-Performance Flexible Broadband Photodetector Based on Organolead Halide Perovskite. *Adv. Funct. Mater.* **2014**, *24*, 7373–7380.

(114) You, J.; Hong, Z.; Yang, Y. M.; Chen, Q.; Cai, M.; Song, T.; Chen, C.; Lu, S.; Liu, Y.; Zhou, H.; *et al.* Low-Temperature Solution-Processed Perovskite Solar Cells with High Efficiency and Flexibility. *ACS Nano* **2014**, *8*, 1674–1680.

(115) Li, Y.; Meng, L.; Yang, Y. (Michael); Xu, G.; Hong, Z.; Chen, Q.; You, J.; Li, G.; Yang, Y.; Li, Y. High-Efficiency Robust Perovskite Solar Cells on Ultrathin Flexible Substrates.

*Nat. Commun.* **2016**, *7*, 10214.

(116) Kim, B.-J.; Kim, dong H.; Lee, Y.-Y.; Shin, H.-W.; Han, G. S.; Hong, J. S.; Mahmood, K.; Ahn, T.; Joo, Y.-C.; Hong, K. S.; *et al.* Highly Efficient and Bending Durable Perovskite Solar Cells: Toward Wearable Power Source. *Energy Environ. Sci.* **2015**, *8*, 916–921.

(117) Shin, S. S.; Yang, W. S.; Noh, J. H.; Suk, J. H.; Jeon, N. J.; Park, J. H.; Kim, J. S.; Seong, W. M.; Seok, S. Il. High-Performance Flexible Perovskite Solar Cells Exploiting Zn2SnO4 Prepared in Solution below 100 °C - Supplementary Infomation. *Nat. Commun.* **2015**, *6*, 7410.

(118) Tan, Z.-K.; Moghaddam, R. S.; Lai, M. L.; Docampo, P.; Higler, R.; Deschler, F.; Price, M.; Sadhanala, A.; Pazos, L. M.; Credgington, D.; *et al.* Bright Light-Emitting Diodes Based on Organometal Halide Perovskite. *Nat. Nanotechnol.* **2014**, *9*, 1–6.

(119) Wang, J.; Wang, N.; Jin, Y.; Si, J.; Tan, Z.-K.; Du, H.; Cheng, L.; Dai, X.; Bai, S.; He, H.; *et al.* Interfacial Control Toward Efficient and Low-Voltage Perovskite Light-Emitting Diodes. *Adv. Mater.* **2015**, 2311–2316.

(120) Zhou, Q.; Bai, Z.; Lu, W. gao; Wang, Y.; Zou, B.; Zhong, H. In Situ Fabrication of Halide Perovskite Nanocrystal-Embedded Polymer Composite Films with Enhanced Photoluminescence for Display Backlights. *Adv. Mater.* **2016**.

(121) Cho, H.; Jeong, S.-H.; Park, M.-H.; Kim, Y.-H.; Wolf, C.; Lee, C.-L.; Heo, J. H.; Sadhanala, A.; Myoung, N.; Yoo, S.; *et al.* Overcoming the Electroluminescence Efficiency Limitations of Perovskite Light-Emitting Diodes. *Science (80-. ).* **2015**, *350*, 1222–1225.

(122) Wang, N.; Cheng, L.; Ge, R.; Zhang, S.; Miao, Y.; Zou, W.; Yi, C.; Sun, Y.; Cao, Y.;

Yang, R.; *et al.* Perovskite Light-Emitting Diodes Based on Solution-Processed Self-Organized Multiple Quantum Wells. *Nat. Photonics* **2016**, *10*, 699–704.

(123) Zhang, F.; Zhong, H.; Chen, C.; Wu, X.; Hu, X.; Huang, H. Brightly Luminescent and Color- ( X = Br , I , Cl ) Quantum Dots : Potential Alternatives for Display Technology. *ACS Nano* **2015**, *3*, 4533–4542.

(124) Bade, S. G. R.; Li, J.; Shan, X.; Ling, Y.; Tian, Y.; Dilbeck, T.; Besara, T.; Geske, T.; Gao, H.; Ma, B.; *et al.* Fully Printed Halide Perovskite Light-Emitting Diodes with Silver Nanowire Electrodes. *ACS Nano* **2016**, *10*, 1795–1801.

(125) Li, J.; Bade, S. G. R.; Shan, X.; Yu, Z. Single-Layer Light-Emitting Diodes Using Organometal Halide Perovskite/Poly(ethylene Oxide) Composite Thin Films. *Adv. Mater.* **2015**, 5196–5202.

(126) Li, G.; Tan, Z.-K.; Di, D.; Lai, M. L.; Jiang, L.; Lim, J. H.; Friend, R. H.; Greenham, N. C. Efficient Light-Emitting Diodes Based on Nano-Crystalline Perovskite in a Dielectric Polymer Matrix. *Nano Lett.* **2015**, *15*, 2640–2644.

(127) Schmidt, L. C.; Pertegas, A.; Gonzalez-Carrero, S.; Malinkiewicz, O.; Agouram, S.; Espallargas, G. M.; Bolink, H. J.; Galian, R. E.; Perez-Prieto, J. Nontemplate Synthesis of CH 3 NH 3 PbBr 3 Perovskite Nanoparticles. *J. Am. Chem. Soc.* **2014**, *136*, 850–853.

(128) Xing, J.; Yan, F.; Zhao, Y.; Chen, S.; Yu, H.; Zhang, Q.; Zeng, R.; Demir, H. V.; Sun, X.; Huan, A.; *et al.* High-Efficiency Light-Emitting Diodes of Organometal Halide Perovskite Amorphous Nanoparticles. *ACS Nano* **2016**, *10*, 6623–6630.

(129) Deng, W.; Xu, X.; Zhang, X.; Zhang, Y.; Jin, X.; Wang, L.; Lee, S. T.; Jie, J. Organometal Halide Perovskite Quantum Dot Light-Emitting Diodes. *Adv. Funct. Mater.* **2016**, *26*, 4797–4802.

(130) Yang, X.; Mutlugun, E.; Dang, C.; Dev, K.; Gao, Y.; Tan, S. T.; Xun, X. W.; Demir, H. V. Highly Flexible, Electrically Driven, Top-Emitting, Quantum Dot Light-Emitting Stickers. *ACS Nano* **2014**, *8*, 8224–8231.

(131) Liu, H.; Li, M.; Voznyy, O.; Hu, L.; Fu, Q.; Zhou, D.; Xia, Z.; Sargent, E. H.; Tang, J. Physically Flexible, Rapid-Response Gas Sensor Based on Colloidal Quantum Dot Solids. *Adv. Mater.* **2014**, *26*, 2718–2724.

(132) Huang, H.; Zhao, F.; Liu, L.; Zhang, F.; Wu, X. G.; Shi, L.; Zou, B.; Pei, Q.; Zhong, H. Emulsion Synthesis of Size-Tunable CH3NH3PbBr3 Quantum Dots: An Alternative Route toward Efficient Light-Emitting Diodes. *ACS Appl. Mater. Interfaces* **2015**, *7*, 28128–28133.

(133) Lu, H.-Y.; Chou, C.-Y.; Wu, J.-H.; Lin, J.-J.; Liou, G.-S. Highly Transparent and Flexible polyimide–AgNW Hybrid Electrodes with Excellent Thermal Stability for Electrochromic Applications and Defogging Devices. *J. Mater. Chem. C* **2015**, *3*, 3629–3635.

(134) Dai, X.; Zhang, Z.; Jin, Y.; Niu, Y.; Cao, H.; Liang, X.; Chen, L.; Wang, J.; Peng, X. Solution-Processed, High-Performance Light-Emitting Diodes Based on Quantum Dots. *Nature* **2014**, *515*, 96–99.

(135) Su, S. J.; Chiba, T.; Takeda, T.; Kido, J. Pyridine-Containing Triphenylbenzene Derivatives with High Electron Mobility for Highly Efficient Phosphorescent OLEDs. *Adv. Mater.* **2008**, *20*, 2125–2130.

(136) Zhang, Q.; Zhou, Q.; Cheng, Y.; Wang, L.; Ma, D.; Jing, X.; Wang, F. Highly Efficient Green Phosphorescent Organic Light-Emitting Diodes Based on CuI Complexes. *Adv. Mater.* **2004**, *16*, 432–436.

(137) Kim, S. Y.; Jeong, W. I.; Mayr, C.; Park, Y. S.; Kim, K. H.; Lee, J. H.; Moon, C. K.;

Brütting, W.; Kim, J. J. Organic Light-Emitting Diodes with 30% External Quantum Efficiency Based on a Horizontally Oriented Emitter. *Adv. Funct. Mater.* **2013**, *23*, 3896–3900.

(138) Pfister, G. R. Hopping Transport in a Molecularly Doped Organic Polymer. *Phys. Rev. B - Condens. Matter Mater. Phys.* **1977**, *16*, 3676–3687.

(139) Fu, Q.; Chen, J.; Shi, C.; Ma, D. Solution-Processed Small Molecules as Mixed Host for Highly Efficient Blue and White Phosphorescent Organic Light-Emitting Diodes. *ACS Appl. Mater. Interfaces* **2012**, *4*, 6579–6586.

(140) Sun, Q. J.; Fan, B. H.; Tan, Z. A.; Yang, C. H.; Li, Y. F.; Yang, Y. White Light from Polymer Light-Emitting Diodes: Utilization of Fluorenone Defects and Exciplex. *Appl. Phys. Lett.* **2006**, *88*, 86–89.

(141) Zhu, R.; Chung, C. H.; Cha, K. C.; Yang, W.; Zheng, Y. B.; Zhou, H.; Song, T. Bin; Chen, C. C.; Weiss, P. S.; Li, G.; *et al.* Fused Silver Nanowires with Metal Oxide Nanoparticles and Organic Polymers for Highly Transparent Conductors. *ACS Nano* **2011**, *5*, 9877–9882.

(142) Scheideler, W. J.; Smith, J.; Deckman, I.; Chung, S.; Arias, A. C.; Subramanaian, V. A Robust, Gravure-Printed, Silver Nanowire/metal Oxide Hybrid Electrode for High-Throughput Patterned Transparent Conductors. *J. Mater. Chem. C* **2016**, *4*, 3248–3255.

(143) Trung, T. Q.; Ramasundaram, S.; Hwang, B. U.; Lee, N. E. An All-Elastomeric Transparent and Stretchable Temperature Sensor for Body-Attachable Wearable Electronics. *Adv. Mater.* **2016**, *28*, 502–509.

(144) Li, J.; Liang, J.; Li, L.; Ren, F.; Hu, W.; Li, J.; Qi, S.; Pei, Q. Healable Capacitive Touch Screen Sensors Based on Transparent Composite Electrodes Comprising Silver Nanowires

and a Furan / Maleimide Diels-Alder Cycloaddition Polymer. *ACS Nano* **2014**, *8*, 12874–12882.

(145) Cho, Y. J.; Yook, K. S.; Lee, J. Y. A Universal Host Material for High External Quantum Efficiency close to 25% and Long Lifetime in Green Fluorescent and Phosphorescent OLEDs. *Adv. Mater.* **2014**, *26*, 4050–4055.

(146) Wu, Z.; Ma, D. Recent Advances in White Organic Light-Emitting Diodes. *Mater. Sci. Eng. R* **2016**, *107*, 1–42.

(147) Brütting, W.; Frischeisen, J.; Schmidt, T. D.; Scholz, B. J.; Mayr, C. Device Efficiency of Organic Light-Emitting Diodes: Progress by Improved Light Outcoupling. *Phys. Status Solidi Appl. Mater. Sci.* **2013**, *210*, 44–65.